SPECTROSCOPIC CONSTANTS, LIFETIMES AND PREDISSOCIATION RATES FOR Bi$_2$ $A(0_u^+)$

DISSERTATION

Michael Wayne Dolezal, Captain, USAF

AFIT/DS/ENP/01-01

DEPARTMENT OF THE AIR FORCE
AIR UNIVERSITY

AIR FORCE INSTITUTE OF TECHNOLOGY

Wright-Patterson Air Force Base, Ohio

20010612 122

The views expressed in this dissertation are those of the author and do not reflect the official policy or position of the United Sates Air Force, Department of Defense, or the U.S. Government.

SPECTROSCOPIC CONSTANTS, LIFETIMES AND PREDISSOCIATION RATES FOR $Bi_2\, A(0_u^+)$

DISSERTATION

Presented to the Faculty

Department of Engineering Physics

Graduate School of Engineering and Management

Air Force Institute of Technology

Air University

Air Education and Training Command

in Partial Fulfillment of the Requirements for the

Degree of Doctor of Philosophy

Michael Wayne Dolezal, B.S., M.S.
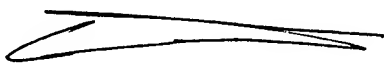
Captain, USAF

March 2001

SPECTROSCOPIC CONSTANTS, LIFETIMES AND PREDISSOCIATION RATES FOR $Bi_2 A(0_u^+)$

Michael Wayne Dolezal, B.S., M.S.
Captain, USAF

Approved: Date

_____
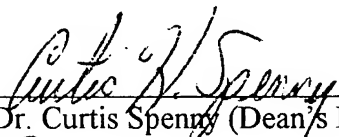LtCol Glen Perram (Chairman)   05 MAR 01

_____
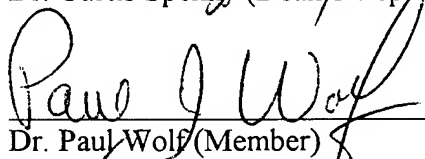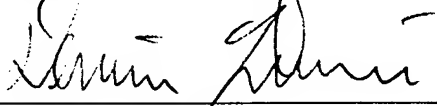Dr. Curtis Spenny (Dean's Representative)   9 March 01

_____
Dr. Paul Wolf (Member)   6 mar 01
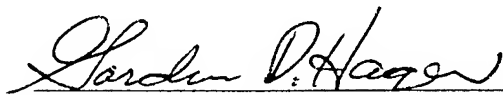
_____
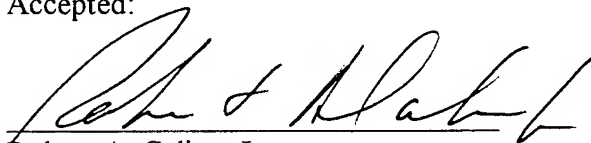Dr. Dennis Quinn (Member)   6 MAR 01

_____
Dr. Gordon Hager (Laboratory Representative)   March 11 2001

Accepted:

_____
Robert A. Calico, Jr.   13 March 01
Dean, Graduate School of Engineering and Management   Date

Acknowledgments

I have been extremely fortunate to work with several individuals who have had a profound positive influence on my life, my academic ambitions, and my career. Without a doubt, I consider Dr. Lee Whitney to be my inspiration for pursuing this degree and my motivation for enveloping myself in this profession. During the short period of time I worked with Dr. Whitney nearly a decade ago, he taught me respect and enthusiasm for this discipline. Along with the help of my coworkers Tom, Joe, Chuck and Ron, I was able to learn and develop a passion for science and foster an eagerness to further my education in physics.

My pursuit of this degree has taken me on a journey through several educational institutions and placed me in contact with several outstanding educators along the way. I would be remiss if I did not take this opportunity to thank the individuals who have left a positive impression on me throughout my education. My high school physics teacher, Dick Snydle, first planted the seed of interest that has grown to this point. My collegiate professors from the University of Minnesota, Dr. Mortin Hammermesh and Dr. Fred Greenlees, and from the University of North Dakota, Dr. Hen Sonpaa, continued to inspire and guide me through the labyrinth of undergraduate education. As I pursued my Masters Degree at Creighton University, my advisor, Dr. Sam Cipolla, along with Dr. Robert Kennedy, Father Tom McShane and Dr. Janet Seager continued the tradition of excellence in instruction I needed every step along the way.

I would like to thank Lieutenant Colonel Glen Perram for his patients and guidance during the course of my experimental work. His experience, knowledge and insight helped guide me through many areas of uncertainty encountered during my research. My gratitude also extends to the members of my committee for their insightful and meaningful contributions over the past four years of my studies. Finally, without the help of Dr. Won Roh, Dr. William Bailey, Dr. David Weeks, Major Craig Largent and Mr. Greg Smith, I would have never been able or ready to sit down and write these words.

Many thanks to my family, friends, especially Mark, and coworkers for their encouragement and support over the years. My classmates Jeremy, Mark, and Rob deserve recognition for their professionalism and willingness to help with problems both simple and complex. Also, without the continual help from Sam, Chad and Ted, I would have never finished this dissertation. Thanks to my friends and extended family for your support, help, endless understanding and scheduling of events around my research. Special recognition must go out to my mother, Dixie, and father, Harold, who, throughout my life, have stressed the importance of education, self-discipline, and hard meaningful work. Endless thanks and love to Maria, Jonathan, and my wife Jennifer, I will never be able to fully convey to you how much your love, understanding and support has helped me through these stress-filled times.

Most importantly, I thank God for all He has done for my family and I.

<div align="right">Michael Wayne Dolezal</div>

Table of Contents

List of Figures

List of Tables

List of Symbols

Category	Symbol	Definition
Energy	$V(\mathbf{R})$	Bound-State Potential
	T_e	Minimum Bound-State Energy
	$V_{rep}(\mathbf{R})$	Repulsive-State Potential
	G_v	Vibrational Energy
	ΔG	Vibrational Second Difference
	$F_v(J)$	Ro-Vibrational Energy
	$\Delta_2 F(J)$	Rotational Second Difference
	E_p	Photon Energy
Lifetimes	τ	Total State Lifetime
	τ_{rad}	Radiative Lifetime
	τ_0	Collision-Free Lifetime
Operators	$\mathbf{H}_{molec}$	Molecular Hamiltonian
	$\mathbf{H}'$	Born-Oppenheimer Cross Term
	∇_A	Nuclear Operator
	∇_i	Electronic Operator

Category	Symbol	Definition
Physical	$\mathbf{r}$	Electronic Coordinate Vector
	$\mathbf{R}$	Nuclear Coordinate Vector
	Z_A	Atomic Number (Atom A)
	M_A	Nuclear Mass (Atom A)
	m_e	Electron Mass
	μ	Reduced Mass
	P	Pressure
Rates	k_q	Collisional Deactivation Rate
	Γ_o	Collisionless Decay Rate
	Γ_{pd}	Heterogeneous Predissociation Probability
	Γ_{rad}	Radiative Decay Rate
	$A_{v',v'}$	Einstein A Coefficient
	$k_{pd,v'}$	Predissociative Rate
Wave Functions	Ψ_{molec}	Total Molecular Wave Function
	ψ_{elec}	Electronic Wave Function
	χ_N	Total Nuclear Wave Function
	χ_{vib}	Nuclear Vibrational Wave Function
	χ_{rot}	Nuclear Rotational Wave Function

Category	Symbol	Definition
Spectroscopic	A	Upper Bound State
	X	Ground Electronic State
	v	Vibrational Quantum Number
	J	Rotational Quantum Number
	ν_0	Band-Head
	P(J)	P-Branch
	R(J)	R-Branch
	ω_e $\omega_e\chi_e$ $\omega_e y_e$	Vibrational Term Values
	B_e D_e α_e γ_e δ_e	Rotational Term Values
	$Y_{i,k}$	Dunham Expansion Coefficients

Abstract

More than 100,000 spectral features from a $Bi_2(X^1\Sigma_g^+ \rightarrow A(0_u^+))$ absorption spectrum, encompassing $0 \le v' \le 91$, $0 \le v'' \le 7$ and $J \le 203$, have been assigned. Analysis of this data has resulted in improvements to vibrational and rotational spectroscopic constants for $Bi_2(A)$. Ground state constants, reported by Barrow et al. [1], remain unchanged. The new constants are used to redefine the A-state potential using traditional RKR methods and to set the dissociation energy at $D_e = 29,913$ cm^{-1}, which correlates A-state dissociation products to $^4S + {}^2D$ atoms. A pulsed dye laser apparatus was used to obtain lifetime data for $Bi_2(A(0_u^+) \rightarrow X^1\Sigma_g^+)$ transitions. The collision-free lifetimes for $v'=20$ to $v'=39$, and $J \le 105$, were investigated for effects of heterogeneous predissociation. The observed predissociation rates, $\Gamma = k_{pd,v'}J(J+1)$, establish the range $k_{pd,v'} = 153$ sec^{-1} to 1.5×10^5 sec^{-1} for $v'=21$ to $v'=39$. Rapid predissociation and the dense $Bi_2(A \rightarrow X)$ spectrum required both traditional lifetime measurements and synthetic spectrum fits to determine the full range of observed rates. Extensive numerical analysis fails to produce an appropriate analytic repulsive potential responsible for the observed A-state predissociation implying that current numerical tools, theoretical constructs, and knowledge of the low-lying electronic states in Bi_2 are inadequate to describe the predissociation found in this study.

SPECTROSCOPIC CONSTANTS, LIFETIMES

AND PREDISSOCIATION RATES FOR $Bi_2 A(0_u^+)$

1. Introduction

1.1. Overview

The bismuth atom, Bi, has an atomic number of 82 and an atomic mass of nearly

209 atomic mass units (amu) making the bismuth diatom, Bi_2, the heaviest stable diatomic

molecule. Of all transitions within Bi_2, the $A(0_u^+) \leftrightarrow X^1\Sigma_g^+$ electronic transition has been

the most investigated. Several previous spectroscopic [1-7] and lifetime [8-10] studies

have been performed in an effort to characterize this transition. None of the spectroscopic

studies contain a comprehensive analysis of the entire range of available vibrational and

rotational levels within $Bi_2(A)$. Results presented in the lifetime studies are, at best,

incomplete and there has been no effort to evaluate the type or rates of predissociation

reported to exist in the $A(0_u^+)$ state. This dissertation presents a complete research effort

which has improved spectroscopic constants, confirmed dissociation products of $Bi_2(A)$,

defined lifetimes, and determined predissociation rates for the A-state. Additionally,

theoretical treatments are explored in an effort to determine an acceptable analytic form

for the repulsive $^7\Sigma_u^+(1_u)$ potential thought responsible for predissociation in the A-state.

1.2. Air Force Interests

Soon after the demonstration of the first laser device in the 1960's the Air Force

became interested in the laser as a potential weapon system. Several types of lasers have

been considered as possible weapon system candidates including chemical lasers, excimer

lasers and free electron lasers [11]. Since 1976, when "a commitment was made to

develop a (high power) HF/DF chemical laser within 5 years," [11] the chemical laser

program has moved to the forefront of laser weapons technology research.

Chemical laser systems, which create a population inversion in the lasing medium

through an exothermic chemical reaction, have proven to be very efficient. They produce

a large output for each unit mass of laser reactant consumed. For systems which utilize

pure chemical initiation (i.e., the chemical reaction drives the entire process without the

use of external power) the mass efficiencies are on the order of 150 kJ/kg for the HF laser

and 300 kJ/kg for the Chemical Oxygen Iodine Laser (COIL) [12]. The goal is to reach

mass efficiencies of 1 MJ/kg in future systems [13]. These types of efficiencies are not

only desirable but also necessary for airborne and space based laser weapon applications.

In 1978, at the Air Force Weapons Laboratory, the first electronic transition

chemical laser, COIL, was demonstrated. The development of COIL as a potential

weapon system has progressed to the point where the Air Force is currently testing

deployment of COIL on a modified Boeing 747 aircraft for use as a theater missile defense system. COIL operates at a wavelength of 1.315 μm.

One measure of a laser's performance, which determines the maximum power obtainable on the target, is the brightness, B, which has units of W/sr. The brightness of a laser can be expressed as $B = PD^2/\pi\lambda^2$, where D is the aperture diameter, P is the output power and λ the operating wavelength [11]. For diffraction limited systems, the advantage of shorter operating wavelengths is obvious, considering that $B \propto 1/\lambda^2$. For example, the power, P, generated by COIL would need to be nearly eight times greater than the power output of a laser operating in the blue range of the visible spectrum to produce the same brightness.

This potential power advantage has lead researchers to investigate candidates for visible wavelength chemical lasers. One promising candidate is an excited state $NF(a^1\Delta)$ driven laser system. $NF(a^1\Delta)$ acts as a metastable energy carrier which, by collision, can transfer its energy to an atomic or molecular system [13,14,15]. Capelle and Sutton have shown that the rate of energy transfer to bismuth metal vapor is both fast and efficient [14]. The near resonant energy transfer from NF to Bi is better than that for other atomic systems they had investigated. In 1993, the threshold oscillation of a $NF(a^1\Delta)/BiF$ laser operating at 470nm was first observed [16]. This demonstration was performed with a gaseous organic bismuth molecule, $Bi(CH_3)_3$, which proved undesirable due to the rapid collisional quenching associated with the methyl radicals.

Therefore, the ability to produce a NF/BiF laser, which utilizes metallic vapor bismuth atoms, is desirable. Unfortunately, the production of Bi vapor, needed to produce

the BiF, is accompanied by a nearly equal production of Bi_2 which acts as a collisional energy deactivation constituent reducing the efficiency of the laser medium.

To completely understand the BiF production process and its efficiency the effects of all constituents in the energy transfer process must be determined. Thus, a thorough evaluation of the spectroscopy, lifetimes, and energy transfer processes of Bi_2 will be necessary in the search for a more efficient BiF visible chemical laser system.

1.3. Spectroscopic Community Interests

Analysis of the $A(0_u^+)$ and $X^1\Sigma_g^+$ states of Bi_2 has resulted in a good determination of the spectroscopic constants for the X-state, and to a lesser degree, for the A-state as well. Most recently Barrow et al., have presented a complete set of Dunham expansion coefficients for $0 \leq v'' \leq 105$ and $0 \leq v'' \leq 11$ for the X-state [1] and Franklin and Perram have presented the most accurate set of coefficients for the excited A-state [6]. However, there still exist the need for "…an extended analysis of the A-X system of Bi_2…"[4]. An interferometer has been used to investigate absorption line positions for the range of accessible rotational, $J \leq 203$, and vibrational, $0 \leq v' \leq 91$ and $0 \leq v'' \leq 7$, levels resulting from transitions from the X to the A-state of Bi_2. Spectral features are identified and used to determine the best spectroscopic constants to date for the A-state. The spectroscopic data is also used in a Brige-Sponer analysis to define D_e, the dissociation energy of the A-state.

Lifetime studies of the excited A-state are only partially complete [8,9,10]. These lifetime studies show inconsistent evidence of the number and nature of predissociative phenomena in the A-state of Bi_2. Blondeau, Gandara, Carette, and Messelyn state, with regard to the complex predissociative nature of $Bi_2(A)$, "An extensive study by means of high resolution absorption and laser induced fluorescence experiments has to be performed to solve this problem[8]." The pulsed dye laser experiment used to investigate the lifetimes of v' in the range $8 \leq v' \leq 40$ with $J \leq 105$ fills this void. The lifetimes measured from this experiment allow for the characterization of the nature of the predissociative phenomena. Once the lifetime data is analyzed as a function of quantum numbers v and J as well as total pressure P, the type of predissociation is determined. With this information, and a new bound A-state potential, characterized by new A-state spectral constants, the form of the repulsive potential responsible for predissociation in the A-state will be extensively explored [17].

1.4.   Problem Statement

A Fourier Transform (FT) interferometer was used to obtain a 0.12 cm^{-1} resolution absorption spectra of the $Bi_2(X(0_g^+) \rightarrow A(0_u^+))$ transition. Within each vibrational manifold, spectroscopic features were identified by position and used to determine the best fit for band-specific rotational constants. The entire group of constants, from all vibrational manifolds accessed, was then analyzed in a global fit routine to determine the best A-state spectroscopic constants and dissociation energy available to date.

A pulsed dye laser experiment was used to obtain both laser excitation spectra and lifetime data, at several different pressures, for the A-state of Bi_2. The A-state was probed over the range $8 \leq v' \leq 40$ with $J \leq 105$. Existence of very strong predissociation is evident in the excitation spectra above $v'=20$. Most of the effort in obtaining lifetime data was, therefore, concentrated at $v'=20$ and above.

The theoretical treatment of spontaneous predissociation in Br_2, presented in a paper by Clyne, Heaven and Tellinghuisen [17], is analogous to the predissociation found here in Bi_2. The newly revised bound state potential and the measured predissociation rates, $k_{pd,v'}$, were used in an effort to determine an analytic solution for the repulsive potential responsible for this predissociation. A detailed analysis reveals that no such potential is definable using available theoretical and numerical techniques.

1.5.   Organization

The theory of spectroscopy for diatomic bismuth, with an emphasis on the effects of heterogeneous predissociation on the spectra, is presented first in Chapter 2. Chapter 3 outlines the computational steps and results of Bi_2 (X→A) absorption spectroscopy, which covers vibrational levels $0 \leq v' \leq 91$ and $0 \leq v'' \leq 7$. Chapter 4 contains a complete analysis of the lifetimes of the excited states of $Bi_2(A)$ within the vibrational manifold range of $v'=20$ to $v'=40$. This analysis provides the radiative lifetime, τ_o, the range of the predissociation rate constant, $k_{pd,v'}$, and information on the potential responsible for predissociation of this state. Chapter 5 includes a Rydberg-Klein-Rees (RKR) calculation

of the bound A-state potential using new spectroscopic constants, determined in Chapter 4, and attempts to identify the repulsive state responsible for the predissociation. The numerical investigation into the analytic form of the repulsive potential is also presented. Lastly, Chapter 6 provides a summary and conclusion of the work contained in this dissertation as well as several recommendations for future analysis of this molecular system.

2. Background Theory

2.1.   The Born-Oppenheimer Approximation

The behavior of a diatomic molecule may be treated with varying levels of sophistication. The primary difficulty associated with determining the energy eigenvalues of the molecule is the complexity of the molecular Hamiltonian [18],

$$\mathbf{H}_{molec} = -\frac{\hbar^2}{2m}\sum_i \nabla_i^2 - \sum_A \frac{\hbar^2}{2M_A}\nabla_A^2 - \sum_{A,i}\frac{Z_A e^2}{\mathbf{r}_{Ai}} + \sum_{A>B}\frac{Z_A Z_B e^2}{\mathbf{R}_{AB}} + \sum_{i>j}\frac{e^2}{\mathbf{r}_{ij}} \tag{1}$$

where the terms on the right hand side correspond to the electron kinetic energy, the nuclear kinetic energy, the electron-nuclear attraction, the nuclear-nuclear repulsion, and the electron-electron repulsion, respectively.

The Born-Oppenheimer approximation asserts that electronic motions in molecules occur quickly enough, relative to the motion of the nuclei, to assume the nuclear coordinate, $\mathbf{R}$, remains constant during electronic transitions. As a result, electronic and nuclear wave functions are separable. Therefore, the molecular wave function, Ψ_{molec}, may be written as the product of the electronic, ψ_{elec}, and nuclear, χ_N, wave functions:

$$\Psi_{molec}(\mathbf{r},\mathbf{R}) = \psi_{elec}(\mathbf{r},\mathbf{R})\chi_N(\mathbf{R}) \tag{2}$$

Note, the electronic wave function $\psi_{elec}(\mathbf{r}, \mathbf{R})$ is a function of both the electronic

coordinate $\mathbf{r}$ and the nuclear coordinate $\mathbf{R}$, whereas the nuclear wave function $\chi_N(\mathbf{R})$ is a

function of the nuclear coordinate $\mathbf{R}$ alone. Substitution of equations (1) and (2) into

Schrodinger's equation,

$$H_{molec}\Psi_{molec}(\mathbf{r},\mathbf{R}) = E_{total}\Psi_{molec}(\mathbf{r},\mathbf{R}), \tag{3}$$

yields the following expression

$$
\begin{aligned}
\chi_N &\left[-\frac{\hbar^2}{2m}\sum_i \nabla_i^2 - \sum_{A,i}\frac{Z_A e^2}{\mathbf{r}_{Ai}} + \sum_{i>j}\frac{e^2}{\mathbf{r}_{ij}} \right]\psi_{elec} + \\
&\psi_{elec}\left[-\frac{\hbar^2}{2M_A}\sum_A \nabla_A^2 + \sum_{A>B}\frac{Z_A Z_B e^2}{\mathbf{R}_{AB}} \right]\chi_N - \\
&\left[\frac{\hbar^2}{2M_A}\sum\left(2\nabla_A\psi_{elec}\nabla_A\chi_N + \chi_N\nabla_A^2\psi_{elec} \right) \right] = E_{total}\psi_{elec}\chi_N
\end{aligned}
\tag{4}
$$

The last term in square brackets in equation (4) is the cross term in the Born-

Oppenheimer approximation, which will be called $\mathbf{H}'$. For this term only, the electronic

wave function $\psi_{elec}(\mathbf{r}, \mathbf{R})$ cannot be separated from the effect of the nuclear operator ∇_A,

which operates on the nuclear coordinate $\mathbf{R}$. The contribution of this term to the

electronic energy is on the order of $(m_e/M_A)E_{elec} \approx (2.6\times10^{-6})E_{elec}$ for bismuth [18].

Neglecting $\mathbf{H}'$ in (4) and applying separation of variables to the remaining terms, the

electronic and nuclear eigenvalue equations become

$$\left[-\frac{\hbar^2}{2m} \sum_i \nabla_i^2 - \sum_{A,i} \frac{Z_A e^2}{\mathbf{r}_{Ai}} + \sum_{i>j} \frac{e^2}{\mathbf{r}_{ij}} \right] \psi_{elec}(\mathbf{r};\mathbf{R}) = E_{elec}(\mathbf{R})\psi_{elec}(\mathbf{r};\mathbf{R}) \tag{5}$$

and

$$\left[-\frac{\hbar^2}{2M_A} \sum_A \nabla_A^2 + E_{elec}(\mathbf{R}) + \sum_{A>B} \frac{Z_A Z_B e^2}{\mathbf{R}_{AB}} \right] \chi_N(\mathbf{R}) = E_{total}\chi_N(\mathbf{R}) \tag{6}$$

respectively. The energy eigenvalues associated with solutions of equation (6) will determine the majority of the spectroscopy of the bismuth diatom.

2.2. *Rotational, Vibrational, and Electronic Energy Levels of Diatomic Molecules*

The solution to the nuclear eigenvalue equation, (6), provides the energies of translation, vibration, and rotation. Each of these energies is treated as independent so the total energy of the diatomic system can be written as

$$E_{total} = E_{trans} + (E_{vib} + E_{rot}) + E_{elec} \tag{7}$$

where the electronic energy, E_{elec}, is determined from solving equation (5) for given inter-nuclear separations $\mathbf{R}$. E_{vib} and E_{rot} have been bracketed together to indicate their inescapable interdependence, which will be outlined in the discussion that follows. The nuclear motions of rotation and vibration are considered to be in a space-fixed reference

frame, thus eliminating the translational energy contribution, E_{trans}, from the total energy

term. Furthermore, the additive nature of the energy terms requires the total wave

function, Ψ_{total}, to be the product of individual wave functions [19], that is

$$\Psi_{total} = \chi_N \psi_{elec} = \chi_{vib} \chi_{rot} \psi_{elec} \tag{8}$$

The vibrational energy of the molecule results from the periodic oscillatory

motion of the bound nuclei of the diatomic system. Consider, as a first approximation,

the solution to the simple harmonic oscillator (SHO) whose quantized energy levels are

positive integer multiples of $h\nu$, $E_v = h\nu(v + \frac{1}{2})$. The actual potential, by which the

diatomic system is bound, is much more complex than the simple parabolic potential of

the SHO. The potential is far more repulsive than R^2 as $R \to 0$ and eventually tends to a

zero slope as $R \to \infty$, in the limit of dissociation. Borrowing the form of the harmonic

oscillator solution, the energy levels are cast as a series expansion in terms of $(v + \frac{1}{2})$.

By convention this equation is written in energy units of cm^{-1} as

$$G_v = \omega_e \left(v + \frac{1}{2}\right) - \omega_e \chi_e \left(v + \frac{1}{2}\right)^2 + \omega_e y_e \left(v + \frac{1}{2}\right)^3 + \dots \tag{9}$$

Similarly, the simple dumbbell rigid rotor model may be used to approximate the

rotational energy levels in the molecule. In this case energy levels are of the form

$E_{rot} = BJ(J+1)$, where B is the rotational constant in units of cm^{-1}. Paralleling the

development of the vibrational energy term, the rotational energy is written as a series expansion of J(J + 1), resulting in energy levels of

$$E_{rot} = B_v J(J+1) - D_v \left[J(J+1) \right]^2 + H_v \left[J(J+1) \right]^3 + ... \qquad (10)$$

Note the introduction of the subscript v in equation (10). Even though our original hypothesis called for independence in energy for electronic, vibrational and rotational motions, we must now, by physical necessity, redefine E_{rot} in terms of both v and J, to account for the rotation-vibration dependence of this term. This is necessary to allow for rotational dependence on the vibrating diatomic whose internuclear separation changes as the molecule undergoes vibrational motion. Thus, further expansion of equation (10), to include vibrational effects, is accomplished by including terms of $(v + \frac{1}{2})$ within the rotational constants

$$B_v = B_e - \alpha_e (v + \tfrac{1}{2}) + \gamma_e (v + \tfrac{1}{2})^2 + \delta_e (v + \tfrac{1}{2})^3 + ... \qquad (11)$$

$$D_v = D_e - \beta_e (v + \tfrac{1}{2}) + ... \qquad (12)$$

and so on. By substitution, of equations (11) and (12) into equation (10), the rotation-vibration energy term, denoted by $F_v(J)$, becomes

2-5

$$F_v(J) = \left[B_e - \alpha_e(v + \tfrac{1}{2}) + \gamma_e(v + \tfrac{1}{2})^2 + \ldots \right] J(J+1)$$
$$- \left[D_e - \beta_e(v + \tfrac{1}{2}) + \ldots \right] \left[J(J+1) \right]^2 + \ldots \tag{13}$$

Thus, for a given set of vibrational and rotational quantum numbers (v, J), the total energy of a state can be written as

$$E_{v,J} = E_{elec} + G_v + F_v(J) \tag{14}$$

2.3.   The Spectra

The energy of a single emitted photon is simply the difference between the energy of the upper $E_{v',J'}$ energy level and the lower $E_{v'',J''}$ energy level. Thus the emitted photon energy, E_p (cm^{-1}), is given by

$$E_p \equiv E_{v',J'} - E_{v'',J''} = \left[T_e' + G_{v'} + F_{v'}(J') \right] - \left[T_e'' + G_{v''} + F_{v''}(J'') \right] \tag{15}$$

where T_e denotes the minimum of the electronic potential energy curve. In this study only transitions to the ground state are of interest, so $T_e''(X) = 0$ and only $T_e'(A)$ will appear in (15), which becomes

$$E_p = T_e' + \left[G_{v'} - G_{v''}\right] + \left[F_{v'}(J') - F_{v'}(J'')\right] \qquad (16)$$

The determination of the energy of the emitted photons is complete. However, not all transitions between states are allowed.

2.4.   Allowed Molecular Transitions

For Bi_2 it has been established [5,7,10] that the A↔X transition is a transition between the excited electronic state A(0_u^+) and the ground electronic state X($^1\Sigma_g^+$). When a transition is made between electronic energy levels changes in the vibrational quantum number v and the rotational quantum number J also take place. Some changes in these values are allowed while others are forbidden. Here, selection rules for both vibration and rotation are explored.

The transition probability between two vibrational levels of differing electronic states, the upper level being denoted by v' and the lower level by v'', is determined by the degree of overlap of the vibrational wave functions of the upper and lower states, $\chi_{vib'}$ and $\chi_{vib''}$ respectively. More precisely, the strength, or intensity of this transition, is proportional to the square of the transition moment integral

$$\mathbf{M}_{u,l} = \int \Psi_{molec'}^* \boldsymbol{\mu} \Psi_{molec''} d\tau \qquad (17)$$

Once again note that the Born-Oppenheimer approximation asserts that $\Psi_{molec} = \psi_{elec}\chi_{vib}$.

The dipole moment, μ, may be written in terms of its electronic and nuclear components as $\mu = \mu_{elec} + \mu_N$. It can be shown [18,20, 22] that substitution of these two terms into equation (17) yields

$$\begin{aligned} \mathbf{M}_{u,l} &= \int \psi_{elec'}^{*}\mu_e\psi_{elec''}d\tau_{elec} \int \chi_{v'}^{*}\chi_{v''}d\tau_N \\ &= \mathbf{M}_e(\mathbf{R})\langle \chi_{v'}|\chi_{v''}\rangle \end{aligned} \tag{18}$$

where, $\mathbf{M}_e(\mathbf{R})$ is the electronic transition dipole moment and $\langle \chi_{v'}|\chi_{v''}\rangle$ is the overlap integral. Since $\mathbf{R}$ remains constant during an electronic transition, $\mathbf{M}_e(\mathbf{R})$ remains constant. The Frank-Condon factor, $q_{v',v''}$, is, therefore, defined as

$$q_{v',v''} \equiv \left|\langle \chi_{v'}|\chi_{v''}\rangle\right|^2 = \left|\int \chi_{v'}^{*}\chi_{v''}dr\right|^2 \tag{19}$$

The Frank-Condon factor is simply the probability of transition between the two states. In other words, it is a measure of the intensity of a transition between two vibrational states of differing electronic energy levels. A large Frank-Condon factor indicates the transition from v' to v'' is intense.

Attention is now turned to the closely spaced rotational line structure in Bi_2. Analysis of rotational selection rules reveals the dipole selection rule for the rotational quantum number J applies as usual, namely $\Delta J = 0, \pm 1$ [18]. This selection rule gives rise

to the familiar P(J), Q(J) and R(J) branches within the rotational spectrum. The Bi_2(A-X) transition has no Q(J) branch. To understand this statement one must first look at the angular momentum coupling cases. Hund's case (c) applies to the heavier diatomics such as Br_2, I_2 and Bi_2. In this case, the orbital angular momentum quantum number, **L,** and the spin angular momentum quantum number, **S,** are coupled together to form **J = L + S.** [18]. The projection of **J** onto the internuclear axis is labeled Ω, as shown in Figure 2-1. If Ω = 0 for both the upper and lower electronic states, as is the case for Bi_2(A↔X), then ΔJ = 0, i.e., the Q(J) branch, is disallowed by the selection rules and only P(J) and R(J) branches appear in the rotational spectra.
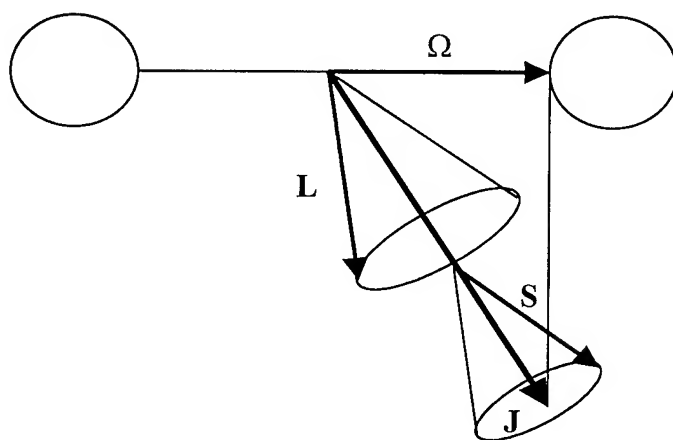
Figure 2-1. Addition of angular momenta for heavy diatomics, Hund's Case (c)

2.5. Determination of Spectroscopic Constants from Experimental Data

The final, and for purposes of this dissertation, most useful application of this theoretical discussion on spectroscopy will be to determine the spectroscopic constants

for the A↔X transition of Bi_2. To accomplish this nontrivial task, the spectrum must be assigned. That is to say the position and responsible transition for each of the thousands of spectral lines, which comprise the $Bi_2(A↔X)$ spectrum, must be determined. Traditionally, a systematic approach to define and eliminate spectral lines based on their spacing relative to one another is used.

Recall the frequency of an individual spectral feature is given by equation (16). To simplify the analysis of data, initially neglect the rotational energies within each vibrational manifold leaving only the frequencies of the vibrational band origins

$$\nu_o = T_e' + G_{v'} - G_{v''} \tag{20}$$

The energy spacing between successive vibrational band origins, known as the vibrational second difference, ΔG, in the spectrum is given by

$$\Delta G = G_{v+1} - G_v = \omega_e - 2(v+1)\omega_e\chi_e + O(\omega_e y_e) \tag{21}$$

The construction of a Deslandres Table aids in the assignment of the vibrational spectrum. Such a table is constructed by ordering the observed transitions such that the relative spacing, ΔG, between successive levels is consistent with equation (21). The vibrational spectroscopic term values (ω_e, $\omega_e\chi_e$, $\omega_e y_e$,...) are then determined by plotting ΔG verses v+1 and fitting this data to equation (21) using a least squares technique. The

accuracy of the fit, which is influenced by the resolution and range of available spectral data, determines the number of terms explicitly carried in the fit to equation (21).

For rotation a similar methodology is employed. The rotational second difference, the energy difference between pairs of rotational lines R(J) and P(J), is used to order and assign these features. Using equation (10), to first order in J(J+1) for simplicity, the rotational second differences are

$$\begin{aligned}
\Delta_2 F'(J'') &= R(J) - P(J) \\
&= B_{v'}(J''+1)(J''+2) - B_{v'}(J''-1)(J'') \\
&= 4B_{v'}(J+\tfrac{1}{2})
\end{aligned} \tag{22}$$

and

$$\begin{aligned}
\Delta_2 F''(J'') &= R(J''-1) - P(J''+1) \\
&= 4B_{v''}(J+\tfrac{1}{2})
\end{aligned} \tag{23}$$

Plotting $\Delta_2 F'(J'')$ and $\Delta_2 F''(J'')$ against J + ½ and performing a least squares fit of the data will result in two straight lines which have slopes $4B_{v'}$ and $4B_{v''}$, intercepts of $2B_{v'}$ and $2B_{v''}$, and a terminus at J = - ½. Once again, the number of terms included in (22) and (23) will be dependent on the accuracy of the fit. This fit establishes both the desired rotational constants and the correct rotational numbering. Although equations (22) and (23) establish an absolute rotational numbering of lines in a band, a generalized expression for all rotational features within a vibrational manifold may be written. By

letting m = J+1 for R(J) and m = -J for P(J) the frequency of a spectral line may be

expressed as

$$
\begin{aligned}
v = v_o &+ (B_{v'} + B_{v''})m + (B_{v'} - B_{v''} - D_{v'} + D_{v''})m^2 \\
&- 2(D_{v'} + D_{v''})m^3 - (D_{v'} - D_{v''})m^4 + O(H_{v'}, H_{v''})
\end{aligned}
\tag{24}
$$

where, again, v_0 is the vibrational band origin.

Once a band-by-band spectroscopic analysis is complete, the results are ready for

a global data fit. Consider, for example, a fit of rotational features from two vibrational

manifolds $(v' = 0, v'' = 1)$ and $(v' = 0, v'' = 2)$, which result in rotational term values

$B_{v'=0}(v'' = 1)$ and $B_{v'=0}(v'' = 2)$ which are not equal. Theory correctly predicts the equality

of these two term values, therefore, there must be a common fit, $B_{v'bf}$, which is the best

fit for the set of individual term values $B_{v'=0}(v'' = 1)$ and $B_{v'=0}(v'' = 2)$. To rectify these

apparent inconsistencies across all bands, a simultaneous global fit to all available data

must be made. Essentially, constants are varied and a least squares analysis is performed

stopping only when the best set of constants for the entire data set of assigned spectral

features is found.

At this point the Dunham Expansion Coefficients $Y_{0,0}$, $Y_{1,0}$, $Y_{1,1}$,..., must be found.

Recall the forms of equations (9) and (13). These two sets of equations can be combined

in a series expansion in terms of v and J such that

$$E(v, J) = \sum_{i,k} Y_{i,k} (v + 1/2)^i [J(J+1)]^k \tag{25}$$

where the $Y_{i,k}$ are related to the vibrational and rotational term values by

$$E(v,J) = Y_{0,0} + Y_{1,0}(v + \tfrac{1}{2}) + Y_{2,0}(v + \tfrac{1}{2})^2 + Y_{0,1}J(J+1) + Y_{0,2}[J(J+1)]^2$$
$$+ Y_{1,1}(v + \tfrac{1}{2})J(J+1) + Y_{2,1}(v + \tfrac{1}{2})^2 J(J+1) + \ldots$$

$$\tag{26}$$

$$= T_e + \omega_e(v + \tfrac{1}{2}) - \omega_e \chi_e (v + \tfrac{1}{2})^2 + B_e J(J+1) - D_e [J(J+1)]^2$$
$$- \alpha_e (v + \tfrac{1}{2})J(J+1) + \gamma_e (v + \tfrac{1}{2})^2 J(J+1) + \ldots$$

Note the subtle differences in sign for term values $\omega_e \chi_e$, D_e, and α_e. Knowledge of these $Y_{i,k}$ constants will allow for the calculation of the potential energy curves, which are responsible for the observed bound-bound spectroscopy.

2.6. Derivation of Potential Energy Curves from Spectroscopic Constants

To understand the construct of determining a bound state potential from spectroscopic constants, consider first the inverse problem, finding the energy eigenvalues from a known potential V(**R**). By use of the semiclassical Wentzel-Kramers-Brillouin (WKB) theory [21] the bound state energies and wave functions may be approximated. Specifically, the first-order WKB theory gives the action integral

$$\left(\frac{2\mu}{\hbar^2}\right)^{\frac{1}{2}} \int_{R^-}^{R^+} \left(E - V(R)\right)^{\frac{1}{2}} dR = \pi\left(v + \tfrac{1}{2}\right) \qquad (27)$$

where R^- and R^+ are the classical turning points on either side of the known bound state

potential, $V(R)$, μ is the reduced mass and E is the energy eigenvalue of the state of

interest. The wavefunctions corresponding to equation (27) are given by

$$\psi = A \exp\left(\pm i \left(\frac{2\mu}{\hbar^2}\right)^{\frac{1}{2}} \int [E - V(R)]^{\frac{1}{2}} dR\right) \qquad (28)$$

and the energy eigenvalues are equation (25), the Dunham expansion[22]

$$E(v, J) = \sum_{i,k} Y_{i,k} \left(v + 1/2\right)^i \left[J(J+1)\right]^k \qquad (25)$$

Recall that the $Y_{i,k}$ have been experimentally determined for the diatomic system,

Section 2.5. The task now is to invert the WKB process and find the effective potential,

$V(R)$, knowing the solutions to equation (25). Numerical techniques have been

developed to solve equation (27) by varying R^+ and R^- to arrive at $V(R)$. This process is

known as the Rydberg-Klein-Rees (RKR) method. This is the preferred methodology

used to determine potential energy curves from spectroscopic constants when more

simple forms, such as the SHO or Morse potential, are inadequate [18]. This method has

become a simple PC-based numerical procedure for which one enters the spectroscopic

constants into a data file, which determines the allowed energy levels within the potential, and then the numerical routine produces the desired potential, $V(\mathbf{R})$.

2.7. Predissociation in Bi_2

Lifetime studies of the $Bi_2(A\text{-}X)$ transition have shown patterns of behavior which may indicate a predissociative property in the A state of Bi_2 [8,9]. There exist some question as to the exact number, nature and location of these predissociative properties. Blondeau, Gandara, Carette, and Messelyn [8] have shown that the lifetime decreases near $v' = 22$ and is "nonexistent" from $v' = 28$ to $v' = 33$. The predissociative nature of $Bi_2(A)$ will be examined in an attempt to determine the exact crossing point and the analytical form of the repulsive potential responsible for predissociation.

As part of a complete predissociation analysis the electronic energy levels within a molecule must be explored. Bismuth, a group V atom, has an outer shell electronic configuration of $6p^3$ giving rise to spin-orbit term symbols $^4S_{3/2}$, $^2D_{3/2}$, $^2D_{5/2}$, $^2P_{1/2}$, and $^2P_{3/2}$. These atoms combine to form electronic energy states of the diatomic molecule given, in order from least to most energetic, by the combinations $^4S_{3/2} + {}^4S_{3/2}$, $^4S_{3/2} + {}^2D_{3/2}$, $^4S_{3/2} + {}^2D_{5/2}$, $^4S_{3/2} + {}^2P_{1/2}$, and $^4S_{3/2} + {}^2P_{3/2}$. The atomic term symbols, molecular combinations, and their respective energy levels are given in Table 2-1.

Combining the experimental results presented by Barrow et al. [1] with the ab initio calculations given by Das et al. [10] and Balasubramanian and Liao [7] the known set of low-lying electronic energy levels within Bi_2 are determined, see Figure 2-2. In

addition to the bound states shown in Figure 2-2 a theoretically proposed repulsive state, 1_u ($^7\Sigma_g^+$) is depicted. This state, as will be further discussed in Chapter 5, is thought to be the state most likely causing the predissociation in $Bi_2(A)$.

Table 2-1. Term symbols and energies for the lowest lying molecular states of Bi_2

Atomic Term Symbol	Atomic Energy (cm^{-1}) [23,24]	Separated Atom State	Atomic Energy + D_e'' (cm^{-1})
$^4S_{3/2}$	0	$^4S_{3/2} + {}^4S_{3/2}$	16,534
$^2D_{3/2}$	11,419	$^4S_{3/2} + {}^2D_{3/2}$	27,953
$^2D_{5/2}$	15,438	$^4S_{3/2} + {}^2D_{5/2}$	31,972
$^2P_{1/2}$	21,661	$^4S_{3/2} + {}^2P_{1/2}$	38,195
$^2P_{3/2}$	33,165	$^4S_{3/2} + {}^2P_{3/2}$	49,699

Obviously, the separated atom configurations give rise to many more electronic energy levels than those shown in Figure 2-2. According to Mulliken there exist more than 50 possible electronic states for these separated atom combinations. There exist ten states for $^4S_{3/2} + {}^4S_{3/2}$ (3u, 2u, 2g, 1u, 1g, 1u, 0g$^+$, 0u$^-$, 0g$^+$, 0u$^-$), fourteen states for $^4S_{3/2} + {}^2D_{3/2}$ (3g, 3u, 2u, 2u, 2g, 2g, 1u, 1u, 1g, 1g, 0g$^+$, 0u$^-$, 0g$^+$, 0u$^-$), ten states for $^4S_{3/2} + {}^2P_{1/2}$ (2u, 2g, 1u, 1u, 1g, 1g, 0g$^+$, 0u$^-$, 0g$^+$, 0u$^-$), and so on. The vast number of electronic states along with the large mass of the molecule make a detailed theoretical or experimental analysis of the electronic energy levels within Bi_2 extremely difficult to perform [1,7,10].
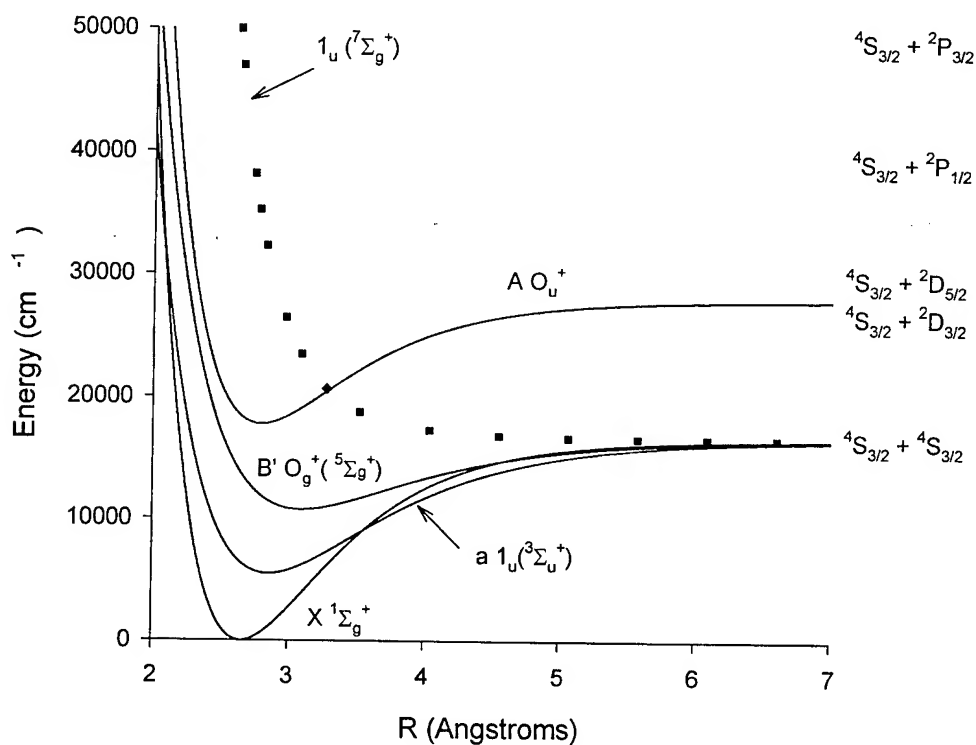
Figure 2-2. Known electronic energy levels of Bi_2 (—) and the predicted $1_u(^7\Sigma_g^+)$ potential (⋯) thought responsible for predissociation in $Bi_2(A)$

2.8. *Experimental Investigation of Heterogeneous Predissociation*

Interactions between a bound state and a purely repulsive dissociative state may occur at potential energy curve crossings. For an excited molecule in a bound electronic state the primary decay mechanisms are considered to be fluorescence and collisional quenching. However, more detailed analysis shows additional non-radiative processes

may influence the lifetime of each state. Figure 2-3 provides an illustrative example of the possible mechanisms responsible for removing molecules from their excited state. Once a state is populated by a pump mechanism, it undergoes changes in population due to several processes including collisional quenching, k_q, fluorescence, $A_{v',v'}$, and predissociation $k_{pd,v}$. Predissociation reduces the number of exited molecules in the bound state by dissociating them into the continuum of separated atoms. A method of
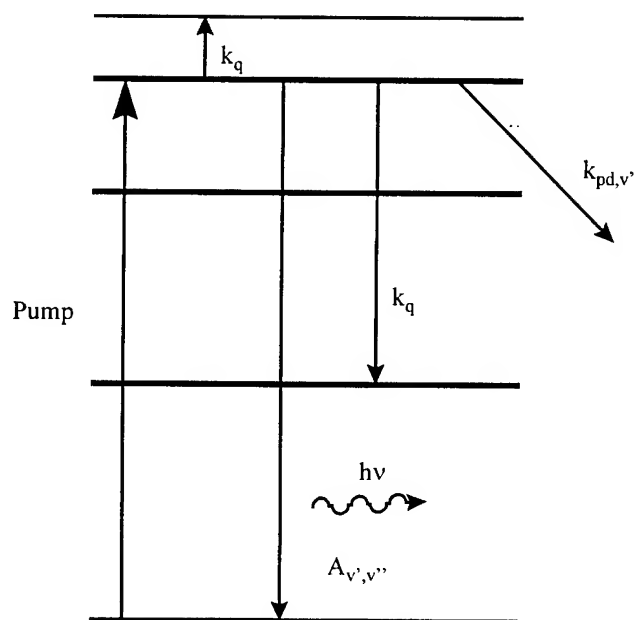
Figure 2-3. Schematic diagram for decay mechanisms influencing state lifetimes

extracting the heterogeneous predissociation rate constant, $k_{pd,v}$, contribution from the total lifetime must be developed for the diatomic system under investigation.

Experimentally, the pulse from a tunable laser is used to instantaneously populate a specific (v', J') level. The spontaneous emission of photons from the populated state

create the fluorescence intensity, I(t), observed as a function of time. This time-dependent signal will decay exponentially at a rate of $1/\tau$, where τ is defined as the lifetime of the state. The intensity of the fluorescence is given by

$$I(t) = I_o e^{-t/\tau} \tag{29}$$

Figure 2-4 shows a notional plot of the intensity, I(t) and the natural log of the intensity, ln I(t), as a function of time. The plot of ln I(t), which is proportional to $-1/\tau$, allows for the determination of the lifetime of the populated state.
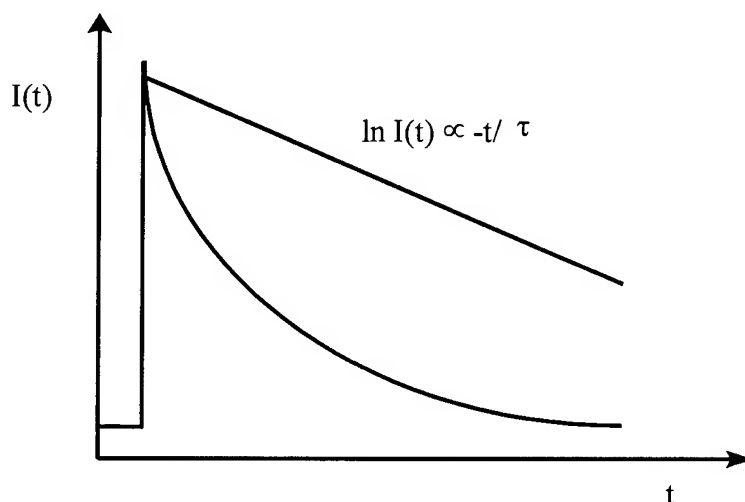
Figure 2-4. Notional plot of fluorescence intensity I and ln(I) as a function of time

The determination of several lifetimes, τ, at differing pressures allows for the discovery of the collision-free lifetime τ_o by noting that $1/\tau$ can be written as [25,26]

$$\frac{1}{\tau} = \frac{1}{\tau_o} + k_q P \tag{30}$$

where k_q denotes the quenching rate and P the pressure of the gas. This pressure-dependent lifetime data, plotted as $1/\tau$ vs. P in a Stern-Volmer plot, Figure 2-5, allows for the calculation of the intercept $1/\tau_o$, and thus the collision-free lifetime, τ_o.
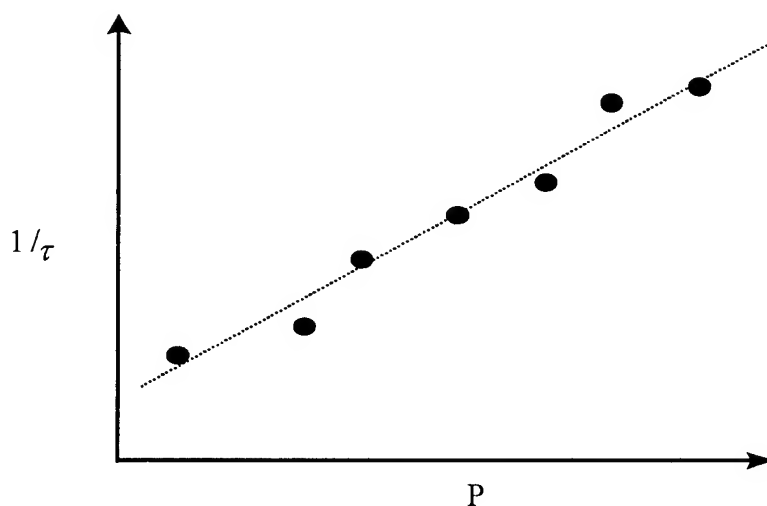
Figure 2-5. Notional Stern-Volmer Plot, inverse radiative lifetime verses pressure P

Now only collisionless processes remain to investigate. It will soon be shown, Section 2.9, equation (38), that the transition probability for heterogeneous predissociation is given by $\Gamma_{pd} = k_{pd,v} J(J+1)$. Then the collision-free lifetime τ_o can be written in terms of radiative and predissociative terms, i.e.,

$$\frac{1}{\tau_o} = \frac{1}{\tau_{rad}} + k_{pd,v}J(J+1) \qquad (31)$$

A plot of $1/\tau_o$ verses $J(J+1)$, Figure 2-6, allows the calculation of the predissociative rate constant $k_{pd,v}$. Since this rate constant is a function of the vibrational energy level with which it is associated, this information may be used to determine both the form of the repulsive potential and the location of the curve crossing. The link between the form of $k_{pd,v}$ and the potential is outlined next.
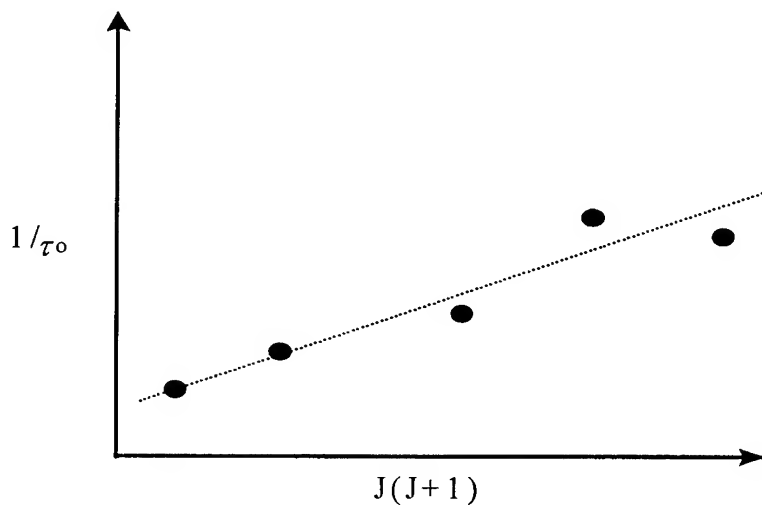
Figure 2-6. Notional plot of inverse collision-free lifetime, $1/\tau_o$, verses $J(J+1)$

2.9. Determining Repulsive Potentials from Lifetime and Predissociation Data

Following the theoretical development presented by Clyne, Heaven and Tellinghuisen [17], the non-radiative probability for predissociation, Γ_{pd}, may be written in terms of the bound state and continuum state wave functions, Ψ_b and Ψ_c, as well as the neglected term in the molecular Hamiltonian, H', reference equation (4). This term couples the bound and repulsive electronic states of the molecule following the selection rules for predissociation, namely $\Delta J = 0, \pm 1$, $\Delta\Omega = 0, \pm 1$, $u \leftrightarrow u$, $g \leftrightarrow g$. The predissociation probability, Γ_{pd}, is proportional to $\left|\langle \Psi_c \mid H' \mid \Psi_b \rangle\right|^2$, where

$$\left|\langle \Psi_c \mid H' \mid \Psi_b \rangle\right|^2 \propto \left|\langle \Omega = 0, \pm 1, J = 0 \pm 1 \mid H'_{rot} \mid \Omega, J \rangle\right|^2 \tag{32}$$

and

$$H'_{rot} = B[\mathbf{J} - \mathbf{L} - \mathbf{S}]^2 = \frac{h}{8\pi^2 c\mu} \frac{1}{\mathbf{R}^2}[\mathbf{J} - \mathbf{L} - \mathbf{S}]^2 \tag{33}$$

The cross terms in H'_{rot} provide for like, $\Delta\Omega = 0$, homogeneous, and unlike, $\Delta\Omega = \pm 1$, heterogeneous, electronic-rotational coupling. The predissociation phenomena in Bi_2 $A(0_u^+)$, investigated in this research, is a heterogeneous perturbation.

The predissociation probability, Γ_{pd}, is written as

$$\Gamma_{pd} = \left(\frac{2\pi}{\hbar}\right)\left|\left\langle \Psi_c \left| \mathbf{H}' \right| \Psi_b \right\rangle\right|^2 \tag{34}$$

where $\mathbf{H}'$ is proportional to $[J'(J'+1) - \Omega_b(\Omega_b \pm 1)]^{\frac{1}{2}}$ for rotational-electronic coupling. Thus, substitution of $\mathbf{H}'$ into equation (34), with appropriate proportionality constants, yields, according to Clyne, Heaven and Tellinghuisen

$$\left|\left\langle \Psi_c \left| \mathbf{H}' \right| \Psi_b \right\rangle\right|^2 = \frac{\hbar^3}{8\pi\mu^2 c}[J'(J'+1) - \Omega_b(\Omega_b \pm 1)]\left|\left\langle \chi_c \left| \mathbf{W}_e(\mathbf{R})\mathbf{R}^{-2} \right| \chi_b \right\rangle\right|^2 \tag{35}$$

where χ_c and χ_b are the vibrational wave functions of the continuum and bound states respectively and $\mathbf{W}_e(\mathbf{R})$ is a dimensionless quantity which remains constant for these electronic transitions. Since $\Omega_b = 0$ for the predissociation found in $Bi_2 A(0_u^+)$, see Section 2.4, $\mathbf{R} \approx$ constant, and $\mathbf{W}_e(\mathbf{R}) \approx$ constant, Γ_{pd} may be expressed as

$$\Gamma_{pd} = \frac{\hbar^2}{4\mu^2 c}[J'(J'+1)]\left|\mathbf{W}_e(\mathbf{R})\right|^2 \left|\left\langle \chi_c \left| \mathbf{R}^{-2} \right| \chi_b \right\rangle\right|^2 = k'[J'(J'+1)]P_{v'} \tag{36}$$

where

$$k' = \frac{\hbar^2}{4\mu^2 c}\left|\mathbf{W}_e(\mathbf{R})\right|^2 \tag{37}$$

and

$$P_{v'} = \left| \left\langle \chi_c \left| \mathbf{R}^{-2} \right| \chi_b \right\rangle \right|^2 \qquad (38)$$

such that

$$k_{pd,v'} = k' P_{v'} \qquad (39)$$

and, therefore,

$$\Gamma_{pd} = k_{pd,v'} J'(J'+1) \qquad (40)$$

The dependence of $k_{pd,v'}$ on v' is sensitive to the form of the repulsive potential $V_{rep}(\mathbf{R})$ via the continuum state wave functions χ_c and its subsequent "overlap" onto the bound state wave function χ_b. The continuum-state wave function is determined from the time-independent Schrodinger equation

$$\frac{\hbar^2}{2\mu^2} \frac{d^2 \chi_c}{d\mathbf{R}^2} + \left[\frac{\hbar^2 J'(J'+1)}{2\mu\mathbf{R}^2} + V_{rep}(\mathbf{R}) \right] \chi_c = E\chi_c \qquad (41)$$

via a computational approach supplied by Heaven [27]. The analytical form of $V_{rep}(\mathbf{R})$, which produces the best fit to $k_{pd,v'}$, will be the repulsive potential deemed the cause of predissociation in $Bi_2(A)$. The intersection of the repulsive $V_{rep}(\mathbf{R})$ potential and the bound-state RKR potential, $V(\mathbf{R})$, determines the crossing point, $\mathbf{R}_{cross}$, associated with vibrational level v'.

2.10.   *Summary*

The theoretical development presented in this chapter represents a treatment for traditional spectroscopic analysis of the energy levels, lifetimes, potential energy curves and predissociation rates for diatomic molecules in general and Bi_2 in particular. The remaining four chapters of this dissertation present the results and difficulties associated with applying this theory to an actual complex diatomic system. In fact, since the spectral content of Bi_2 is so dense and the predissociation of the A-state so strong, it will be shown that these traditional analyses must be supplemented with some novel non-conventional computational methods to arrive at meaningful conclusions.

3. *Spectroscopy of the Bi$_2$ A→X Transition*

3.1. *Introduction*

The spectroscopy of the $X\,^1\Sigma_g^+$ and $A(0_u^+)$ electronic states of the bismuth diatom has been studied in various levels of detail by several authors. Recent spectroscopic data on these states appears in papers by: Barrow et al.[1], Gerber, Sakurai and Broida [2], Ehret and Gerber [3], Gerber, Honninger and Janes [4], Effatin et al. [5], Franklin and Perram [6], as will as Balasubramanian and Liao [7]. A variety of techniques, ranging from traditional absorption and emission spectroscopies to more exotic polarization labeling spectroscopy, have been used by these authors in an attempt to develop a somewhat limited set of spectral constants for the Bi$_2$(X) and Bi$_2$(A) states.

The 1996 paper by Barrow et al. presents the most current and accurate ground state constants for Bi$_2$. Their research involved recording laser induced fluorescence spectra of Bi$_2$ using a Fourier transform spectrometer. For the ground electronic state of Bi$_2$, spectral constants "were obtained from a simultaneous least-squares fit to 7396 lines of the A-X and a-X systems [1]." The standard deviation for this set of spectroscopic data is reported to be 0.002 cm^{-1}.

Most recently, the 1999 paper by Franklin and Perram presents the best known Dunham coefficients for Bi$_2$(A). Using a ring dye laser apparatus, whose linewidth was less than .003 cm^{-1}, they were able to achieve doppler-limited laser excitation spectra of

low lying, $0 \le v' \le 4$, vibrational levels within Bi_2(A). Extensive analysis of the

rotational structure within each vibrational manifold, accessing rotational levels $J < 211$,

lead Franklin and Perram to conclude that previously reported rotational coefficients have

been off by as much as 0.08 cm^{-1}. A summary of the spectroscopic coefficients reported

by Barrow et al. for the ground state and Franklin and Perram for the excited A-state of

Bi_2 is presented in Table 3-1. These coefficients represent the best available

spectroscopic data for these two states to date.

Table 3-1. Reported spectroscopic constants for the $A(0_u^+)$ and $X(^1\Sigma_g^+)$ states of Bi_2

Electronic State: Source: Range of Study: Units:	$Bi_2\, A(0_u^+)$ Perram and Franklin [6] v' = 0 – 4 (cm^{-1})	$Bi_2 X(^1\Sigma_g^+)$ Barrow et al. [1] v"=0-11 (cm^{-1})
Y_{00}	17740.696(29)	
Y_{10}	132.383(11)	173.0309(3)
Y_{20}	-0.31092(97)	-0.37521(7)
Y_{30}	-2.75(23)×10^{-4}	-5.595(69)×10^{-4}
Y_{40}		-1.445(320)×10^{-6}
Y_{50}		-6.14(70) ×10^{-8}
Y_{60}		5.81(56) ×10^{-10}
Y_{01}	0.0196663(17)	0.02280577(93)
Y_{11}	-4.991(33) ×10^{-5}	-5.23632(94) ×10^{-5}
Y_{21}	-1.32(12) ×10^{-7}	-1.0370(82) ×10^{-7}
Y_{31}		-9.90(31) ×10^{-10}
Y_{41}		-6.15(40) ×10^{-12}
Y_{02}	-1.74935(26) ×10^{-9}	-1.580(16) ×10^{-9}
Y_{12}	-7.700(66) ×10^{-12}	-7.050(66) ×10^{-12}
Y_{22}		1.415(21) ×10^{-13}
Y_{03}		-1.31(67) ×10^{-16}

Unfortunately, the A-state constants presented in Table 3-1 are derived from a spectroscopic study that has limited range in v'. Therefore, further analysis is necessary to determine a final set of acceptable values for these Dunham expansion coefficients. Improvements would result from accessing nearly the entire range of available vibrational levels within $Bi_2(A)$ by either high-resolution laser induced fluorescence or Fourier transform experiments. Fourier transform absorption spectroscopy has been used in this research. This chapter details this experimental approach and presents the results of this spectroscopic study. The range of A-state vibrational manifolds assigned has increased to $v' \leq 91$ with rotational assignments within each manifold in the $20 \leq J \leq 207$ range. The extension of spectroscopic range has allowed for some of the A-state constants to be redefined.

3.2. *Experimental Apparatus*

An Oriel 6333 quartz-tungsten-halogen (QTH) lamp was used as a broadband white-light source for the spectral absorption experiment. The QTH lamp, contained in an Oriel Q-Series lamp housing, was powered by an Oriel 68806 constant current power supply. An Oriel 60076 UV grade fused silica f/1 condensing lens assembly, mounted to the lamp housing, was aligned along the longitudinal axis of a two-inch diameter, five-
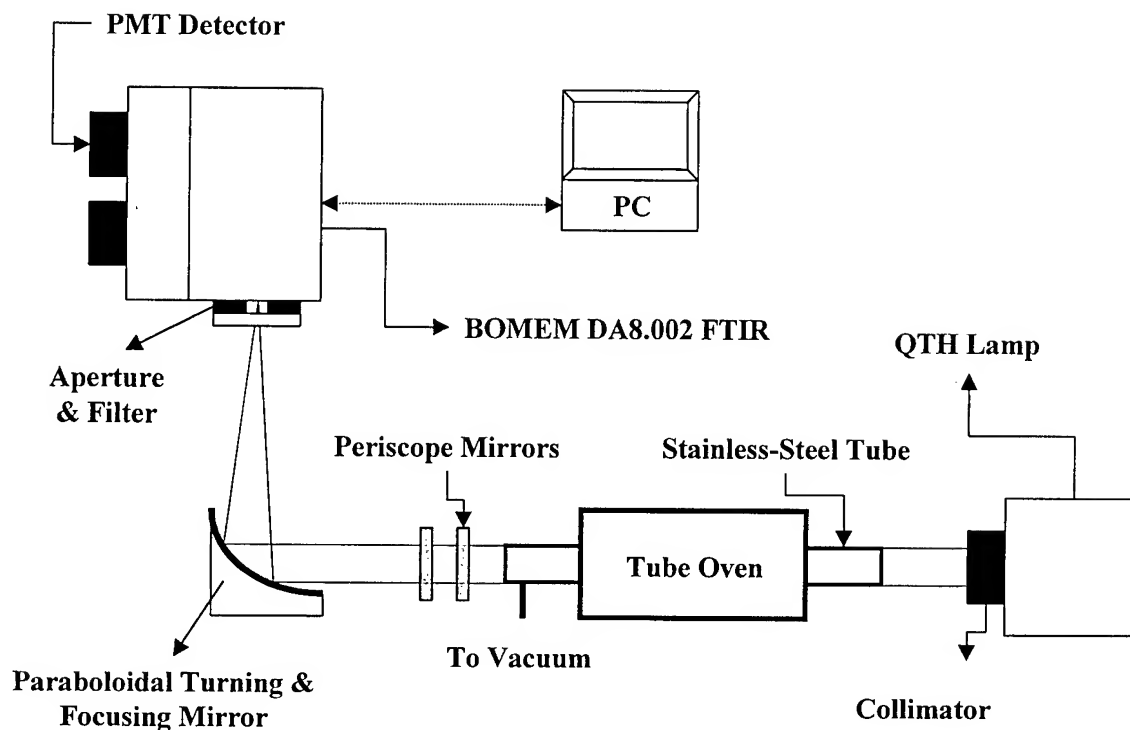
Figure 3-1. Experimental apparatus used in the $Bi_2(X \rightarrow A)$ absorption experiment

foot long stainless-steel tube, allowing for the complete illumination of the interior of the tube, see Figure 3-1.

Each end of the stainless-steel tube was equipped with a two-inch diameter removable quartz window. The tube was centered in a three-foot long Lindberg tube oven. Approximately five grams of metallic bismuth shot was place near the center of the tube and the oven set to 835 °C, which produced a vapor of nearly equal parts Bi and Bi_2; trace amounts of Bi_3 and Bi_4 were also present [8]. At this temperature, the bismuth vapor lasted nearly three hours before plating out on the cool walls near the end of the tube.

The pressure within the tube was monitored by a MKS 1 torr heated baratron and controlled with a mechanical vacuum pump and valve arrangement. The vacuum pump was attached to the purge port, located near one end of the tube. With this arrangement, pressures were maintained near 800 mtorr ±20 mtorr for the duration of the absorption runs.

The collimated output from the QTH lamp, after it passed through the stainless-steel tube, was redirected by a periscope apparatus, consisting of two Melles Griot two-inch square ultra violet (UV) enhanced aluminum coated mirrors, toward a paraboloidal turning mirror. The Melles Griot UV enhanced 63.5 mm diameter 59.7 mm focal length off-axis paraboloidal mirror focused the light onto the external entrance aperture of a Bomem DA8.002 Fourier Transform Interferometer.

The interferometer, equipped with a two-meter scanning mirror tube assembly, has a maximum resolution capability of 0.002 cm^{-1} [33]. The instrument's counting of stable single-mode HeNe laser fringes ensures the absolute wavenumber accuracy for the interferometer to be ± 0.002 cm^{-1}. The DA8 was equipped with a visible quartz beam splitter and a PMT for the detector, which together had an effective spectral range from 11,000 to 28,000 cm^{-1}, see Figure 3-2. In this configuration the interferometer was used to produce an interferogram of the absorption spectra of the $Bi_2(X{\rightarrow}A)$ transition. Using a set of band pass filters, Figure 3-2, five interferograms were taken at instrument resolutions of 0.10 cm^{-1} covering the spectral region from 13,000 cm^{-1} to 27,500 cm^{-1}. These interferograms were transformed to spectrographs via the DA8's internal Fourier Transform Vector Processor. The spectrum was then exported to an Intel®-based 486-

computer for display, storage and analysis. The peak locations for the spectra were
determined using Bomem-Grams peak analysis software suite [33].
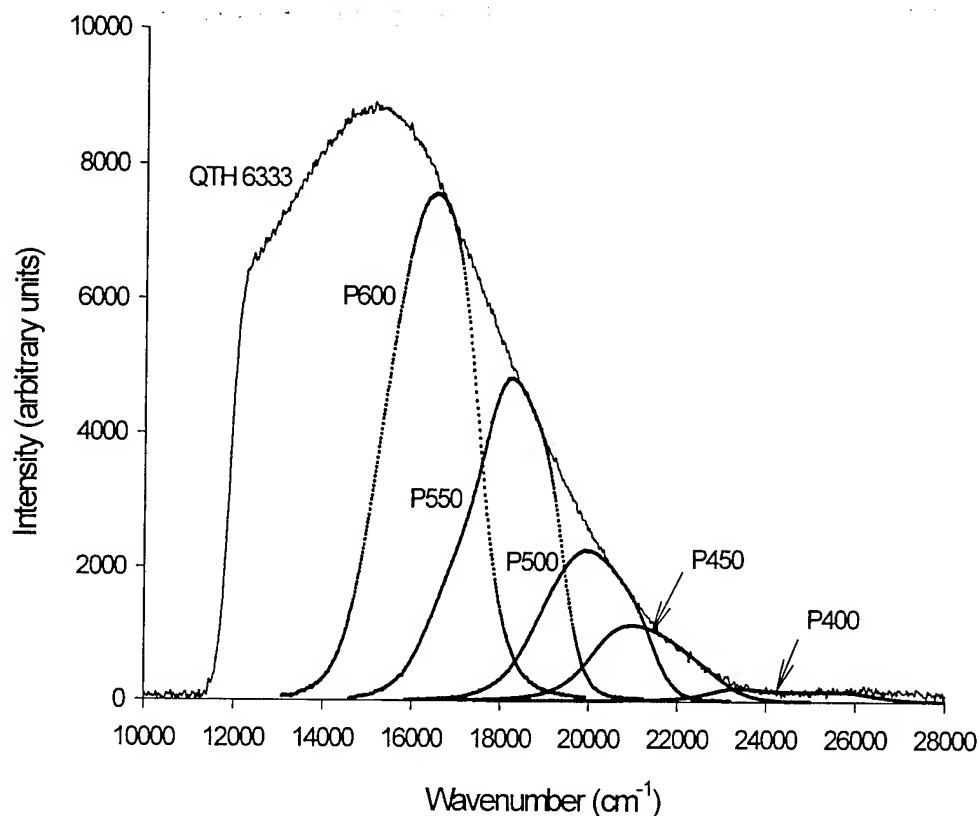
Figure 3-2. Lamp (—) and filter (···) spectral profiles for the absorption experiment

3.3.   Spectroscopic Analysis of $Bi_2(A0_u^+)$

The maximum resolution obtained in for this experimental configuration was
$0.12cm^{-1}$. This limitation is a combination of several different factors. First, at visible

wavelengths and shorter, the vector processor internal to the DA8 has memory limitations. Secondly, the number of scans necessary to produce an acceptable signal to noise ratio had to be found within the constraint that the Bi_2 vapor, within the stainless steel tube, would last only two and a half to three hours. Lastly, to eliminate ringing in the spectrum, a Bartlett apodization function was chosen. This apodizing function is triangular and produces positive, highly damped sidelobes, a $sinc^2x$ function. Optimizing the spectrum to account for all of these constraints led to the 0.12 cm^{-1} resolution limitation. Even at this resolution, however, the GRAMS software was able to produce over 125,000 peak positions. The bandwidth was large enough to capture the entire spectral range for transitions between vibrational bands $0 \le v' \le 91$ and $0 \le v'' \le 7$.

The assignment process, for over 100,000 spectral features, was, as would be expected, involved and time consuming. The steps in this process can be broken down into: (1) the acquisition of the spectra, (2) locating peak positions in the spectra, (3) assigning individual features to transitions, (4) fitting sets of assigned spectral features to theoretical models, (5) determining the best global fit for all spectral constants and, (6) determining the Dunham expansion coefficients from the global fit data. The first step in the process has been explained and limitations outlined. The peak location feature in Bomem GRAMS is a simple step that populates an enormous database with spectral peak location information. It is this data which is used to ultimately determine the spectral constants of $Bi_2(A)$.

The assignment of spectral features of any diatomic molecule is a lengthy task under any circumstance. In the case of Bi_2 this task becomes more difficult due to the

large moment of inertia of the Bi_2 molecule. The moment of inertia is inversely proportional to the size of the rotational constant making the rotational constant for Bi_2 extremely small, on the order of $0.02cm^{-1}$. Thus, rotational lines are numerous and closely spaced. Additionally, a large number of spectral features from nearby vibrational bands overlap. Finally, the relatively low resolution of our spectra adds to assignment difficulties. Addressing these complexities required the development of a systematic method to assign state-to-state transitions.

First, using the spectroscopic constants presented by Barrow et al. and Franklin and Perram, Table 3-1, predicted line positions were calculated using equation (24),

$$\nu = \nu_o + (B_{v'} + B_{v^-})m + (B_{v'} - B_{v^-} - D_{v'} + D_{v^-})m^2 - 2(D_{v'} + D_{v^-})m^3 - (D_{v'} - D_{v^-})m^4 \quad (24)$$

These calculated line positions were then compared to the peaks located in the absorption spectra and patterns were observed. Once a definitive rotational progression was found, within a given vibrational manifold, the set of rotational features was fit to equation (24) using Table Curve™ 2D Version 4.0 software [28], see Figure 3-3 and Appendix A. Barrow's values for ground state constants were held fixed during the fits allowing adjustments to only upper-state term values. During this procedure it was determined that terms higher than D_v are not appropriate to include as fit parameters.

Figure 3-4 shows the difference between what was considered a good fit, the (31,2) band, and poor fit, the (95,0) band. Notice both the increases in residual size, larger than spectral resolution, and the "weighted behavior" for the poor fit.

Approximately 60 out of 285, or about 20%, of the attempted rotational line fits were

discarded due to rotational line fit residual similar to the (95,0) case.
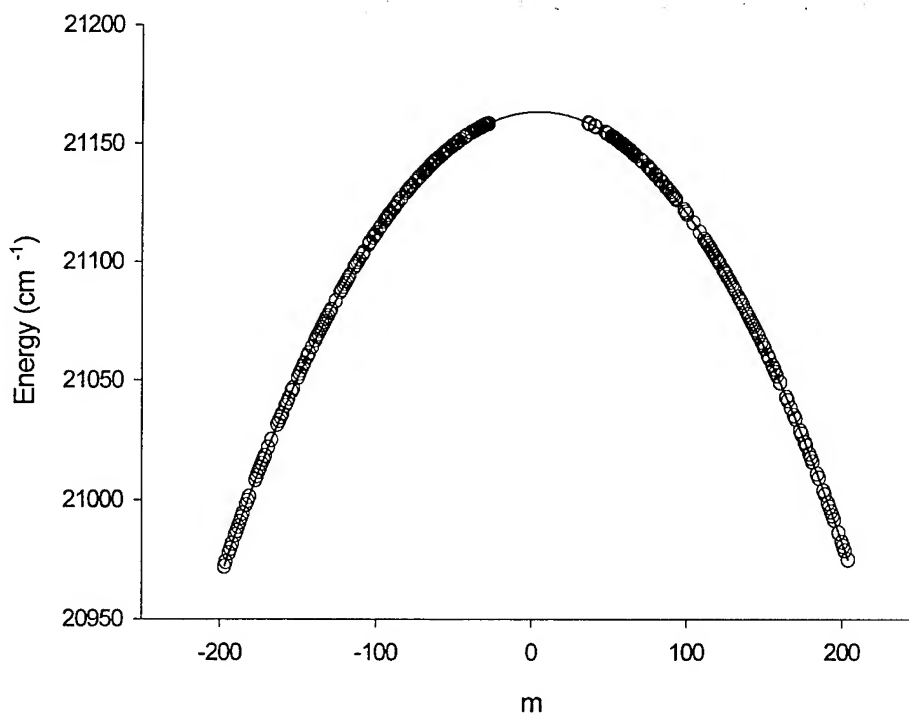
Figure 3-3. Experimental rotational line positions as a function of m (○) and the
corresponding fit (−) to Equation (24) for vibrational band (31,2)

These steps were repeated numerous times for each vibrational manifold of

interest. It became apparent that this process would be applicable to automation using the

same methodology employed for the manual peak selections. Software was designed and

developed [29] to emulate the peak location and identification process. All non-standard
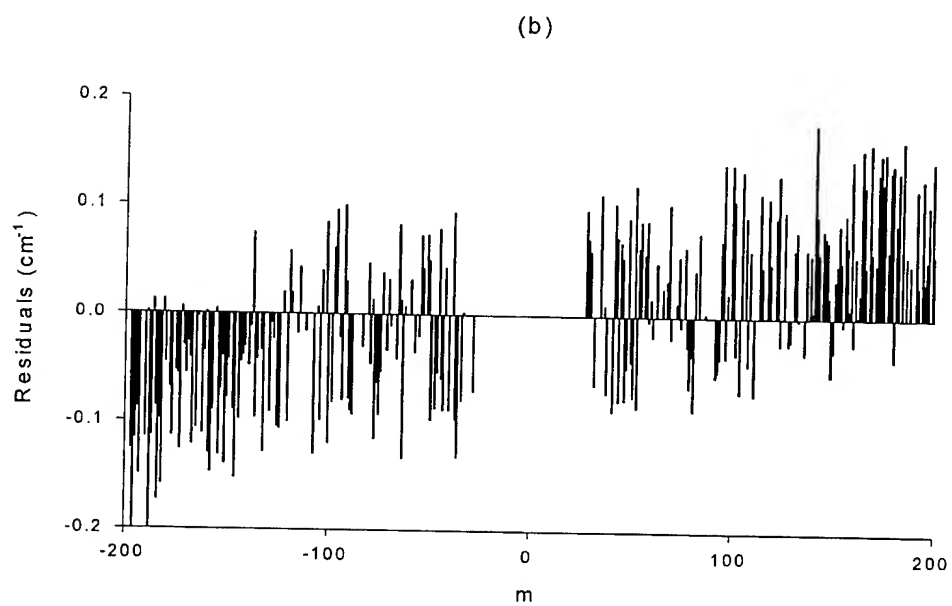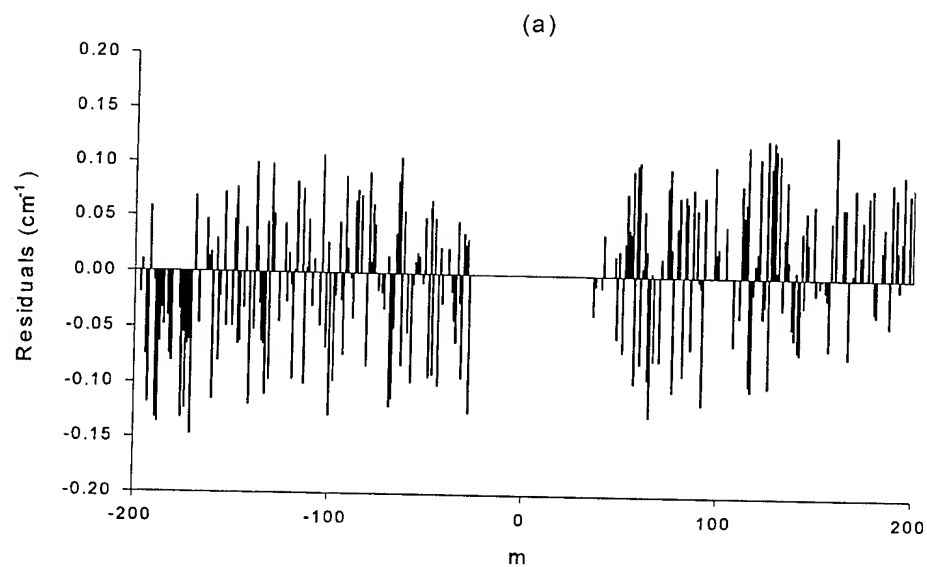
Figure 3-4. Residual plots for vibrational bands (31,2), (a), and (95,0), (b)

results were re-evaluated for correctness of fit. The DataFit software tool has proven to be much more robust than a simple manual peak identification could ever be for such a large amount of data. For example, constants could be systematically varied numerous times and results analyzed for a best fit, thus extending the usefulness of the assignment process.

After nearly 100,000 spectral features were assigned and their state-to-state term values fit, see Table B-1, Appendix B, the entire set of data was processed in a global fit routine. Software written by Franklin [30] served as a model for the more generalized GlobalFit software designed by Dolezal and Herbert [31]. This Visual Basic software tool essentially allows the user to input, either by file or by hand, spectroscopic constants and compares them with an experimental data set of peak locations. The calculated peak positions are compared to the experimental data and a least-squares-fit routine is employed to minimize the error of each fit by adjusting spectroscopic term values. The routine continues to adjust constants until the best global data fit has been determined. The output returns the best fit for each state desired. These constants, Figure 3-5 and Appendix C are then used to determine the Dunham expansion coefficients.

In addition to defining a set of spectroscopic constants, the spectral data is used to determine the dissociation energy of the A-state of Bi_2. A Birge-Sponer plot of $\Delta G_{v'+1/2}$ vs. $v'+\frac{1}{2}$ is shown in Figure 3-6 for the spectroscopic data analyzed in this chapter. An extrapolation of this data predicts the dissociation level of $Bi_2(A)$ to occur at $v' = 171 \pm 1$. The dissociation energy is $D_e = 12,165$ cm^{-1} with error bounds of $D_e^{MAX} = 12,234$ cm^{-1} and
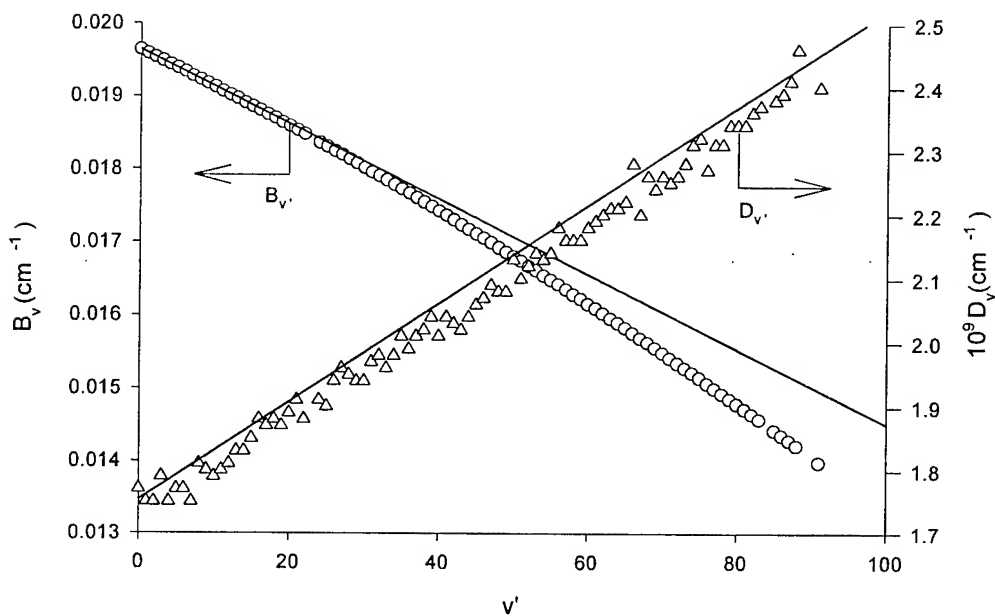
Figure 3-5. Global fit results for term values $B_{v'}$ (○) and $D_{v'}$ (△) for the $Bi_2(A)$ state shown with extrapolated term values $B_{v'}$ and $D_{v'}$ (—) from Franklin and Perram [6]

$D_e^{MIN} = 11,978$ cm^{-1} implying that the A-state dissociates at an energy of 29,905 cm^{-1}. Therefore, the dissociation products are the $^4S + {}^2D$ atoms, see Table 2-1 and Figure 2-2.

Section 2.1 predicts the change in energy associated with a predissociation perturbation to be on the order of $(m_e/M_A)E_{elec} \approx 0.05$cm^{-1} for this system. Unfortunately, due to limited resolution, no changes in state-to-state values were attributed to predissociative effects.
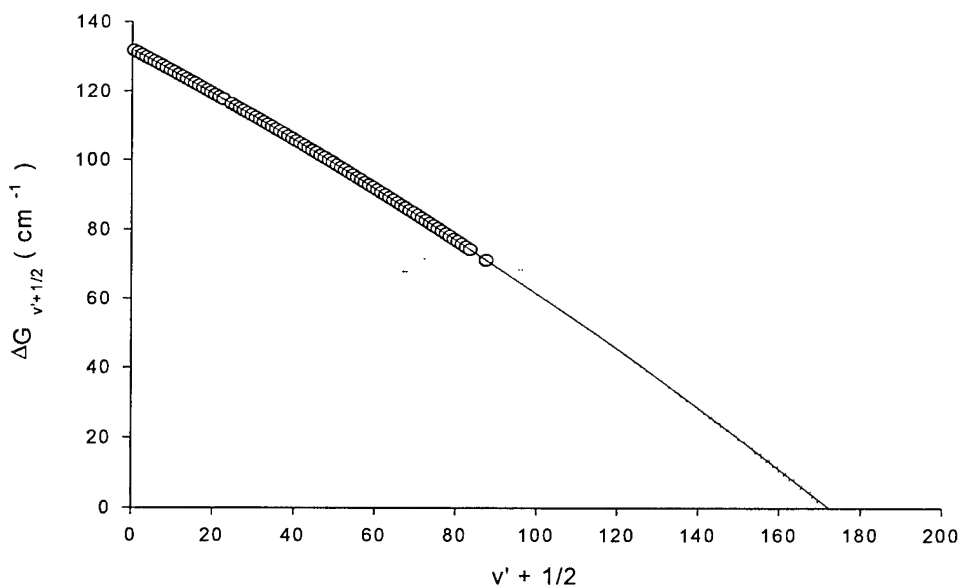
Figure 3-6. Birge-Sponer plot of experimental vibrational energy differences in $Bi_2(A)$

3.4. Summary

The global fitting procedure, outlined in Section 3.3, produced 226 sets, i.e., $B_{v'}$

and $D_{v'}$, of state-to-state term values for transitions between $0 < v' < 91$ and $0 < v'' < 7$.

The GlobalFit software reduced this data down to 88 sets of globally fit parameters,

shown in Figure 3-5 above. Also shown in Figure 3-5 are linear extrapolations of the $B_{v'}$

and $D_{v'}$ values presented by Franklin and Perram, which reported term values for the

range $0 \leq v' \leq 4$. There exist agreement in $B_{v'}$ below $v' = 20$ and the $D_{v'}$ values

presented here are consistently smaller than the extrapolation predicts.

The accurate representation of a bound potential begins with the quality and extent of the experimental spectral data used to determine that potential. In fact, "For bound states which are less well characterized experimentally, the RKR method may not be appropriate [32]." Thus, for electronic states, such as $Bi_2(A)$, the extrapolation of a few low-lying term values to higher ro-vibrational levels is inadequate especially in the determination of an accurate RKR potential. Figure 3-5 clearly indicates problems associated with extrapolations to higher levels. Therefore, this work provides for a significant improvement to the accuracy of the bound $Bi_2(A)$-state potential since the extent of the available spectral data has been vastly increased. In fact, this data now extends over the majority of the accessible levels within the $Bi_2(A)$ electronic state.

The Dunham expansion coefficients for this data were calculated using a least squares fit routine in Table Cuve™, and are provided in Table 3-2 where they are shown alongside values reported by Franklin and Perram. The ground state data from Barrow et al. and the A-state data from the current work will be used, in Section 5.2, to determine RKR potentials for the bound states of $Bi_2(X)$ and $Bi_2(A)$.

The most significant contribution of this spectroscopic analysis is the determination of the total dissociation energy of $Bi_2(A)$. The dissociation limit of 29,905 cm^{-1} confirms that the dissociation products of this state are $^4S + {}^2D$ atoms. This directly contradicts the theoretical papers presented by Balasubramanian and Liao [7] and of Das et al. [10]. These papers imply that the dissociation products are $^4S + {}^2P$, which is clearly incorrect.

Table 3-2. Dunham coefficients for $Bi_2(A)$ from current work and Franklin and Perram

Electronic State: Source: Range of Study: Units:	$Bi_2\,A(0_u^+)$ Current Work $v' = 0\text{-}91$ (cm^{-1})	$Bi_2\,A(0_u^+)$ Perram and Franklin [6] $v' = 1-4$ (cm^{-1})
Y_{00}	17740.6927(24)	17740.696(29)
Y_{10}	132.38356(25)	132.383(11)
Y_{20}	-0.3109311(69)	-0.31092(97)
Y_{30}	$-2.7494(5)\times10^{-4}$	$-2.75(23)\times10^{-4}$
Y_{01}	0.0196412(2)	0.0196663(17)
Y_{11}	$-5.0078(13)\times10^{-5}$	$-4.991(33)\times10^{-5}$
Y_{21}	$-1.3167(15)\times10^{-7}$	$-1.32(12)\times10^{-7}$
Y_{02}	$-1.7409(52)\times10^{-9}$	$-1.74935(26)\times10^{-9}$
Y_{12}	$-6.81(27)\times10^{-12}$	$-7.700(66)\times10^{-12}$

4. Lifetimes of Bi₂(A) Ro-Vibrational States

4.1. Introduction

Lifetime studies of the $Bi_2(A(0_u^+) \rightarrow X^1\Sigma_g^+)$ transition indicate the existence of at

least one repulsive potential passing through the $A(0_u^+)$ state causing reductions in

radiative lifetimes due to predissociation [8,9]. Due to the limited amount of information

contained in these studies, there still exist uncertainty as to the number, nature, form and

location of these repulsive features. A complete lifetime analysis the $Bi_2(A \rightarrow X)$ system,

accessible via the pulsed dye laser experiment described below in Section 4.2, provides a

complete set of lifetimes and predissociative rate constants for vibrational levels $v' = 8$ to

$v' = 39$.

The lifetime study presented by Blondeau et al. [8] used laser induced fluorescence

techniques to produce lifetime data for vibrational levels $5 \leq v' \leq 40$. They noted a

strong decrease in lifetimes over the range $22 \leq v' \leq 27$ and failed to observe

fluorescence signals from $v' = 28$ to $v' = 33$. Reported lifetimes from levels

$34 \leq v' \leq 40$ again showed the trend of decreasing lifetime accompanied by decreases in

fluorescence signal intensity, Figure 4-1. These findings lead to the conclusion that levels

above $v' = 22$ are strongly perturbed by some predissociative phenomena while levels

below $v' = 22$ remain unaffected. $Bi_2(A)$ state lifetimes for $v' < 22$ showed $\tau \cong 0.260 \mu s$.

The lack of sufficient information in Blondeau's experimental data did not allow for the

extraction of further information on the state(s) responsible for these predissociation-like

phenomena.
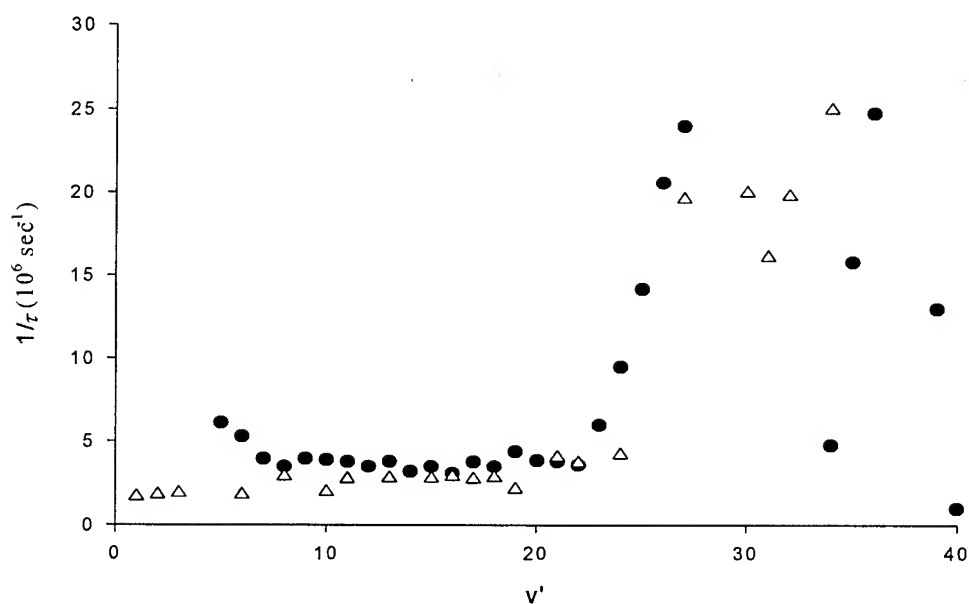
Figure 4-1. State lifetimes as a function of vibrational level, v', reported by
($\bullet$) Blondeau et al. [8] and (Δ) Ehret and Gerber [9]

Subsequent lifetime analysis by Ehret and Gerber [9], also presented in Figure 4-1,

was again performed using laser induced fluorescence spectroscopy. Their investigation

reported lifetimes covering approximately the same vibrational bands as that of Blondeau

et al., $1 \le v' \le 34$. The results confirm the decrease of lifetime near $v' = 22$ but did not

show correlation with the previously published trend near $v' = 34$. The average effective

lifetime, $\tau_{eff} \cong 0.420\mu s$, reported by Ehret and Gerber for levels $1 \le v' \le 19$ is within a

factor of two of that reported by Blondeau et al. Ehret and Gerber performed a limited

investigation on dependence of lifetime with rotational quantum number J' and vibrational quantum number v'. Although their data is far from complete, they reported finding "a slight increase of the decay rate with increasing J' values."

The lifetime analysis presented in the two aforementioned studies, as a function of ro-vibrational level (v', J'), is essentially non-existent. For example, the tabulated data reported by Blondeau et al. reports $Bi_2(A)$ state lifetimes for $5 \leq v' \leq 40$ at J=0. However, considering the dense Bi_2 spectra, it is not possible to populate and observe J=0 independent from other low-J spectral features, which becomes problematic when the lifetimes are a function of J(J+1), see equation (31). Furthermore, the data presented by Ehret and Gerber contained too few J levels to arrive at any conclusive results. These shortfalls will be overcome in the experimental and theoretical findings presented in this chapter. Finally, a theoretical paper by Das et al. [10] contradicts the findings of the experimental lifetimes reported by Blondeau et al. Namely, "the radiative lifetime of the $A0_u^+$ state is calculated to be 72μs, whose result indicates that a previous study…needs to be reevaluated."

In addition to the determination of a definitive value for the $A(0_u^+)$ state lifetime, τ_{rad}, the lifetime analysis presented here will further address the relationship between the ro-vibrational level (v', J') and the observed rate of predissociation, $k_{pd,v'}$, Section 4.3.2. This analysis combines experimental results with the theory outlined in Section 2.8. In brief, it will be shown that the radiative lifetime of the $A(0_u^+)$ state is $\tau_{rad} \approx 0.57$μs, Table

4-1, and the observed predissociation rates, $\Gamma_{pd} = k_{pd,v'}J(J+1)$, establish the range of $k_{pd,v'}$

to be $k_{pd,v'} = 153\,\text{sec}^{-1}$ to $1.5\text{x}10^5\,\text{sec}^{-1}$ for v'=21 to v'=39.

4.2. Experimental Apparatus

A Spectra Physics Quanta Ray® DCR-3G pulsed Nd:YAG laser operating at 20Hz serves as the pump source for a Spectra Physics Quanta Ray® PDL-3G continuously tunable pulsed dye laser, Figure 4-2. The dye laser has a tunable range of 10,400 cm^{-1} to 26,315 cm^{-1} using various laser dyes and pumping configurations. A series of transversely pumped Exciton dyes (Coumarin 460, Coumarin 480 and Coumarin 500) were used to excite A-state ro-vibrational levels with energies ranging from 18,725 cm^{-1} to 21,950 cm^{-1}. This configuration allowed us to populate and produce fluorescence from vibrational manifolds $v' = 8$ to $v' = 42$.

The dye laser produces an elliptically shaped beam approximately 1mm in width and 3 mm in height. The intensity of the beam is monitored by a Coherent power meter. Typical energies obtained are on the order of 10 mJ per pulse. This probe beam was directed through a periscope apparatus into a stainless steel six-way cross, shown in Figure 4-3.

The lower arm of the cross is equipped with a pair of feed-through copper leads which supply current to a tungsten basket located a few centimeters below the center of the chamber. Within the basket sits a 0.5 in diameter aluminum oxide crucible containing
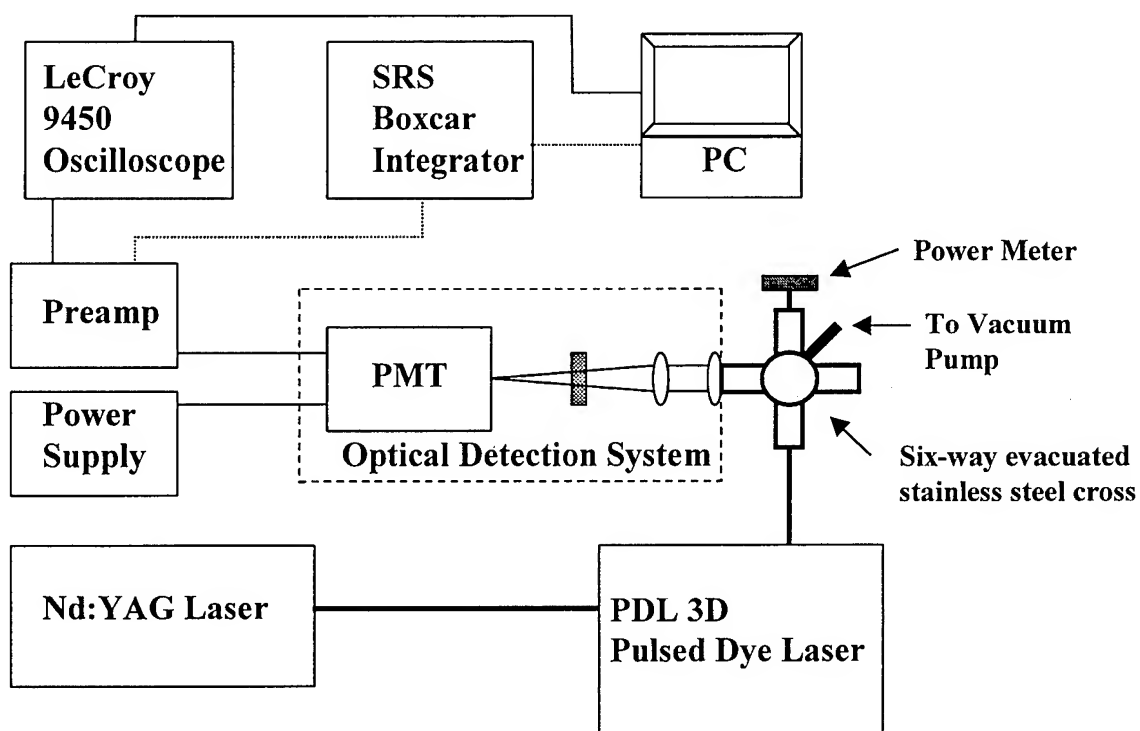
Figure 4-2. Block diagram of experimental apparatus used to collect both the pulsed lifetime data (—) and laser excitation spectra (⋯)

granular metal bismuth. A Hewlett Packard 6453A power supply provides the necessary current, approximately 30 to 40 amps at 3 volts, to the tungsten basket, which, at these powers, heats the metallic bismuth to temperatures around 900 $^{\circ}$C producing a vapor of nearly equal parts Bi and Bi_2. Fluorescence signal strength and available run time are optimized when the total power supplied to the tungsten basket is approximately 95 watts.
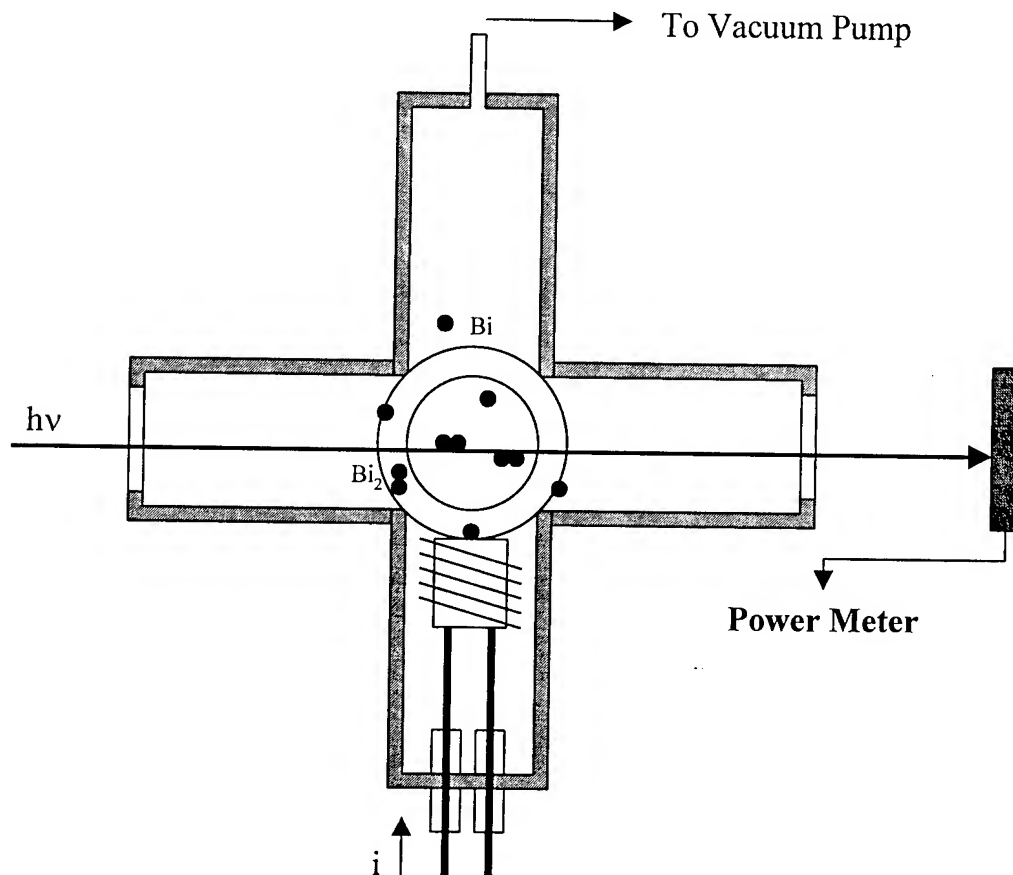
Figure 4-3. Cross sectional view of the stainless-steel six-way cross

As discussed in Section 2.8, once excited by the dye laser, $Bi_2(A)$ may predissociate to the continuum of free atoms or transition back to the ground state via fluorescence or collisional deactivation. The fluorescence signal $(A \rightarrow X)$ is focused through a series of lenses and filters onto a vertically oriented adjustable rectangular aperture positioned at the entrance of a RCA C31034 A03 photo multiplier tube (PMT).

The PMT is powered by a Stanford Research Systems Model PS325 High Voltage Power Supply operating at 1200 V. The output from the PMT is amplified by a EG&G Instruments Model 5185 Wideband Preamplifier and may be used as an input to either a

LeCroy 9450A Dual 300MHz Oscilloscope or to a Stanford Research Systems SR250 Gated Integrator, see Figure 4-2.

The laser excitation spectra were obtained by routing the PMT signal through the preamplifier and into the gated integrator while scanning the dye laser, at a rate of 0.00556 nm/sec, over the desired spectral range. Optimum resolution was obtained by offsetting the gate beyond the duration of the laser pulse and setting the gate width between 30 ns and 300 ns depending on fluorescence signal lifetime. Typically, 30 to 100 shots were averaged together to produce the cleanest signal possible. The output of the integrator is a voltage proportional to the area under the fluorescence decay curve as limited by the gate width. This area is proportional to the strength of the fluorescence signal and, therefore, may be used to produce an excitation spectrum for each of the laser dyes used. The averaged output is sent through an analog-to-digital (A/D) converter and stored in an ASCII file on a PC. The pressure within the six-way cross, monitored by a MKS 1torr heated baratron and controlled with a mechanical vacuum pump and valve arrangement, was held near 25 mtorr for the duration of the fluorescence runs.

Alternately, for the lifetime analysis, the output of the preamplifier was routed to the oscilloscope, which was used to capture and average fluorescence decay curves and send data to a PC for further analysis. The fluorescence intensity decay curves were averaged for 1000 shots and recorded at various pressures for each spectral feature of interest. The buffer gas used to vary the pressure was simply the outgas products produced by heating the crucible and the stainless steel vessel's walls. This buffer gas consisted of non-constant concentrations of Bi, Bi_2, aluminum oxide crucible outgas

products, and the outgas products from the walls of the stainless steel cross. The effects

of pressure, on lifetimes ranging from 10 mtorr to 150 mtorr, were investigated.

4.3. *Laser Excitation Spectra*

4.3.1 *Overview*

Three laser excitation spectra, covering the spectral region from 18,725 cm^{-1} to

21,950 cm^{-1} were taken and analyzed, one for each laser dye used. Each vibrational band,

from these laser excitation spectra, was identified and band location confirmed by use of

a Deslandres table, see Figure 4-4 and Table D-2, Appendix D. The data from Table D-2

is graphically compared to data generated from the results of Chapter 3 in Figure 4-4

below. A least squares fit of the experimental second difference to ΔG, equation (21),

yields $\omega_e = 132.64$ cm^{-1} and $\omega_e \chi_e = 0.34$ cm^{-1}. Therefore, the vibrational constants

obtained are in generally good agreement with the results cited in Chapter 3.

Furthermore, the spectra visually confirm the presence of a very strong predissociative

phenomena for all levels accessed above $v' = 22$, see Figure 4-5 through Figure 4-7. In

fact, the effects of predissociation are prevalent up to the highest vibrational level probed,

$v' = 42$.

The first laser excitation spectrum acquired, shown in Figure 4-5, was taken using

Coumarin 500 dye in the PDL-3D dye laser. This spectrum, ranging from 18,725 cm^{-1} to

20,233 cm^{-1}, shows no signs of predissociation and is, therefore, representative of a

typical bound-bound spectrum. Vibrational band labels for v′ appear across the top of

the laser excitation plots and the corresponding v″ levels are shown to their right.

The most striking spectra is shown in Figure 4-6. This spectrum was obtained

using Coumarin 480 dye over the range 20,195 cm^{-1} to 21,265 cm^{-1}. Here we can clearly

see the onset of predissociation by noticing the degradation of the rotational features in

the spectrum for levels v′ = 22 and above. In fact, the predissociation is so strong that,
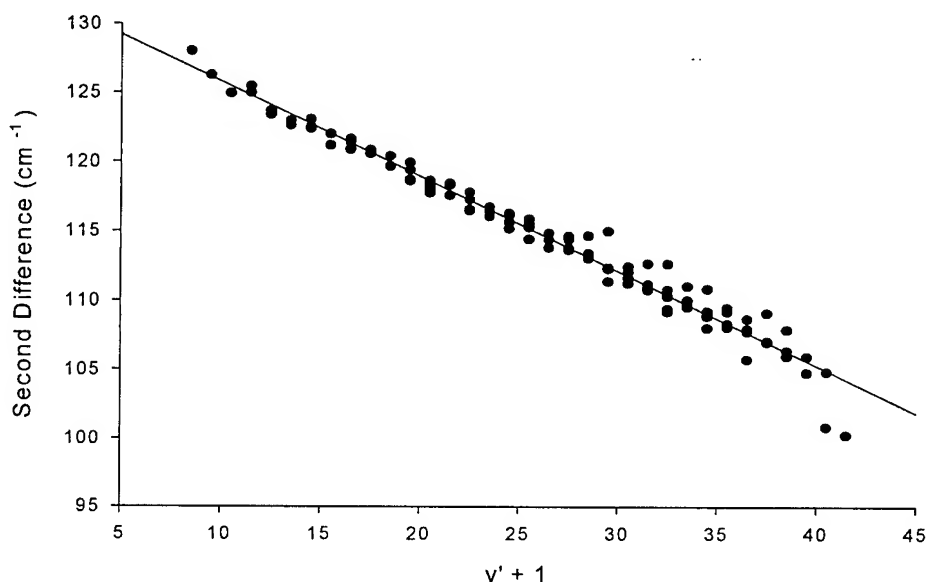
Figure 4-4. Vibrational second differences, ΔG plot as a function of v′ + 1. Deslandres
table results (●) are compared to Chapter 3 predictions (—)

for levels v′ = 23 and above, no rotational features can be identified. The decrease in

lifetime, as a function of ro-vibrational level (v′,J′), can best be investigated by a

traditional analysis, see Section 2.8, of the lifetimes in vibrational manifolds

$(v',v'') = (21,0)$ and $(22,0)$. For these manifolds only, rotational levels could be assigned, see Table D-3 Appendix D, and predissociation rates determined directly. This analysis, Section 4.3.2, will show that the onset of predissociation is indeed evident in $v' = 21$ and $v' = 22$. The vast increase in the predissociative rate, which occurs for levels $v' = 23$ and above, can only be treated by employing the novel numerical techniques introduced in Section 4.3.3.

The last of the laser excitation spectra is shown in Figure 4-7. Coumarin 460 dye was used to access spectral features over the range $21,042\text{cm}^{-1}$ to $21,966\text{cm}^{-1}$. The effects of predissociation remain strong and do not dissipate with increasing v'. This trend is in general agreement with the work of Ehret and Gerber, see Figure 4-1.

4.3.2   Traditional Analysis: $v' = 21$ and $v' = 22$.

Peak locations within vibrational manifolds $(21,0)$ and $(22,0)$ were determined using BMGRAMS/386 peak analysis software [33]. The rotational features within these manifolds were assigned as either R(J) or P(J) features, see Table D-1, Appendix D. The experimentally determined rotational second differences, $\Delta F(J) = R(J) - P(J)$, were fit to equation (22) and values of $B_{v'=21} = 0.019\text{cm}^{-1}$ and, $B_{v'=22} = 0.018\text{cm}^{-1}$ were found, see Figure 4-8. With knowledge of the J level pumped, exploration into the size and nature of the predissociative rate constant $k_{pd,v'}$ begins.
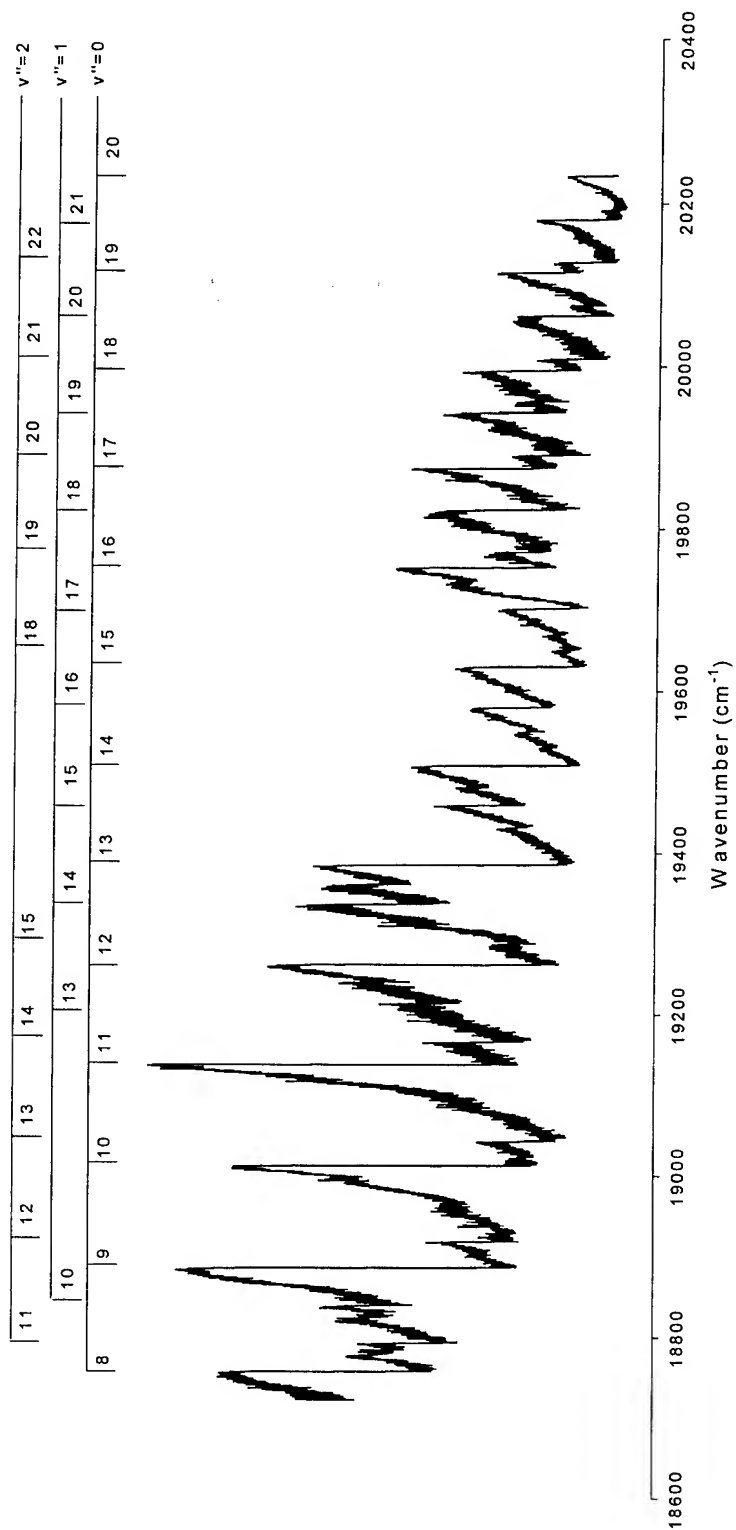
Figure 4-5. Laser excitation spectrum created using Coumarin 500 dye
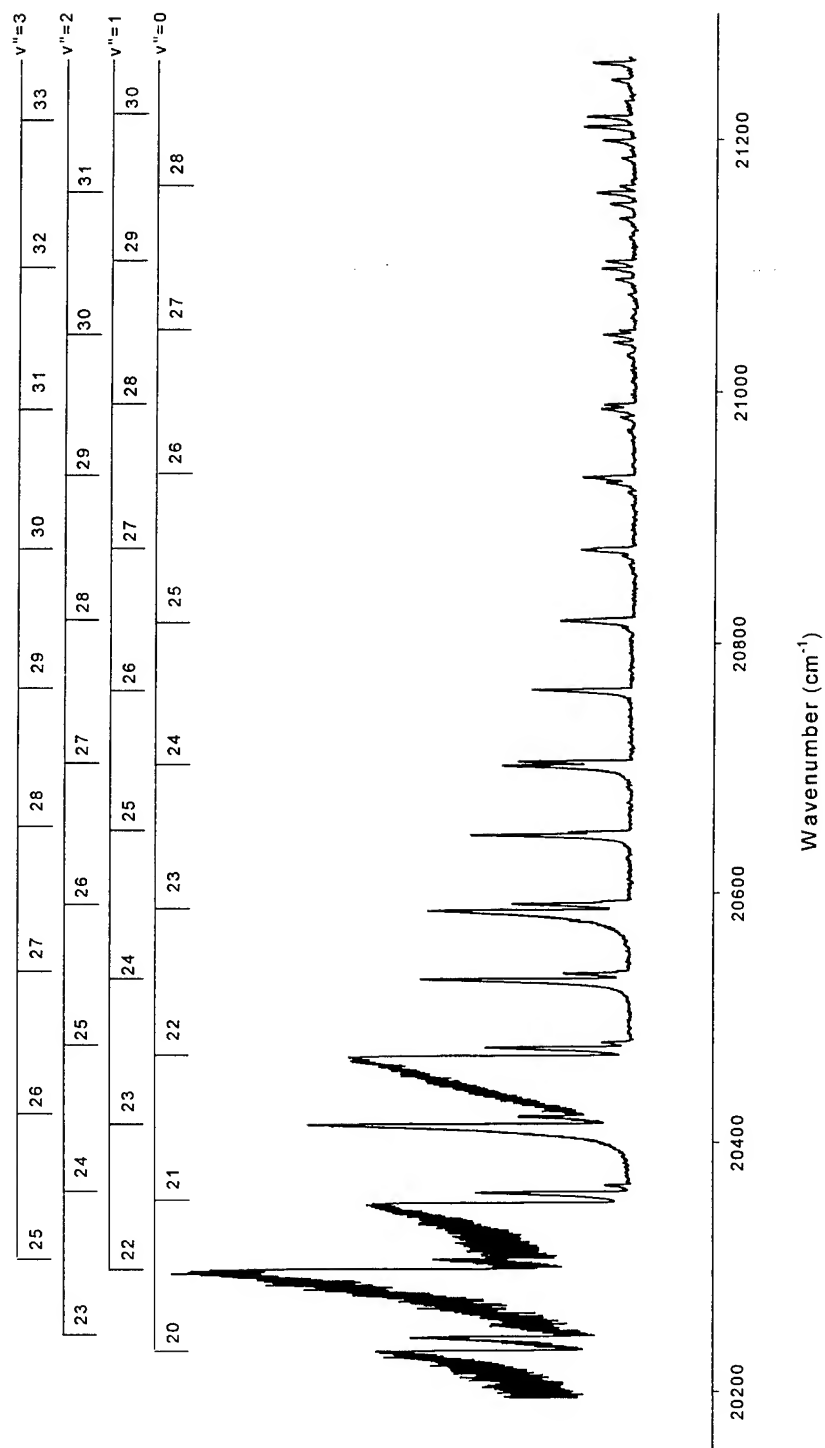
Figure 4-6. Laser excitation spectrum created using Coumarin 480 dye
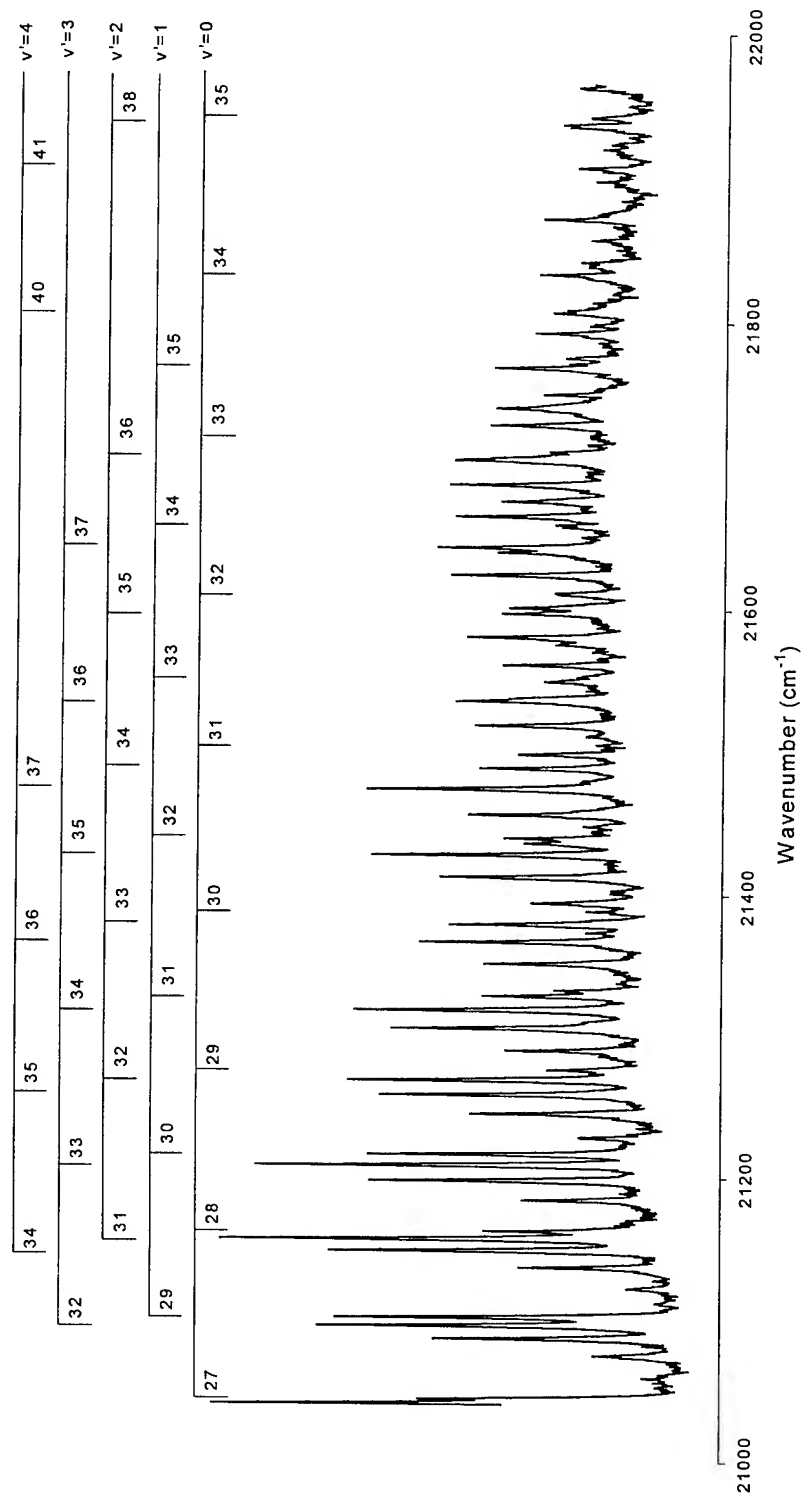
Figure 4-7. Laser excitation spectrum created using Coumarin 460 dye
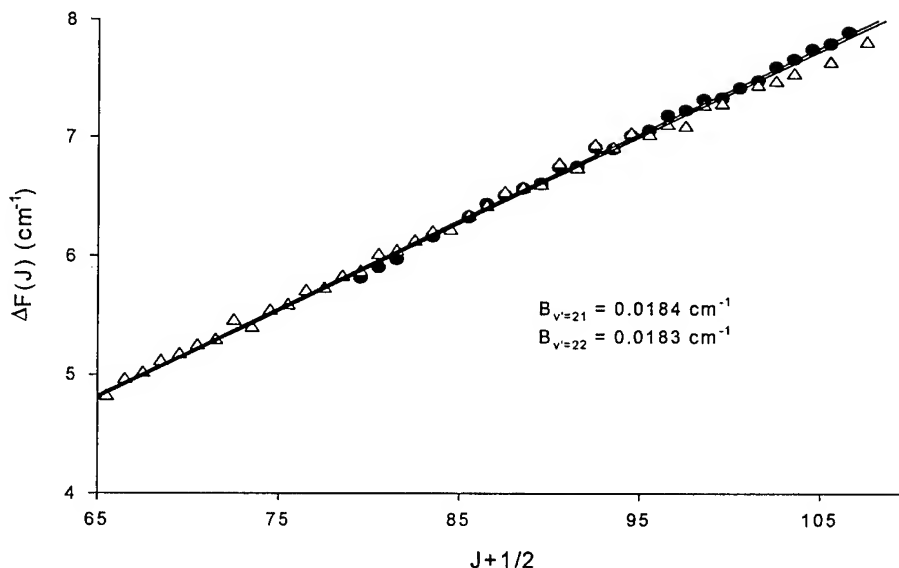
Figure 4-8. Rotational second differences, $\Delta F(J)$, plot as a function of $J+\frac{1}{2}$ for vibrational bands (21,0), (●), and (22,0), (Δ) along with their respective fits (—)

A plot of the natural logarithm of the fluorescence intensity verses time, Figure 4-9, confirms that the data obtained from the time-resolved fluorescence intensity analysis, for $v' = 21$ and $v' = 22$ is single exponential over at least six e-folds. A least squares fit of equation (29) to this exponential decay gives the inverse-lifetime, $1/\tau$, of the transition. A fit is performed on each fluorescence decay curve, one for each combination of pressure, P, and rotational level, J, explored within the vibrational manifold. This analysis produces a set of values $\tau(v', J, P)$ and associated error $\sigma_\tau(v', J, P)$.
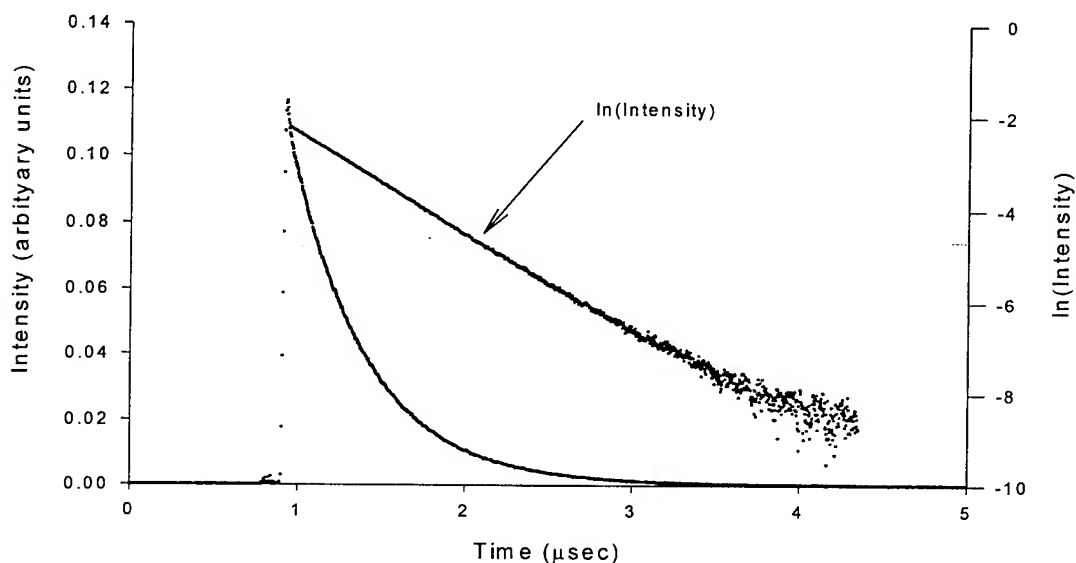
Figure 4-9. 1000-shot-averaged time-resolved fluorescence intensity signal for $(v',v'') = (21,0)$, $J' = 50$ and $P = 100$ mtorr in both ln and linear scales

The error in τ is translated to error in $1/\tau$ by use of the relationship

$$\sigma_{f(\tau)}^2 = \left(\frac{\partial f(\tau)}{\partial \tau} \right)^2 \sigma_\tau^2 \quad \Rightarrow \quad \sigma_{f(\tau)} = \frac{\sigma_\tau}{\tau^2} \tag{40}$$

where $f(\tau) = 1/\tau$ [34]. This data is presented in Appendix E, Tables E-1 and E-2.

Data is gathered together by J-level at varying pressures P. Stern-Volmer plots are then used to determine both the collisional deactivation rate, k_q, and the collision free lifetimes, τ_o, for each J-level of interest, see Figure 4-10, and Appendix E, Tables E-1 and E-2. Note that the quenching rates, k_q, reported in Appendix E have limited meaning since the outgas collision partners are not well known, see Section 4.2. However, the

4-15
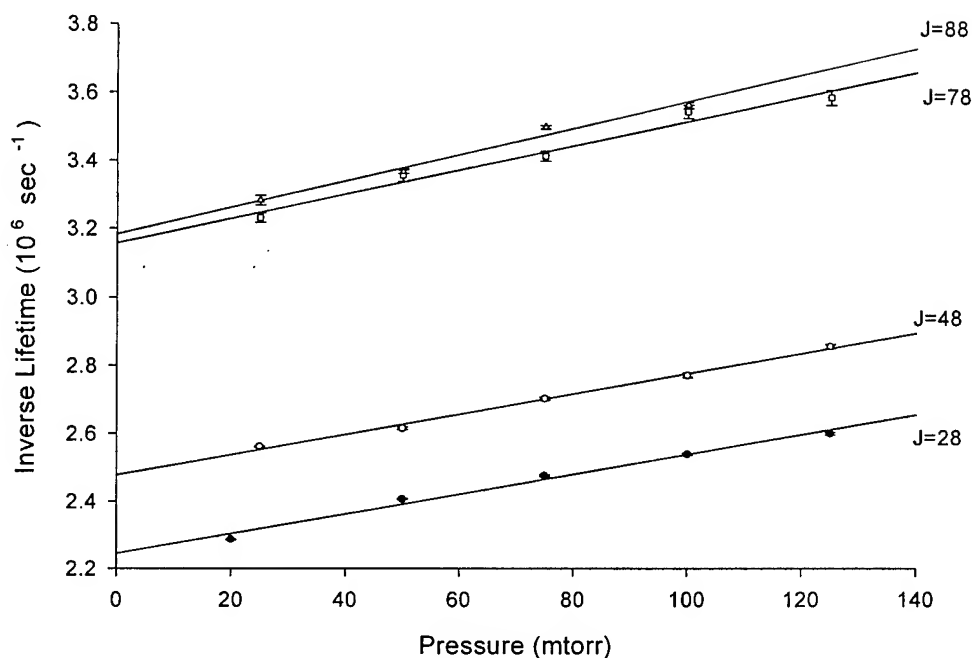
Figure 4-10. Stern-Volmer plots showing the $(v',v'') = (21,0)$ transition for rotational levels J=28 ($\bullet$), 48(o), 78( ) and 88(Δ) along with their respective fits($—$)

most important values obtained, the intercepts of the Stern-Volmer plots, $1/\tau_0$, are

independent of the buffer gas composition. Typically, four or five pressures, ranging

from 20 mtorr to 150 mtorr, were taken for each J level of interest.

The resulting set of data contains two pieces of useful information. Recalling the

form of the inverse collision free lifetime, $1/\tau_0$, equation (31), it has been shown that

$$\frac{1}{\tau_o} = \frac{1}{\tau_{rad}} + k_{pd,v'}J(J+1) \tag{31}$$

Thus, a plot of $1/\tau_o$ vs. J(J+1) results in a straight line with non-zero slope for those

vibrational levels which have lifetimes influenced by heterogeneous predissociation, as

seen in Figure 4-11.
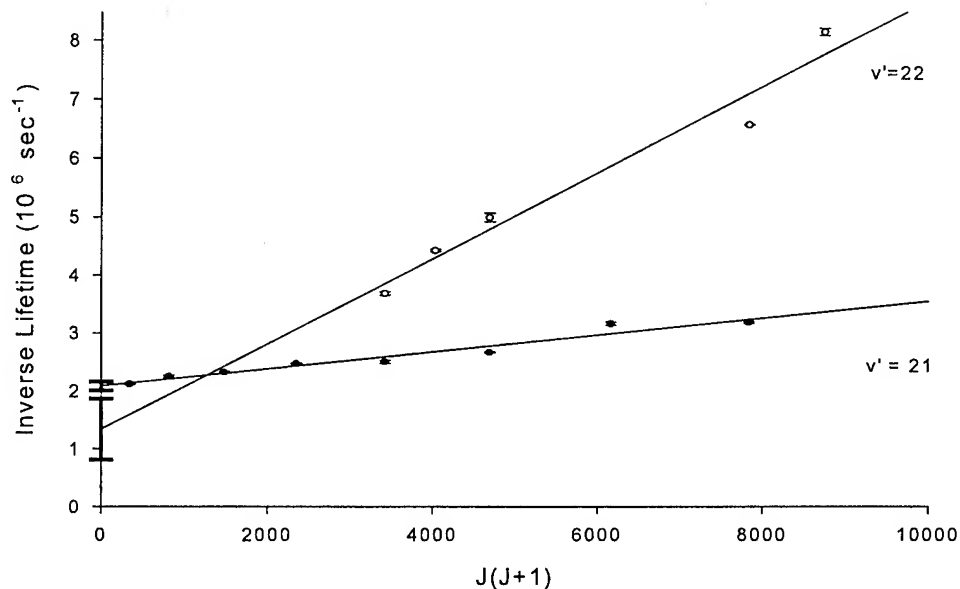
Figure 4-11. Inverse collisionless lifetime, $1/\tau_o$, verses J(J+1) for vibrational manifolds
$v' = 21$ (●) and $v' = 22$ (o) along with their respective fits (—) and intercept errors (**I**)

For vibrational manifolds above $v' = 22$ the curvature in the ln(I) becomes

evident, see Figure 4-12, and the details of the rotational spectrum disappear, leaving

little or no ability for a traditional lifetime analysis to be performed. Specifically,

equation (29), the single exponential function, no longer adequately represents the data.

The non-linearity in the natural logarithm of the fluorescence intensity signal along with

difficulties associated in determining the J-level pumped has required the abandonment of

traditional lifetime analysis techniques in favor of a more pragmatic numerical approach.
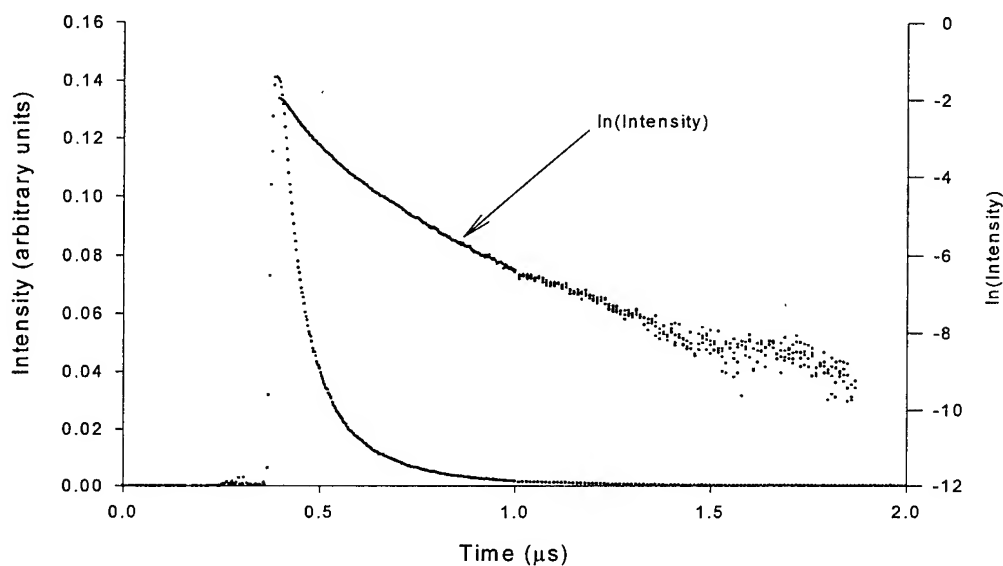
Figure 4-12. 1000-shot-averaged time-resolved fluorescence intensity signal for $(v',v'') = (23,0)$, $J' = 20$ and $P = 100$ mtorr in both ln and linear scales

4.3.3   Spectral Mathematical Model: $23 \leq v' \leq 39$

For vibrational manifolds $v' = 23$ and above the traditional approach of Section

4.3.2 loses its utility. The combination of strong predissociation, along with the limited

resolution of the PDL-3D dye laser leaves no ability to assign the rotational features of

the spectra. Further, both qualitative and quantitative efforts to determine J as a function

Table 4-1. Radiative decay, Γ_{rad}, and predissociation, $k_{pd,v'}$, rates for $Bi_2(A)$ vibrational levels $9 \le v' \le 39$

v', v''	Γ_{rad} $(\sigma_{\Gamma_{rad}})$ $[10^6 \text{ sec}^{-1}]$	Traditional $k_{pd,v'}$ $(\sigma_{k_{pd,v'}})$ $[\text{sec}^{-1}]$	Maximum Slope $k_{pd,v'}$ $[\text{sec}^{-1}]$	Minimum Slope $k_{pd,v'}$ $[\text{sec}^{-1}]$	Synthetic $k_{pd,v'}$ $[\text{sec}^{-1}]$
9,0	1.73 (0.019)				
11,0	1.83 (0.021)				
13,0	1.75 (0.012)				
21,0	2.08(0.076)	153.09 (15.81)			153.09
22,0	1.34(0.531)	793.11 (53.22)			793.11
23,0			21374.25	5644.93	22,000
24,1			94322.94	11179.50	45,000
25,2			116689.16	16376.74	70,000
27,3					95,000
28,0					125,000
29,1					110,000
30,1					140,000
31,3					110,000
32,3					110,000
33,3					150,000
34,4					140,000
35,4					140,000
36,2					140,000
36,3					140,000
36,4					140,000
36,5					140,000
37,5					110,000
38,5					95,000
39,6					95,000

of the pump wavelength, within some experimental error, have failed to yield physically

meaningful results. The inability to determine the range of J-levels pumped as well as

each J-level's contribution to the lifetime of the state has proven almost insurmountable. However, the maximum and minimum slopes of the nonlinear ln I(t) vs. t plots for vibrational manifolds (23,0), (24,1) and (25,2) were used to place bounds on the expected predissociation rates from these levels. The bounds for the expected $k_{pd,v'}$ values of this slope analysis, given in Table 4-1 and shown in Figure 4-18, are consistent with the synthetic analysis to follow. A direct determination of lifetime, τ, as a function of J(J+1), i.e., a traditional analysis, has been abandoned for the following numerical treatment.

A synthetic spectrum may be created by summing the contributions from each spectral line it contains. In the case of a diatomic molecule, within a given vibrational manifold, the shape and intensity of each line is determined by several factors. These factors include the statistical distribution of states, the lineshape function and other functions associated with predissociation. Although these functions contain experimental parameters, if a model is developed that has $k_{pd,v'}$ as its only adjustable parameter the rate constant may be adjusted until the synthetic spectra "fits" the observed excitation spectra. This "best fit" rate constant then becomes the solution for $k_{pd,v'}$. The synthetic spectral model therefore determines the shape of a single vibrational manifold based upon the summation of the set of predissociated rotational lineshape functions $f(\nu,J)$.

Consider first the pulse from the dye laser that excites the spectral features. The linewidth of the dye laser is much larger than the doppler linewidth associated with the transition. Therefore, use, as the resulting spectral lineshape, the lineshape function of the laser described here by the combined Gaussian function,

$$f(v) = N\left[(1-A)\exp\left(\frac{-4\ln 2[v_o - v]^2}{\Delta v_D^2}\right) + A\exp\left(\frac{-4\ln 2[v_o - v]^2}{\Delta v_{ase}^2}\right)\right] \qquad (43)$$

where terms for the laser linewidth and the amplified spontaneous emission (ASE), which was present in our apparatus, have been included. Each of these Gaussian functions is weighted by a normalization constant, N, outside the square brackets, and a weighting constant, A, inside the square brackets. The weighting constant, $0 \leq A \leq 1$, is a measure of the fraction of the input signal which is produced by ASE. The primary result of the ASE term is to add sufficient baseline to the synthetic spectrum to match the observed experimental spectrum.

The intensity of each lineshape must include the effects of the statistical distribution of states, the effects of predissociation, and the width and location of the gate used on the boxcar integrator. The first of these effects, the statistical distribution of states, is given by the Maxwell-Boltzmann distribution function

$$f_{MB}(J) = (2J+1)\exp\left[\frac{-B''J(J+1)}{kT}\right] \qquad (44)$$

The second of the modifiers, mentioned above, is developed to account for the effects of predissociation on the J level pumped. For a level with non-zero $k_{pd,v'}$ the

4-21

fluorescence yield, i.e., the ratio of the radiative decay rate, Γ_{rad}, to the collisionless decay

rate, Γ_o, is less than unity. This quantity is expressed as

$$f_{pd}(J) = \frac{\Gamma_{rad}}{\Gamma_{rad} + k_{pd,v'}J(J+1)} \tag{45}$$

When the synthetic spectrum was compared to the experimental spectrum a

significant discrepancy in the shape of the manifold was found. The curvature of the

synthetically produced spectrum would simply not match that of the experimental

spectra. In fact, several trial solutions were discarded as new fit parameters were

investigated. Then the experimental setup itself was considered as a factor in the shape of

the predissociated vibrational manifold. The intensity of the laser excitation spectrum is

dependent upon the gate-width set on the boxcar integrator. Mathematically, the change

in the fluorescence signal intensity is dependent on the non-constant ratio of calculated

gate area to the total area of the signal. The ratio may be expressed by dividing the area

under the decay curve bound by the gate width by the total area under the fluorescence

decay curve. Specifically,

$$f_{gate}(J) = \frac{\int_{t_o}^{t_f} C\exp(-t/\tau)dt}{\int_0^\infty C\exp(-t/\tau)dt} = \frac{-\tau\ C\left[\exp(-t/\tau)\right]_{t_o}^{t_f}}{-\tau\ C\left[\exp(-t/\tau)\right]_0^\infty} = \exp(-t_o/\tau) - \exp(-t_f/\tau) \tag{46}$$

where, once again, $1/\tau = \Gamma_o + k_{pd,v'}J(J+1)$. This point is significant since, for non-predissociated spectra, equation (46) is constant, e.g. not dependent on J. Therefore, with this formalism, an accurate picture of the laser excitation spectra has been found.

Each term is put together in its final form to reproduce the experimental spectrum. For each J transition the appropriately weighted lineshape function is given by the combination of equations (43), (44), (45) and (46):

$$f(v,J) = f(v)f_{MB}(J)f_{pd}(J)f_{gate}(J) \tag{47}$$

Summing over all J levels accessed, the final expression for the intensity of the experimental spectrum, within a given vibrational manifold, is

$$\text{Intensity}(v) = \sum_J f(v,J) \tag{48}$$

This entire routine has been programmed as a Mathcad 7.0 Professional Workbook, see Appendix F. The constants used in the synthetic fits are provided in Table 4-2.

Table 4-2. Constants used in synthetic spectrum fit analysis

Constant	Value
Δv_D	0.3 cm^{-1}
Δv_{ase}	1.55 cm^{-1}
A	20 %
T	300 K [30]
Γ_{rad}	$1.76 \times 10^6 \text{ sec}^{-1}$
t_o	$9.2 \times 10^{-9} \text{ sec}$
t_f	$77.8 \times 10^{-9} \text{ sec}$

Figure 4-14, on the following page, illustrates the agreement of these synthetically derived spectra with the experimental spectra of the pulsed dye-laser experiment. The predissociation rate selected for the synthetic spectra fit is the previously determined value of $k_{pd,v'} = 153.09 \, \text{sec}^{-1}$, see Section 4.3.2. Figure 4-14 and Figure 4-15 differ from Figure 4-13 only by variation in the value of $k_{pd,v'}$, which by variation, allows the synthetic spectra to replicate the major features of the experimental spectra. Finally, Figure 4-16 shows, on a single plot with "common" band origin, an illustration of the sensitivity of spectral decay on selection of predissociative rate constant, $k_{pd,v'}$. Further note that, for those transitions for which it could be verified, $k_{pd,v'}$ does indeed remain consistent for each v' independent of the v'' level to which the transition had taken place, see Table 4-1 transitions (36,X).

An error analysis was performed on each of the fit spectra by varying the value of $k_{pd,v'}$ by 5 to 25 percent for any given spectral fit. It is evident, see Figure 4-17, that the error associated with $k_{pd,v'}$ is approximately 15% for these spectra. Values of $k_{pd,v'}$ which varied by more than 15% were universally unacceptable as fit results. Analysis of all accessible levels, that have no interference from nearby spectral features, results in a comprehensive set of predissociative rate constants, $k_{pd,v'}$, for the entire range of v' accessed. The complete set of predissociative rate data, Table 4-1, is shown graphically in Figure 4-18 and Figure 4-19. In addition to the synthetic spectrum values for $k_{pd,v'}$, Table 4-1 and Figure 4-18 contain comparative results from maximum slope,
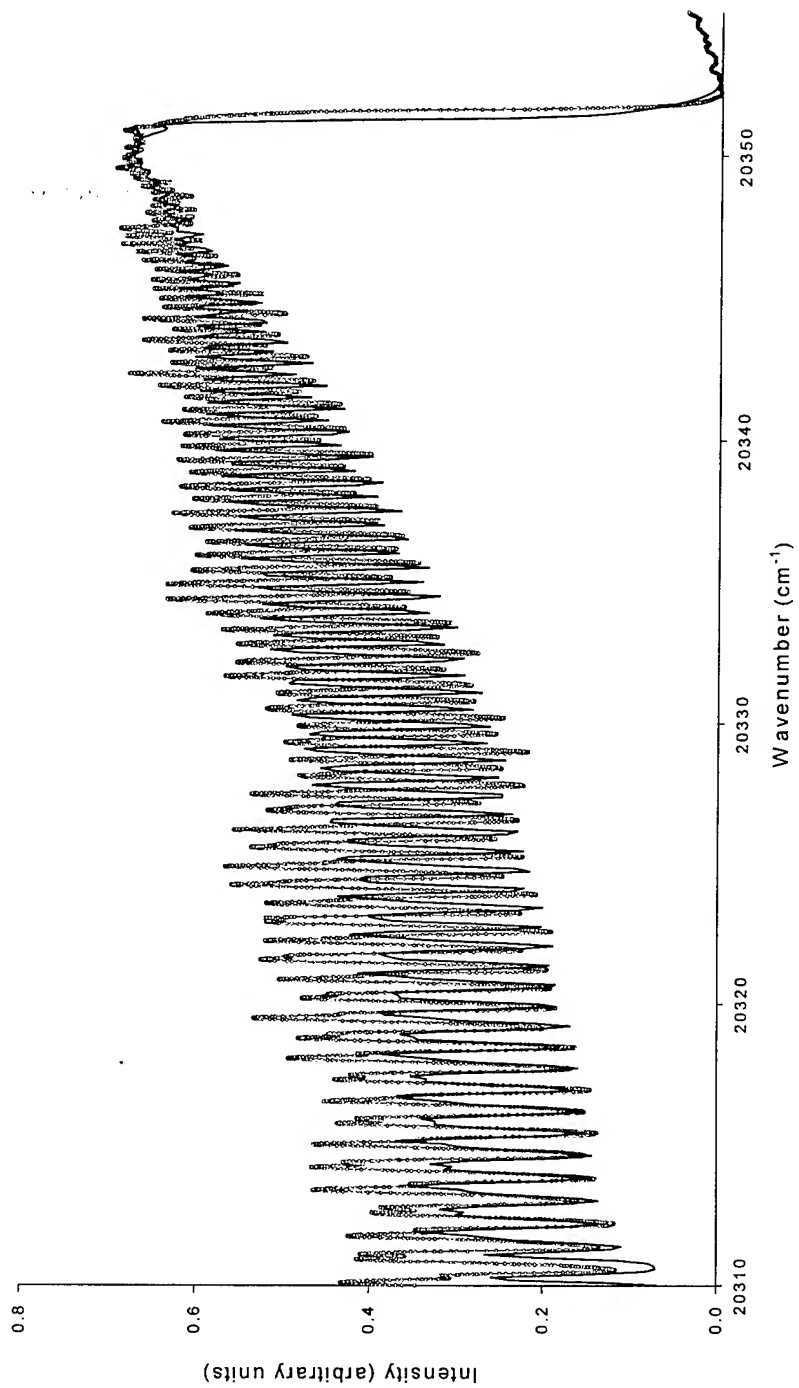
Figure 4-13. Synthetic and experimental spectrum comparison for (21,0)
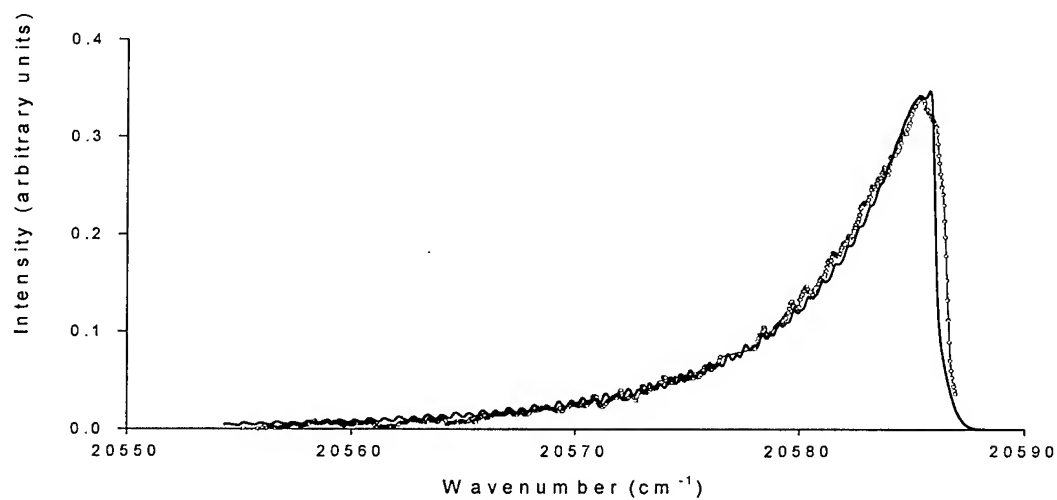
Figure 4-14. Synthetic (—) and experimental (o) spectrum for $(v',v'') = (23,0)$
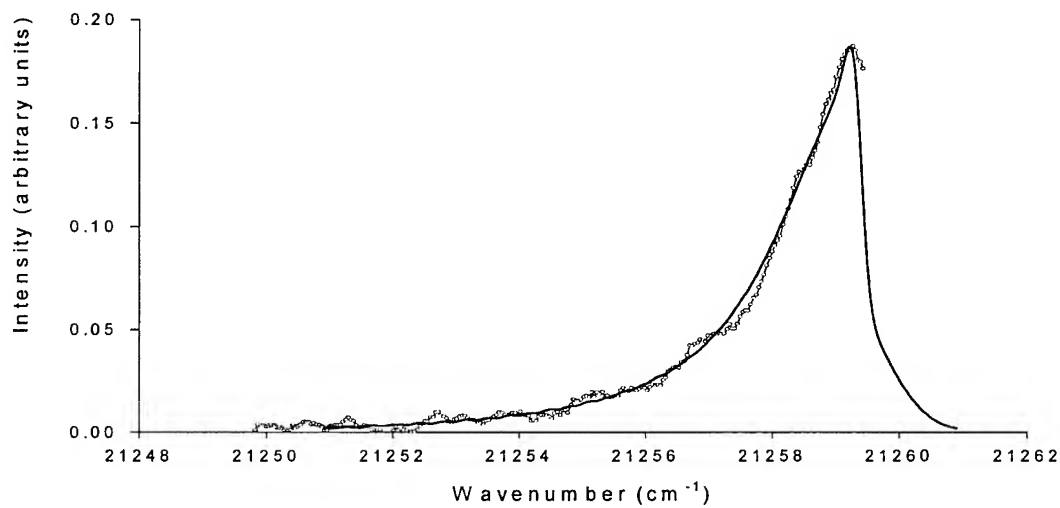
Figure 4-15. Synthetic (—) and experimental (o) spectrum for $(v',v'') = (35,4)$
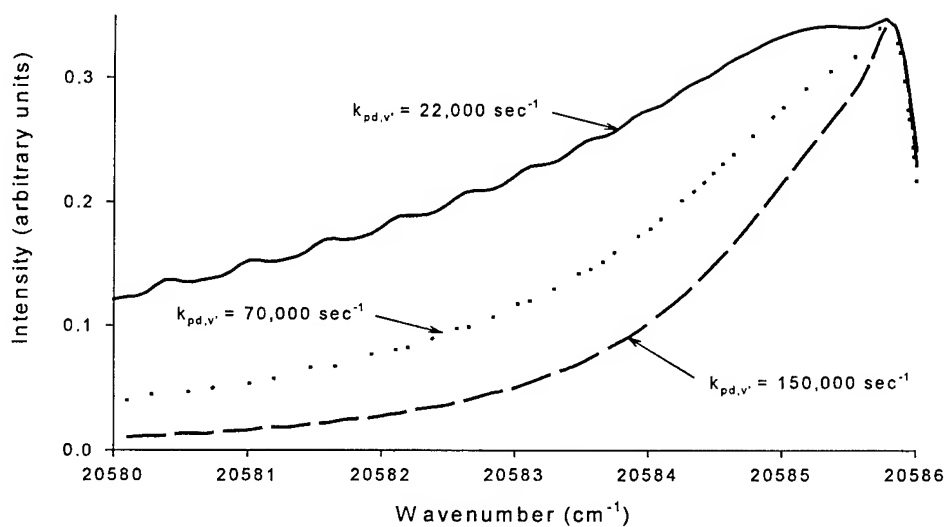
Figure 4-16. Comparative plot of synthetic spectra from vibrational bands (23,0) [—],
(25,2) [⋯], and (33,3) [---] each with different assigned values for $k_{pd,v'}$ as shown
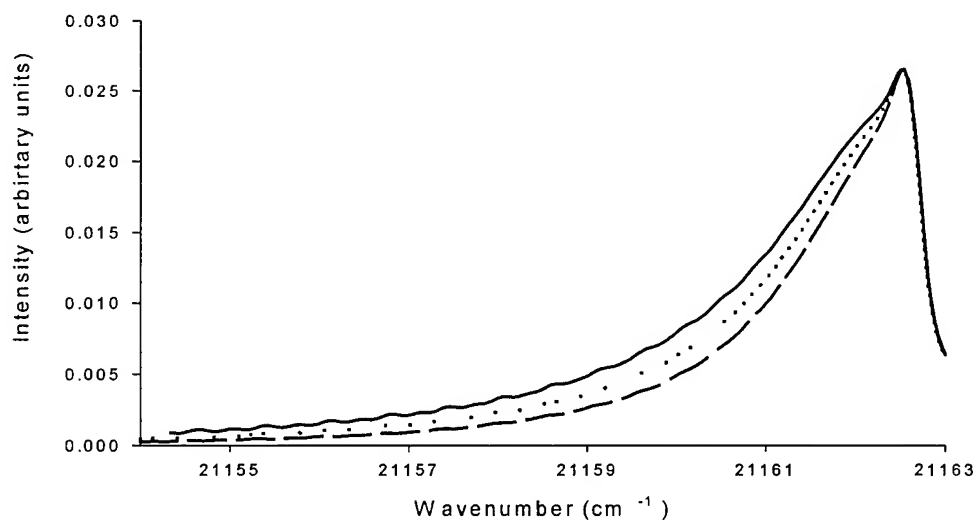
Figure 4-17. Comparative plot of synthetic spectra from vibrational band (28,0) [⋯]
showing the effects of increasing [---] and decreasing [—] $k_{pd,v'}$ by 15%
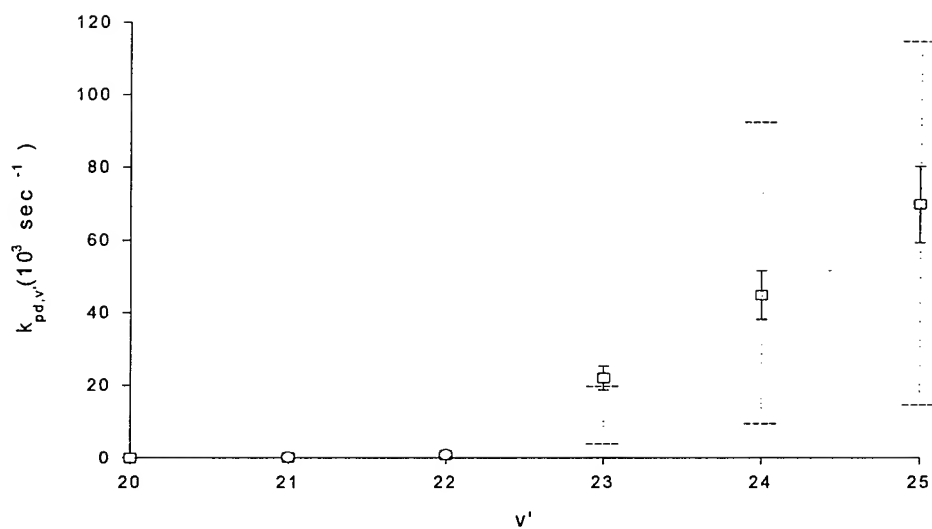
Figure 4-18. $k_{pd,v'}$ verses v' for vibrational levels $20 \leq v' \leq 25$ for traditional [o], maximum and minimum slope bounds [---] and synthetic fit [□] analysis
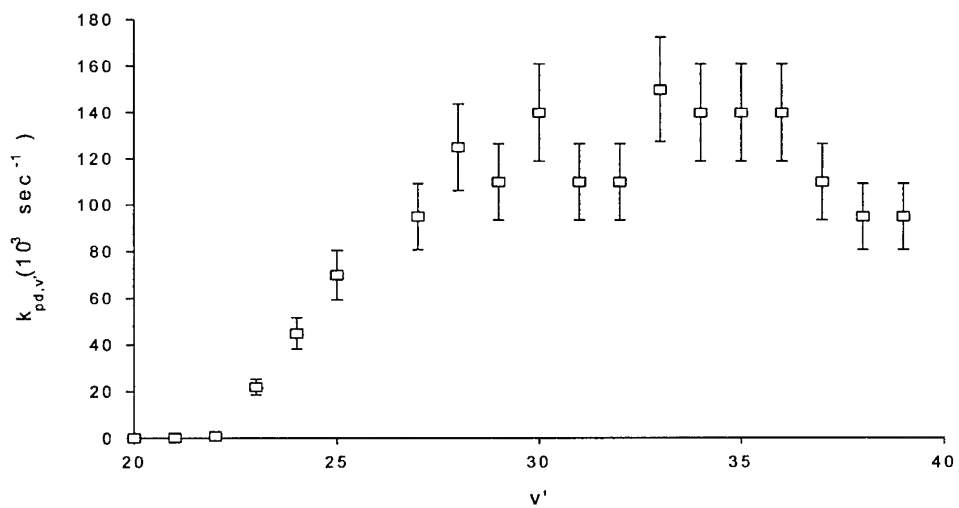
Figure 4-19. $k_{pd,v'}$ vs. v' [□] and associated 15% error determined from synthetic spectra

minimum slope, and traditional $k_{pd,v'}$ analysis. As previously asserted, in Section 4.3.2, only the $v' = 21$ and $v' = 22$ manifolds allowed for traditional analysis. The trend of decreasing $k_{pd,v'}$ above $v' = 36$, shown in Figure 4-19, is real based on the error analysis previously discussed.

4.4. *Summary*

The data presented in this lifetime and predissociation analysis represents the best treatment of predissociation in $Bi_2(A)$ to date. In fact, this is the only complete analysis of the $Bi_2(A)$-state predissociation phenomena. This research has determined lifetimes and predissociation rates in addition to identifying the predissociation as heterogeneous. The rate data presented in this chapter, along with the spectroscopic data of Chapter 3, will be used in combination, in Chapter 5, in an attempt determine the analytic form of the repulsive potential responsible for the predissociative behavior found in $Bi_2(A)$.

5. Determination of the Predissociative Potential

5.1. Introduction

The theoretical and experimental developments of the three preceding chapters of this dissertation are used here, in combination, as a starting point from which to identify the potential energy states investigated in this study. Chapter 2 outlined the theoretical foundation for the identification and calculation of spectroscopic constants, lifetimes, and predissociation rates for $Bi_2(A)$. The absorption spectroscopy experiment and analysis detailed in Chapter 3 lead to improvements in A-state spectroscopic constants. The extensive analysis of Chapter 4 produced lifetimes and predissociation rate data for $Bi_2(A)$. All of this theory and data is brought together in this chapter to calculate RKR potentials for $Bi_2(X)$ and $Bi_2(A)$, review and discuss proposed electronic states responsible for A-state predissociation, and attempt to numerically determine the analytic form of the potential responsible for this phenomena.

5.2. RKR Potential Energy Curves for $Bi_2(X)$ and $Bi_2(A)$

The potential energy curves for $Bi_2(X)$ and $Bi_2(A)$ are calculated using the Dunham expansion coefficients presented in the paper by Barrow et al. [1] for the ground state and the improved coefficients from this dissertation, presented in Table 3-2, for the

A-state. These spectroscopic constants are used as the input data for the PC-based RKR program, supplied by Hornkohl [35]. A brief review of the RKR method is presented in Section 2.6. The output files, which include a synopsis of the input data, are shown in Tables G-1 and G-2, Appendix G, for both states. RKR calculations result in the bound-state potentials plotted in Figure 5-1.

5.3. *Theoretical Determination of the Interactive State*

The selection rules for predissociation require $g \leftrightarrow g$, $u \leftrightarrow u$, and $\Delta\Omega = 0, \pm 1$ [20]. Heterogeneous predissociation is manifest via the rotational-electronic coupling term of Equation (35),

$$\left| \left\langle \Psi_c \left| \mathbf{H}' \right| \Psi_b \right\rangle \right|^2 = \frac{\hbar^3}{8\pi\mu^2 c} \left[J'(J'+1) - \Omega_b(\Omega_b \pm 1) \right] \left| \left\langle \chi_c \left| \mathbf{W}_e(\mathbf{R})\mathbf{R}^{-2} \right| \chi_b \right\rangle \right|^2 \tag{35}$$

and corresponds to the selection rule $\Delta\Omega = \pm 1$. In Chapter 4, it has been shown that the predissociation phenomena investigated does indeed possess a rotational dependence of the form J(J+1) via application of Equation (31)

$$\frac{1}{\tau_o} = \frac{1}{\tau_{rad}} + k_{pd,v} J(J+1) \tag{31}$$
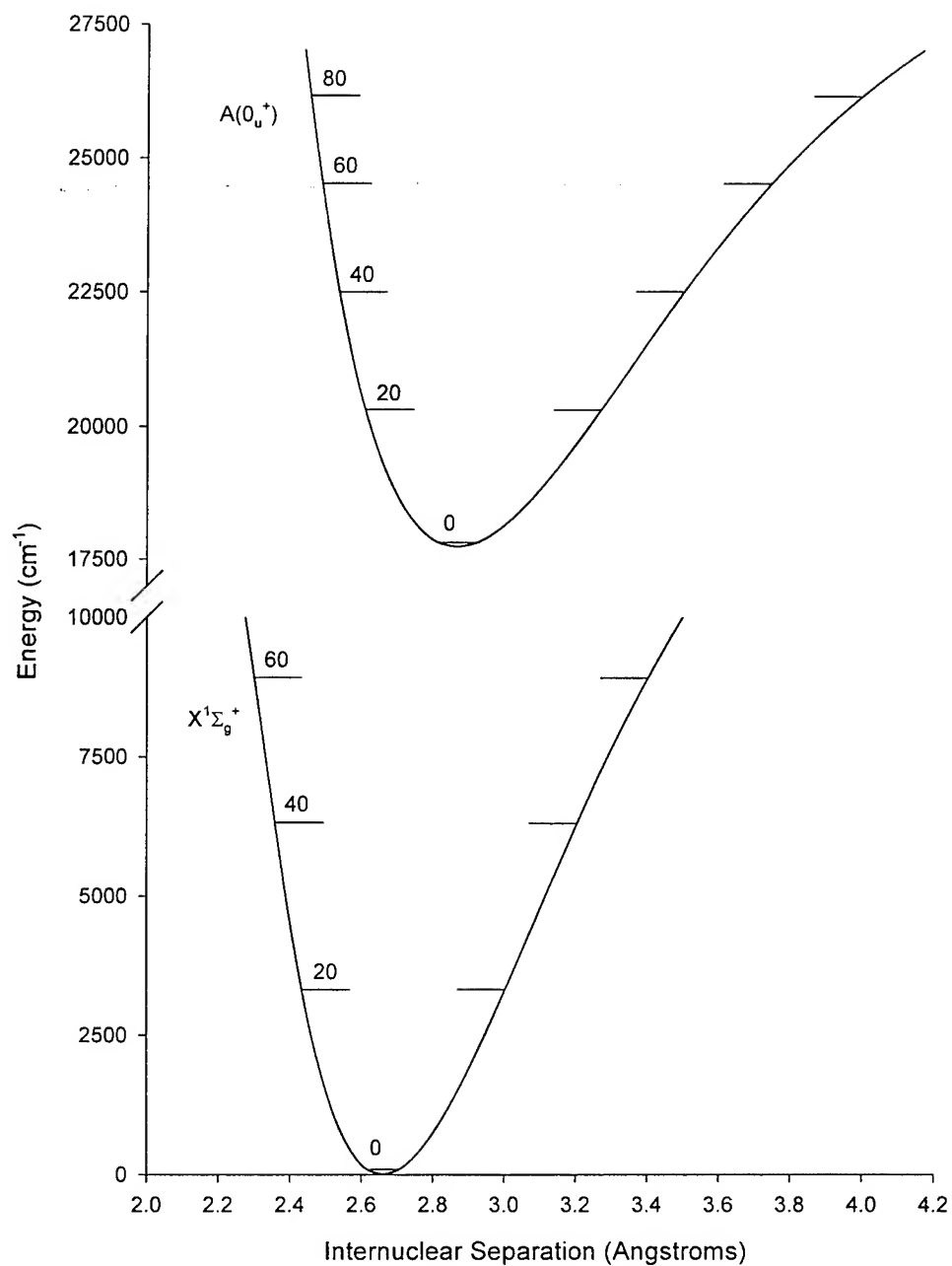
Figure 5-1. RKR-generated potential energy curves for $Bi_2(X)$ and $Bi_2(A)$

Therefore, the symmetry of the interactive state is identifiable, "Since the [bound] state in question is a $^3\Sigma_u^-(0_u^+)$ state, only u states could predissociate this state [7]."

The theoretical configuration of electronic states for Bi_2 has received analysis by Balasubramanian and Liao [7] as well as Das, Liebermann, Buenker, and Hirsch [10]. Both papers agree that the repulsive $^7\Sigma_u^+$ state, which "correlate[s] with the lowest atomic limit [10]," is the ideal candidate for interaction with the $Bi_2A(0_u^+)$ state. This repulsive state is calculated by Balasubramanian and Liao to cross the bound potential of $Bi_2(A)$ at approximately 3.3 Å, see Figure 2-2. This is in remarkable agreement with the onset of rapid predissociation near $v' = 23$, which intersects the $A(0_u^+)$ state at 3.305 Å according to the RKR analysis of Section 5.2. It is therefore concluded, "the observed predissociation in the A – X system is [most likely] due to the predissociation of $^3\Sigma_u^-(0_u^+)$ by $^7\Sigma_u^+(1_u)$ [7]."

5.4.   Determination of a Repulsive Potential $V_{rep}(R)$ for $Bi_2(A)$

The 1982 paper on the predissociation of Br_2, $B^3\Pi(0_u^+)$, by Clyne, Heaven and Tellingheusin [17] provides the model for the analytical treatment of predissociation presented in this chapter. The similarity in the symmetry of the affected bound state, namely 0_u^+, and the type of predissociation treated, heterogeneous, is an analogous to the $Bi_2(A)$ predissociation found in this dissertation. The methodology used by Clyne,

Heaven and Tellingheusin is replicated here in an attempt to determine the analytic form of the repulsive potential responsible for predissociation. Heaven has supplied the numerical code, the FCF program, for use in this research [27].

The probability of predissociation, $P_{v'}$, is a Frank-Condon-like factor defined as the matrix element of $\mathbf{R}^{-2}$ between the bound state wave function, χ_b, and the continuum state wave function, χ_c, Equation (38):

$$P_{v'} = \left| \left\langle \chi_c \left| \mathbf{R}^{-2} \right| \chi_b \right\rangle \right|^2 \tag{38}$$

The bound state wave functions, χ_b, are calculated by a numerical routine within the FCF program. The input data to this routine is the RKR potential data for the $Bi_2 \, A(0_u^+)$ state, which was determined in Section 5.2. In agreement with the analysis of Section 5.3, a simple repulsive potential of the form $V_{rep}(R) = a/(R-d)^b$ is used to determine the bound wave functions, χ_c. Iterative guessing of the constants, a, b and d, produce a "best fit" to the $k_{pd,v'}$ vs. v' data.

A sample input file, prein.dat, for the FCF program is shown in Appendix H. This file contains information on the physical properties of the molecule as well as energy values, E(R), for the A-state potential. A typical output file, preout.dat, is provided in Appendix I. To simplify the process of modifying the input file and viewing the output results, a Visual BASIC FCF program control interface, DataPlot [36], was developed.

Literally thousands of constants were explored exhausting the parameter space for the repulsive guess potential and eliminating uncertainty in these results.

Using Tellinghuisen's work as a guide [32], a systematic approach to exploring possible solutions for $V_{rep}(R)$ was developed. Reference Figure 5-2 and Figure 5-3 for the following discussion. Based on the theoretical predictions of Balasubramanian and Liao [7] the intersection of the repulsive $1_u \, ^7\Sigma_g^+$ potential and the bound $A(0_u^+)$ state occur near $R \approx 3.3\text{Å}$, which is in close agreement with experimental results of Chapter 4. Therefore, a set of repulsive states of varying slope are constrained to intersect the A-state at $v' = 23$ or $R \approx 3.3\text{Å}$. These potentials, labeled V_1, V_2, and V_3, are shown in Figure 5-2. The corresponding probabilities of predissociation are shown in Figure 5-3. Without exception all trial potentials produce oscillatory predissociation probabilities for $v' > 25$. It is clear that a single repulsive state passing through the A-state at $R \approx 3.3\text{Å}$ will not reproduce the form of the $k_{pd,v'}$ vs. v' data shown in Figure 4-19.

Alternately, another family of potential energy curves intersecting the bound $Bi_2(A)$ state at various internuclear separations, R, were explored. The first of these potentials, labeled V_1, in Figure 5-4, represents a potential similar to those of Figure 5-2. Again, these "right-branch" potentials are zero for levels below the intersection point and consist of non-zero, highly oscillatory results for v-levels above the intersection point. These results concur with Tellinghuisen's prediction that, "The most highly structured FCD [i.e., $P_{v'}$] occurs for the right-branch crossing... [32]."
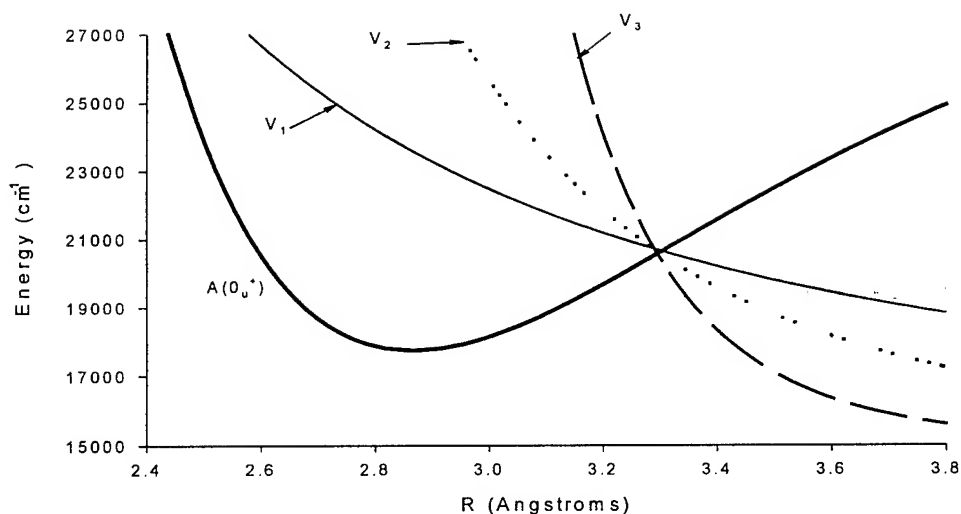
Figure 5-2. Sample potentials, V_1 (—), V_2 (⋯), and V_3(----), along with the bound $Bi_2(A)$ potential (—) used in the numerical investigation of predissociation probabilities
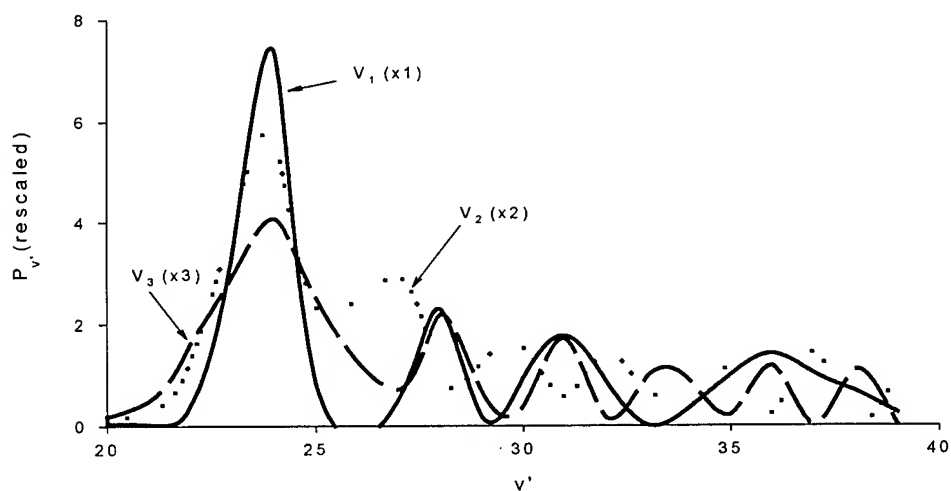
Figure 5-3. Frank-Condon-like factors ($P_{v'}$) calculated over the range $20 \leq v' \leq 39$ corresponding to trial potentials, V_1, V_2, and V_3, in Figure 5-2 shown with scaling factors

The next family of trial potential functions chosen were those associated with crossings closer to the center of the bound state, represented by V_2 in Figure 5-4. Figure 5-5 shows the results of this selection. As these potentials migrate to the left branch of the bound potential it was observed that, "...the two potentials are [become] nearly parallel, and the relative phases change more slowly with v, giving less structure [32]." The further these potentials were moved to the left, the less severe the oscillations in $P_{v'}$ became. However, as with the right-branch potentials, a maxima in $P_{v'}$ occurs near the intersection of the bound and repulsive states since "the phase relation between the bound and free wavefunctions changes rapidly with v (and E) at the point of stationary phase – the curve crossing [32]."

The final case studied was for the family of repulsive potentials that lie to the left, outside the bound potential, potential V_3. When these repulsive curves lie completely outside the bound state, "...there is no point of stationary phase within the bound well, and much of the overlap occurs in the non-classical regions of one or both states [32]." Some agreement with the experimental $k_{pd,v'}$ data was anticipated. What was found is represented by the $P_{v'}$ plot corresponding to V_3 in Figure 5-5. This $P_{v'}$ plot gives the desired zero $P_{v'}$ values below v'=21 but again produces oscillatory values for $k_{pd,v'}$ of higher-lying v-levels. So, this last iteration again failed to reproduce the $k_{pd,v'}$ trend of Chapter 4. Thus, it must be concluded that this numerical method produces no suitable single repulsive potential that can account for the observed predissociation.
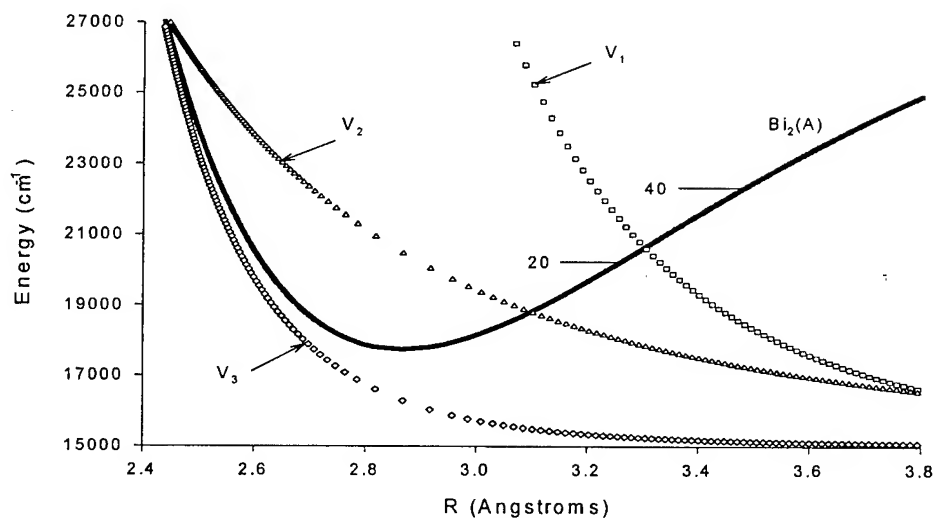
Figure 5-4. Sample potentials, V_1 (□), V_2 (Δ), and V_3(◊), along with the bound $Bi_2(A)$ potential (—)used in the numerical investigation of predissociation probabilities
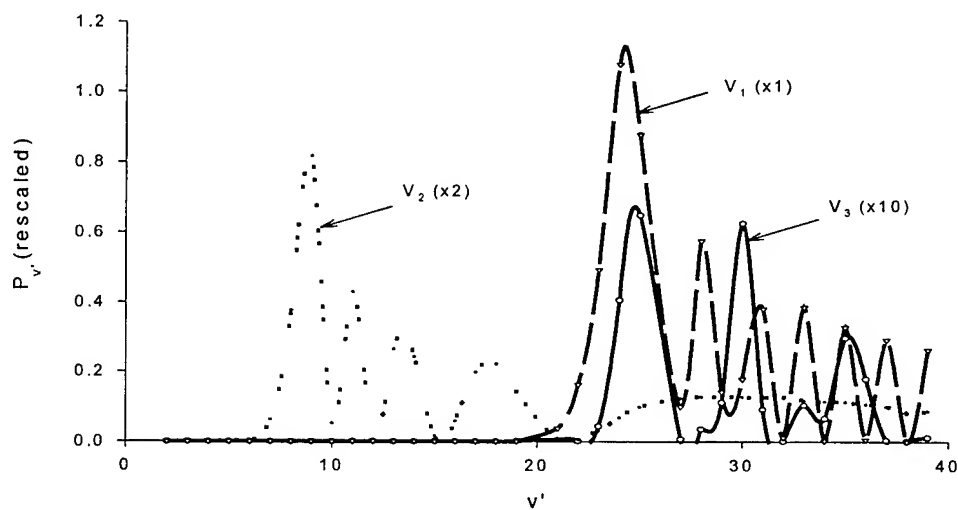
Figure 5-5. Frank-Condon-like factors, $P_{v'}$, calculated over the range $0 \le v' \le 39$ corresponding to trial potentials, V_1, V_2, and V_3, in Figure 5-4 shown with scaling factors

5.5. *Summary*

The results of Section 5.4 clearly indicate a disconnection between experimentally determined $k_{pd,v'}$ rates and those rates predicted by existing theory. Clearly, the data presented in Chapter 4 is essentially accurate. That is to say, there exists sufficient spectral evidence in Figures 4-5 to 4-7 to support the nearly constant $k_{pd,v'}$ trend found in Figure 4-19. The absence of strongly visible variation in the spectroscopic structure is in agreement with the results of Section 4.3. In other words, if such rapid and pronounced oscillatory behavior did exist, as predicted by the FCF program used in Section 5.4, the spectra would bear evidence manifest in the return of less-dissociated spectral bands.

Clearly this evidence suggest that the current state of theoretical analysis for predissociation is insufficient to predict observed trends in k_{pd} for $Bi_2(A)$ by using a single repulsive potential as the perturbing state. The validity of the FCF program supplied by Heaven is not in question. This numeric routine works fine for other cases of predissociation cited in this dissertation. These results necessitate further exploration into both the electronic structure of Bi_2 and the underlying theory of predissociation, which is beyond the scope of this work.

6. Results and Conclusions

6.1. Results

Spectral analysis of the $Bi_2(X\rightarrow A)$ transition, using Fourier Transform absorption spectroscopy techniques, has lead to improved Dunham coefficients for the A-state. The new values presented in Table 3-2 and reproduced below, are the result of a 20-fold expansion in the range of vibrational manifolds probed from $1 \le v' \le 4$ to $0 \le v' \le 91$. The changes to these constants are graphically presented in Figure 3-5. The impact of expanding the accessed spectral range is significant since, "...for diatomic molecules the analysis of discrete transitions can lead to potential curves whose reliability is limited solely by the range and quality of the spectroscopic data [32]."

Table 6-1. $Bi_2(A)$ Dunham coefficients from current work and Franklin and Perram [6]

Electronic State: Source: Range of Study: Units:	$Bi_2\,A(0_u^+)$ Current Work $v' = 0\text{-}91$ (cm^{-1})	$Bi_2\,A(0_u^+)$ Perram and Franklin [6] $v' = 0 - 4$ (cm^{-1})
Y_{00}	17740.6927(24)	17740.696(29)
Y_{10}	132.38356(25)	132.383(11)
Y_{20}	-0.3109311(69)	-0.31092(97)
Y_{30}	$-2.7494(5)\times10^{-4}$	$-2.75(23)\times10^{-4}$
Y_{01}	0.0196412(2)	0.0196663(17)
Y_{11}	$-5.0078(13)\times10^{-5}$	$-4.991(33)\times10^{-5}$
Y_{21}	$-1.3167(15)\times10^{-7}$	$-1.32(12)\times10^{-7}$
Y_{02}	$-1.7409(52)\times10^{-9}$	$-1.74935(26)\times10^{-9}$
Y_{12}	$-6.81(27)\times10^{-12}$	$-7.700(66)\times10^{-12}$

The spectroscopic analysis performed indicates that the proper dissociation products for the $A(0_u^+)$ state are $^4S + ^2D$. Since the calculated dissociation energy lies nearly midway between the $^2D_{3/2}$ and the $^2D_{5/2}$ levels, see Figure 2-2, assignment to a single level was not possible. However, this information clearly leads to the conclusion that the dissociation products are not $^4S + ^2P$. These separated atom states simply lie too far above any reasonable A-state dissociation limit. Therefore, the theoretical work performed by Balasubramanian and Liao [7] and Das et al. [10] on the electronic energy levels within Bi_2 must be reevaluated for validity.

Laser induced fluorescence experiments produced lifetime and predissociation rate data previously unavailable. The radiative lifetime of the A-state, τ_{rad}, was confirmed to be 0.57 μs, which is in good agreement with the experimental results of Blondeau [8] and Ehret and Gerber [9]. These results conflict with the theoretical findings of Das et al. [10], which predict the A-state lifetime to be approximately 72 μs, once again casting doubt on the results of this theoretical paper. An extensive analysis of the (21,0) and (22,0) vibrational bands, by traditional methods, confirmed that predissociative lifetimes of $Bi_2(A)$ are a function of J(J+1). The synthetic spectrum fits of Section 4.3.3 enabled predissociation analysis to continue into regions of the spectrum not otherwise accessible by traditional methods. The combination of traditional analysis and synthetic spectral fits lead to first-ever reporting of $k_{pd,v'}$ values. Over the range $21 \le v' \le 39$ the predissociation rates were found to lie between $153 \text{ sec}^{-1} \le k_{pd,v'} \le 1.5 \times 10^5 \text{ sec}^{-1}$. A

"comparison" between the lifetimes reported by Blondeau and Ehret and Gerber to these rate constants is shown below in Figure 6-1.
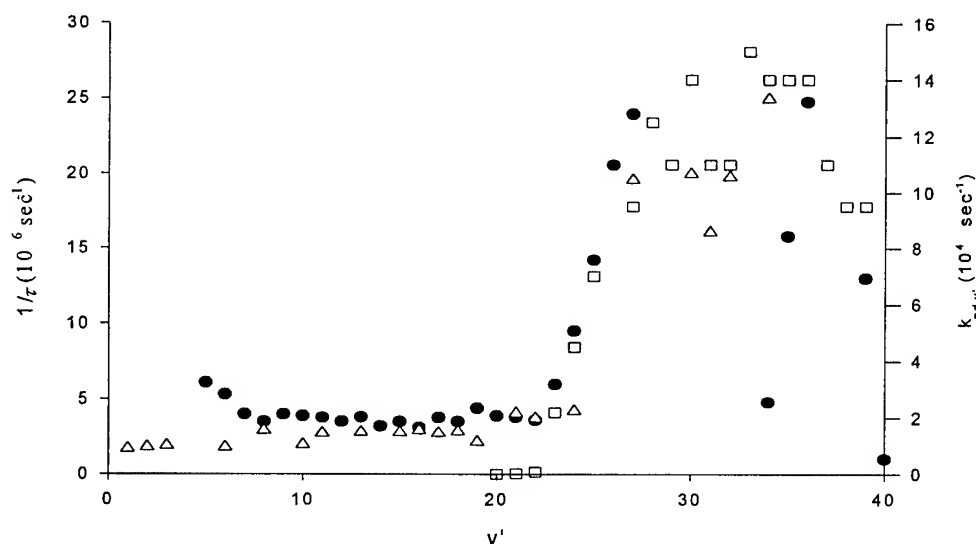
Figure 6-1. Comparison of the reported trends in lifetime behavior for Blondeua [●] and Ehret and Gerber [△] to the predissociation rates [□] reported in this work

Lifetime and spectroscopic data were used in combination to identify and explore a numerical solution for a repulsive state of Bi_2 thought responsible for the observed predissociation. $Bi_2(A)$ RKR potential data and predissociation rates were used as input to a proven numerical model with little success. Results from this extensive analysis indicate that the current methods used to determine analytic forms of the repulsive potentials from predissociation data are inadequate for the case of $Bi_2(A)$ predissociation. The results of Chapter 5 illustrate the interaction between a single repulsive state and the

bound A-state potential is inadequate to replicate the predissociation rates determined in Chapter 4.

6.2. Conclusions

Several important ideas have been conveyed in this dissertation. First, much of this work would not have been possible without the development of novel techniques to address the complexities associated with marrying theoretical constructs to experimental shortcomings, and vice versa. First, in Chapter 3, the difficulties of expanding the current understanding of the spectroscopy of the A-state of Bi_2 were addressed by PC-based mathematical modeling techniques that assisted in both the assignment and fitting of megabytes of spectral data. The extraction of predissociation rate constants from unresolved spectra was another significant achievement presented in this dissertation. The novel approach used in the synthetic spectrum fits complimented the traditional analysis well. Finally, numerical methods were used to determine that the observed predissociation rates could not be adequately represented by current theory. Confidence in this conclusion would not have been possible without the ability to perform an exhaustive study of the available model parameter space.

The most significant findings contained within this dissertation are those of importance to the spectroscopic community as a whole. Foremost amongst these results is the association of A-state dissociation products to $^4S + {}^2D$ separated atoms. The reporting of predissociation rates and a determination that the predissociation is

heterogeneous is also significant. The combination of these results suggests that a significant amount of work remains to be accomplished before a reliable picture of the electronic structure of the bismuth dimer can be determined.

6.3.   Suggestions for Further Studies

Several follow-on studies are indicated. A detailed experimental and theoretical analysis of the electronic states of Bi_2 needs to be performed. One must also address improving existing predissociation theory to account for the predissociation rates reported in Chapter 4. A re-evaluation of existing numerical techniques is needed to address these discrepancies in a practical manner. The modeling process may need to be expanded to include the effects of several interacting states. Any numerical model redesign should include simplification of the trail and error process now involved in selecting candidate potentials.

The density of the spectral features of the $Bi_2(X\leftrightarrow A)$ transition presented the greatest obstacle in defining a permanent set of spectroscopic constants for the $X\leftrightarrow A$ system. A doppler-limited-resolution spectral data set needs to be taken for the basis of any future spectral analysis. Two possibilities exist to produce this data. Either a high-resolution laser induced fluorescence (LIF) experiment, such as that presented by Franklin and Perram [6], or a high-resolution Fourier Transform absorption experiment may be used to piece together an improved spectrum. The absorption experiment would benefit greatly from the use of a heat-pipe arrangement, which could re-cycle the metallic

bismuth providing for longer collection times and, therefore, a reduce noise in the spectrum. Furthermore, an absorption experiment has the benefit of not contending with the strong predissociation present in the higher v-levels.

A doppler-limited absorption spectrum may produce predissociation rate data for the A-state of Bi_2. Since the heterogeneous predissociation of the A-state is a function of $J(J+1)$ and the predissociation rates are so large, the linewidths of affected spectra will dramatically increase with increasing J. Line-broadening data would provide independent comparison and verification of the results presented in Chapter 4. Furthermore, an expanded spectral range may be available for analysis thus extending the range of $k_{pd,v'}$ values reported.

Finally, the opportunity exists to further improve to the software used in this dissertation. The DataFit, GlobalFit, and DataPlot software, written for this research, may be upgraded and/or combined to produce a very robust spectral assignment, fit and analysis package. Ideally, a single software tool could sort through spectral data, assign features in that data, and provide global term value fits. Also, the software from "legacy codes", used by many students, must be updated if it is to remain a viable and reliable tool. Most of these DOS-based programs are simply outdated in the Windows environment.

Table A-1 contains experimentally determined rotational line positions for the

$(v',v'') = (31,2)$ vibrational band of the $Bi_2(X \rightarrow A)$ absorption spectrum.

Table A-1. Rotational line positions and assignment for the (31,2) band

m	v (cm^{-1})	m	v (cm^{-1})	m	v (cm^{-1})
-197	20972.06	-146	21056.86	-95	21117.08
-196	20973.99	-144	21059.71	-94	21117.94
-194	20977.68	-143	21061.18	-93	21118.82
-193	20979.51	-141	21063.79	-92	21119.89
-192	20981.55	-139	21066.58	-91	21120.73
-190	20985.19	-138	21068.09	-89	21122.48
-189	20986.90	-137	21069.35	-88	21123.32
-188	20988.72	-136	21070.63	-87	21124.29
-187	20990.61	-135	21071.91	-86	21125.16
-186	20992.45	-134	21073.22	-84	21126.84
-185	20994.23	-133	21074.48	-81	21129.14
-183	20997.80	-132	21075.93	-80	21130.12
-182	20999.54	-131	21077.07	-79	21130.83
-181	21001.29	-130	21078.54	-78	21131.66
-177	21008.28	-129	21079.76	-77	21132.41
-176	21009.89	-126	21083.39	-75	21133.87
-175	21011.67	-123	21087.13	-73	21135.34
-174	21013.29	-122	21088.26	-72	21136.05
-173	21015.03	-121	21089.49	-70	21137.52
-172	21016.71	-120	21090.64	-69	21138.08
-171	21018.29	-119	21091.72	-68	21138.78
-169	21021.80	-118	21092.98	-67	21139.52
-167	21024.95	-117	21094.21	-66	21140.27
-163	21031.45	-114	21097.60	-65	21140.98
-162	21032.99	-113	21098.53	-64	21141.65
-161	21034.56	-112	21099.74	-63	21142.10
-160	21035.99	-111	21100.88	-62	21142.87
-158	21039.22	-109	21102.96	-60	21143.99
-157	21040.64	-108	21104.07	-58	21145.14
-156	21042.22	-105	21107.14	-57	21145.81
-154	21045.33	-104	21108.33	-56	21146.40
-153	21046.70	-102	21110.18	-55	21146.98
-150	21051.12	-101	21111.27	-54	21147.53
-149	21052.67	-100	21112.10	-52	21148.58
-148	21054.14	-98	21114.08	-51	21149.17
-147	21055.43	-97	21115.12	-49	21150.05

m	ν (cm^{-1})	m	ν (cm^{-1})	m	ν (cm^{-1})
-48	21150.71	76	21139.33	139	21077.84
-47	21151.04	77	21138.52	140	21076.62
-46	21151.66	79	21137.27	141	21075.26
-44	21152.44	80	21136.59	142	21073.96
-43	21153.01	82	21134.98	143	21072.77
-42	21153.40	83	21134.41	144	21071.38
-39	21154.72	84	21133.66	145	21070.14
-37	21155.48	86	21132.00	146	21068.78
-36	21155.84	87	21131.37	148	21066.05
-35	21156.19	89	21129.77	149	21064.75
-34	21156.67	90	21128.90	150	21063.29
-33	21156.95	91	21128.08	152	21060.53
-32	21157.23	92	21127.15	153	21059.13
-31	21157.70	93	21126.51	155	21056.29
-30	21158.02	98	21122.23	156	21054.85
-29	21158.34	99	21121.26	157	21053.36
-28	21158.49	100	21120.37	158	21052.03
36	21158.77	104	21116.70	160	21049.18
37	21158.49	108	21112.75	164	21043.14
40	21157.52	111	21109.80	165	21041.62
41	21157.23	112	21108.90	167	21038.43
47	21154.96	113	21107.85	169	21035.40
48	21154.48	114	21106.83	170	21033.92
49	21154.15	115	21105.85	173	21029.11
51	21153.19	116	21104.58	174	21027.53
52	21152.85	117	21103.51	176	21024.25
53	21152.44	118	21102.53	177	21022.69
54	21151.94	119	21101.48	179	21019.41
55	21151.46	120	21100.40	180	21017.64
56	21151.04	121	21099.39	181	21015.96
57	21150.35	123	21097.02	184	21010.96
58	21150.05	124	21095.90	185	21009.27
59	21149.54	125	21094.92	188	21004.00
60	21148.84	126	21093.55	189	21002.38
61	21148.39	127	21092.59	191	20998.85
62	21147.91	128	21091.45	192	20997.02
63	21147.32	129	21090.27	193	20995.20
64	21146.65	130	21088.98	194	20993.45
65	21146.04	131	21087.89	195	20991.71
66	21145.60	133	21085.34	198	20986.23
67	21144.93	134	21084.18	200	20982.54
70	21143.11	135	21083.00	201	20980.70
71	21142.58	136	21081.69	202	20978.80
74	21140.72	138	21079.12	204	20975.00
75	21140.07				

The following table contains A-state term values determined from Table Curve™ fits to individual vibrational band rotational features. Ground state term values from coefficients presented by Barrow et al. [1] are also included. All constants are quoted in units of cm^{-1}.

Table B-1. Band-by-band term values determined from the Bi$_2$(X→A) spectrum

v'	v"	ν_0	$B_{v'}$	$D_{v'}$	$B_{v''}$	$D_{v''}$
0	4	17035.81	0.01964	1.70E-09	0.02257	1.66E-09
0	7	16530.38	0.01964	1.77E-09	0.02241	1.73E-09
0	5	16866.58	0.01960	1.66E-09	0.02252	1.68E-09
1	2	17508.35	0.01959	1.75E-09	0.02267	1.61E-09
1	3	17337.56	0.01959	1.72E-09	0.02262	1.64E-09
1	4	17167.56	0.01959	1.76E-09	0.02257	1.66E-09
1	5	16998.34	0.01960	1.66E-09	0.02252	1.68E-09
2	2	17639.49	0.01954	1.69E-09	0.02267	1.61E-09
2	3	17468.71	0.01954	1.73E-09	0.02262	1.64E-09
2	4	17298.69	0.01954	1.78E-09	0.02257	1.66E-09
2	5	17129.48	0.01950	1.67E-09	0.02252	1.68E-09
3	0	18113.81	0.01949	1.76E-09	0.02278	1.56E-09
3	1	17941.51	0.01950	1.84E-09	0.02273	1.59E-09
3	2	17769.98	0.01949	1.80E-09	0.02267	1.61E-09
4	0	18243.67	0.01944	1.80E-09	0.02278	1.56E-09
4	1	18071.41	0.01944	1.74E-09	0.02273	1.59E-09
4	2	17899.89	0.01944	1.72E-09	0.02267	1.61E-09
4	3	17729.12	0.01944	1.73E-09	0.02262	1.64E-09
5	0	18372.94	0.01939	1.75E-09	0.02278	1.56E-09
5	1	18372.94	0.01939	1.75E-09	0.02273	1.59E-09
5	2	18029.13	0.01939	1.77E-09	0.02267	1.61E-09
5	3	17858.36	0.01939	1.78E-09	0.02262	1.64E-09
6	0	18501.56	0.01934	1.77E-09	0.02278	1.56E-09
6	1	18329.28	0.01933	1.80E-09	0.02273	1.59E-09
6	2	18157.75	0.01933	1.74E-09	0.02267	1.61E-09
6	3	17986.99	0.01934	1.79E-09	0.02262	1.64E-09
7	0	18629.56	0.01928	1.78E-09	0.02278	1.56E-09
7	1	18457.28	0.01928	1.77E-09	0.02273	1.59E-09
7	2	18285.74	0.01928	1.75E-09	0.02267	1.61E-09
8	0	18756.89	0.01920	1.84E-09	0.02278	1.56E-09
8	1	18584.63	0.01923	1.82E-09	0.02273	1.59E-09

v'	v"	ν₀	Bᵥ	Dᵥ	Bᵥ'	Dᵥ'
8	2	18413.09	0.01923	1.81E-09	0.02267	1.61E-09
8	3	18242.32	0.01923	1.79E-09	0.02262	1.64E-09
9	0	18883.62	0.01920	1.88E-09	0.02278	1.56E-09
9	1	18711.35	0.01918	1.78E-09	0.02273	1.59E-09
9	2	18539.83	0.01918	1.79E-09	0.02267	1.61E-09
9	3	18369.05	0.01918	1.77E-09	0.02262	1.64E-09
10	1	18837.43	0.01912	1.80E-09	0.02273	1.59E-09
10	2	18665.91	0.01913	1.79E-09	0.02267	1.61E-09
10	3	18495.14	0.01913	1.78E-09	0.02262	1.64E-09
11	0	19135.15	0.01907	1.80E-09	0.02278	1.56E-09
11	1	18962.87	0.01907	1.83E-09	0.02273	1.59E-09
11	3	18620.58	0.01907	1.79E-09	0.02262	1.64E-09
12	0	19259.98	0.01902	1.83E-09	0.02278	1.56E-09
12	1	19087.65	0.01902	1.84E-09	0.02273	1.59E-09
12	2	18916.15	0.01902	1.80E-09	0.02267	1.61E-09
13	1	19211.82	0.01897	1.87E-09	0.02273	1.59E-09
13	3	18869.55	0.01897	1.78E-09	0.02262	1.64E-09
14	1	19335.37	0.01891	1.83E-09	0.02273	1.59E-09
14	2	19163.81	0.01892	1.84E-09	0.02267	1.61E-09
15	1	19458.22	0.01886	1.85E-09	0.02273	1.59E-09
15	2	19286.68	0.01886	1.85E-09	0.02267	1.61E-09
16	4	19068.13	0.01881	1.83E-09	0.02257	1.66E-09
17	2	19530.48	0.01875	1.89E-09	0.02267	1.61E-09
17	3	19359.73	0.01875	1.85E-09	0.02262	1.64E-09
18	1	19822.95	0.01869	1.86E-09	0.02273	1.59E-09
18	2	19651.40	0.01870	1.89E-09	0.02267	1.61E-09
18	3	19480.63	0.01870	1.86E-09	0.02262	1.64E-09
18	4	19310.64	0.01870	1.85E-09	0.02257	1.66E-09
19	0	20115.50	0.01864	1.89E-09	0.02278	1.56E-09
19	3	19600.91	0.01864	1.85E-09	0.02262	1.64E-09
20	1	20062.85	0.01858	1.91E-09	0.02273	1.59E-09
20	2	19891.30	0.01859	1.89E-09	0.02267	1.61E-09
20	3	19720.52	0.01859	1.84E-09	0.02262	1.64E-09
20	4	19550.52	0.01859	1.87E-09	0.02257	1.66E-09
21	0	20354.05	0.01853	1.96E-09	0.02278	1.56E-09
21	2	20010.28	0.01853	1.86E-09	0.02267	1.61E-09
21	3	19839.48	0.01853	1.91E-09	0.02262	1.64E-09
22	0	20472.37	0.01848	1.93E-09	0.02278	1.56E-09
22	1	20300.09	0.01847	1.91E-09	0.02273	1.59E-09
22	2	20128.57	0.01848	1.85E-09	0.02267	1.61E-09
22	3	19957.80	0.01848	1.87E-09	0.02262	1.64E-09
23	0	20590.01	0.01842	1.92E-09	0.02278	1.56E-09
23	1	19839.48	0.01864	1.91E-09	0.02273	1.59E-09
23	2	20246.20	0.01842	1.95E-09	0.02267	1.61E-09
23	3	20075.43	0.01842	1.89E-09	0.02262	1.64E-09
24	2	20363.19	0.01836	1.90E-09	0.02267	1.61E-09
24	3	20192.42	0.01836	1.89E-09	0.02262	1.64E-09

v'	v''	v_0	B_v	D_v	$B_{v'}$	$D_{v'}$
25	0	20823.31	0.01831	1.96E-09	0.02278	1.56E-09
25	1	20651.04	0.01830	1.90E-09	0.02273	1.59E-09
25	2	20479.52	0.01831	1.87E-09	0.02267	1.61E-09
25	3	20308.74	0.01831	1.89E-09	0.02262	1.64E-09
26	0	20938.95	0.01825	1.97E-09	0.02278	1.56E-09
26	2	20595.16	0.01825	1.93E-09	0.02267	1.61E-09
27	0	21053.95	0.01820	1.98E-09	0.02278	1.56E-09
27	1	20881.67	0.01819	1.97E-09	0.02273	1.59E-09
27	2	20710.15	0.01819	1.95E-09	0.02267	1.61E-09
27	4	20369.38	0.01819	1.94E-09	0.02257	1.66E-09
28	1	20996.00	0.01814	1.96E-09	0.02273	1.59E-09
28	2	20824.48	0.01814	1.94E-09	0.02267	1.61E-09
29	0	21281.94	0.01808	1.94E-09	0.02278	1.56E-09
29	1	20938.13	0.01808	1.97E-09	0.02273	1.59E-09
29	2	20938.13	0.01808	1.97E-09	0.02267	1.61E-09
30	0	21394.91	0.01802	1.97E-09	0.02278	1.56E-09
30	1	21334.95	0.01796	2.00E-09	0.02273	1.59E-09
30	2	21051.13	0.01802	1.96E-09	0.02267	1.61E-09
31	0	21507.24	0.01796	1.99E-09	0.02278	1.56E-09
31	1	21334.95	0.01796	2.00E-09	0.02273	1.59E-09
31	2	21163.45	0.01796	1.95E-09	0.02267	1.61E-09
32	1	21446.59	0.01790	1.97E-09	0.02273	1.59E-09
32	2	21275.06	0.01791	2.00E-09	0.02267	1.61E-09
33	0	21729.85	0.01785	1.96E-09	0.02278	1.56E-09
33	1	21557.57	0.01784	1.97E-09	0.02273	1.59E-09
33	2	21386.02	0.01785	1.98E-09	0.02267	1.61E-09
34	0	21840.13	0.01779	1.99E-09	0.02278	1.56E-09
34	1	21667.85	0.01778	1.98E-09	0.02273	1.59E-09
34	2	21496.33	0.01789	1.99E-09	0.02267	1.61E-09
35	0	21949.75	0.01773	2.04E-09	0.02278	1.56E-09
35	2	21605.94	0.01773	2.00E-09	0.02267	1.61E-09
36	0	22058.66	0.01767	2.02E-09	0.02278	1.56E-09
36	1	21886.37	0.01767	1.99E-09	0.02273	1.59E-09
37	0	22166.90	0.01761	2.06E-09	0.02278	1.56E-09
37	1	21994.63	0.01761	1.99E-09	0.02273	1.59E-09
37	2	21823.10	0.01761	2.01E-09	0.02267	1.61E-09
38	0	22274.47	0.01755	2.05E-09	0.02278	1.56E-09
38	1	22102.19	0.01755	2.04E-09	0.02273	1.59E-09
38	2	21930.67	0.01755	1.99E-09	0.02267	1.61E-09
39	0	22381.34	0.01749	2.03E-09	0.02278	1.56E-09
39	1	22209.07	0.01749	2.07E-09	0.02273	1.59E-09
39	2	22037.54	0.01749	2.05E-09	0.02267	1.61E-09
40	0	22487.54	0.01743	2.03E-09	0.02278	1.56E-09
40	2	22143.75	0.01743	2.00E-09	0.02267	1.61E-09
41	0	22593.03	0.01737	2.09E-09	0.02278	1.56E-09
41	2	22249.23	0.01737	2.01E-09	0.02267	1.61E-09

v'	v"	ν_0	$B_{v'}$	$D_{v'}$	$B_{v''}$	$D_{v''}$
42	0	22697.85	0.01731	2.08E-09	0.02278	1.56E-09
42	1	22525.58	0.01730	2.03E-09	0.02273	1.59E-09
42	2	22354.04	0.01731	2.03E-09	0.02267	1.61E-09
43	0	22801.98	0.01724	2.02E-09	0.02278	1.56E-09
43	1	22629.70	0.01724	2.05E-09	0.02273	1.59E-09
44	0	22905.40	0.01718	2.06E-09	0.02278	1.56E-09
44	1	22733.12	0.01718	2.04E-09	0.02273	1.59E-09
44	2	22561.59	0.01718	2.06E-09	0.02267	1.61E-09
45	1	22835.85	0.01712	2.08E-09	0.02273	1.59E-09
45	2	22664.31	0.01712	2.05E-09	0.02267	1.61E-09
46	0	23110.15	0.01706	2.06E-09	0.02278	1.56E-09
46	1	22937.86	0.01706	2.13E-09	0.02273	1.59E-09
46	2	22766.35	0.01706	2.05E-09	0.02267	1.61E-09
47	0	23211.49	0.01700	2.08E-09	0.02278	1.56E-09
47	1	23039.21	0.01700	2.11E-09	0.02273	1.59E-09
47	2	22867.66	0.01700	2.11E-09	0.02267	1.61E-09
48	0	23312.13	0.01693	2.07E-09	0.02278	1.56E-09
48	1	23139.84	0.01693	2.12E-09	0.02273	1.59E-09
49	0	23412.06	0.01687	2.10E-09	0.02278	1.56E-09
49	1	23239.79	0.01687	2.08E-09	0.02273	1.59E-09
49	2	23068.25	0.01687	2.09E-09	0.02267	1.61E-09
50	2	23167.47	0.01681	2.13E-09	0.02267	1.61E-09
51	0	23609.80	0.01675	2.13E-09	0.02278	1.56E-09
51	1	23437.52	0.01674	2.12E-09	0.02273	1.59E-09
51	2	23266.02	0.01674	2.08E-09	0.02267	1.61E-09
52	0	23707.61	0.01668	2.15E-09	0.02278	1.56E-09
52	2	23363.81	0.01668	2.11E-09	0.02267	1.61E-09
53	0	23804.73	0.01662	2.17E-09	0.02278	1.56E-09
53	1	23632.44	0.01661	2.11E-09	0.02273	1.59E-09
53	2	23460.93	0.01662	2.15E-09	0.02267	1.61E-09
54	0	23901.14	0.01655	2.17E-09	0.02278	1.56E-09
54	1	23728.85	0.01655	2.13E-09	0.02273	1.59E-09
54	2	23557.32	0.01655	2.14E-09	0.02267	1.61E-09
55	0	23996.81	0.01649	2.18E-09	0.02278	1.56E-09
55	2	23653.01	0.01649	2.12E-09	0.02267	1.61E-09
56	1	23919.49	0.01642	2.17E-09	0.02273	1.59E-09
56	2	23747.97	0.01643	2.19E-09	0.02267	1.61E-09
57	0	24186.04	0.01636	2.19E-09	0.02278	1.56E-09
57	2	23842.24	0.01636	2.15E-09	0.02267	1.61E-09
58	0	24279.59	0.01629	2.15E-09	0.02278	1.56E-09
58	1	24107.31	0.01629	2.18E-09	0.02273	1.59E-09
58	2	23935.78	0.01630	2.19E-09	0.02267	1.61E-09
59	0	24372.42	0.01623	2.18E-09	0.02278	1.56E-09
59	1	24200.13	0.01623	2.17E-09	0.02273	1.59E-09
60	0	24464.51	0.01617	2.23E-09	0.02278	1.56E-09
60	1	24292.23	0.01616	2.17E-09	0.02273	1.59E-09

v'	v"	ν_0	$B_{v'}$	$D_{v'}$	$B_{v''}$	$D_{v''}$
61	0	24555.89	0.01610	2.19E-09	0.02278	1.56E-09
61	1	24383.60	0.01610	2.24E-09	0.02273	1.59E-09
62	0	24646.55	0.01603	2.22E-09	0.02278	1.56E-09
62	1	24474.26	0.01603	2.24E-09	0.02273	1.59E-09
62	2	24302.74	0.01603	2.19E-09	0.02267	1.61E-09
63	0	24736.47	0.01597	2.27E-09	0.02278	1.56E-09
63	1	24564.21	0.01596	2.20E-09	0.02273	1.59E-09
63	2	24392.70	0.01596	2.18E-09	0.02267	1.61E-09
64	0	24825.68	0.01590	2.22E-09	0.02278	1.56E-09
64	2	24481.87	0.01590	2.22E-09	0.02267	1.61E-09
65	0	24914.17	0.01583	2.25E-09	0.02278	1.56E-09
65	1	24741.88	0.01583	2.23E-09	0.02273	1.59E-09
65	2	24570.36	0.01583	2.21E-09	0.02267	1.61E-09
66	1	24829.63	0.01576	2.29E-09	0.02273	1.59E-09
67	0	25088.94	0.01570	2.23E-09	0.02278	1.56E-09
67	1	24916.65	0.01569	2.21E-09	0.02273	1.59E-09
68	0	25175.22	0.01563	2.27E-09	0.02278	1.56E-09
68	1	25002.93	0.01563	2.28E-09	0.02273	1.59E-09
68	2	24831.40	0.01563	2.26E-09	0.02267	1.61E-09
69	0	25260.75	0.01556	2.27E-09	0.02278	1.56E-09
69	1	25088.48	0.01556	2.24E-09	0.02273	1.59E-09
69	2	24916.95	0.01556	2.26E-09	0.02267	1.61E-09
70	1	25173.29	0.01549	2.27E-09	0.02273	1.59E-09
71	0	25429.65	0.01542	2.29E-09	0.02278	1.56E-09
71	1	25257.36	0.01542	2.25E-09	0.02273	1.59E-09
72	0	25512.99	0.01535	2.27E-09	0.02278	1.56E-09
72	1	25340.69	0.01535	2.27E-09	0.02273	1.59E-09
72	2	25169.17	0.01535	2.29E-09	0.02267	1.61E-09
73	1	25423.29	0.01528	2.29E-09	0.02273	1.59E-09
74	0	25677.42	0.01522	2.34E-09	0.02278	1.56E-09
74	1	25505.14	0.01521	2.32E-09	0.02273	1.59E-09
75	0	25758.51	0.01515	2.34E-09	0.02278	1.56E-09
76	0	25838.89	0.01507	2.27E-09	0.02278	1.56E-09
76	2	25495.07	0.01508	2.30E-09	0.02267	1.61E-09
77	0	25918.50	0.01500	2.32E-09	0.02278	1.56E-09
77	1	25746.21	0.01500	2.34E-09	0.02273	1.59E-09
77	2	25574.69	0.01500	2.30E-09	0.02267	1.61E-09
78	0	25997.36	0.01493	2.32E-09	0.02278	1.56E-09
78	1	25825.07	0.01493	2.32E-09	0.02273	1.59E-09
78	2	25653.54	0.01493	2.33E-09	0.02267	1.61E-09
79	0	26075.46	0.01487	2.38E-09	0.02278	1.56E-09
79	1	25903.18	0.01486	2.36E-09	0.02273	1.59E-09
79	2	25731.66	0.01486	2.33E-09	0.02267	1.61E-09
80	1	25980.53	0.01479	2.36E-09	0.02273	1.59E-09
80	2	25809.01	0.01479	2.33E-09	0.02267	1.61E-09

v'	v''	v_0	B_v	D_v	$B_{v''}$	$D_{v''}$
81	0	26229.41	0.01472	2.36E-09	0.02278	1.56E-09
81	2	25885.62	0.01472	2.33E-09	0.02267	1.61E-09
82	0	26305.26	0.01465	2.38E-09	0.02278	1.56E-09
82	2	25961.46	0.01465	2.34E-09	0.02267	1.61E-09
83	0	26380.34	0.01458	2.38E-09	0.02278	1.56E-09
83	2	26036.54	0.01458	2.38E-09	0.02267	1.61E-09
85	0	26528.24	0.01443	2.40E-09	0.02278	1.56E-09
86	1	26428.76	0.01436	2.40E-09	0.02273	1.59E-09
87	0	26673.07	0.01429	2.43E-09	0.02278	1.56E-09
88	0	26744.33	0.01422	2.48E-09	0.02278	1.56E-09
91	0	26953.56	0.01399	2.42E-09	0.02278	1.56E-09

The complete set of band-by-band spectral data from Appendix B, for both the A

and X-states, has been processed using the GlobalFit program [31]. GlobalFit performs a

simultaneous least-squares-fit to all bands and outputs the best global fit results. The X-

state constants were not allowed to vary from the values presented in Table B-1. The fit

results, in units of cm^{-1} are presented below in Table C-1.

Table C-1. Globally fit term values from the GlobalFit program output file

v'	Bv'	Dv'	Std Dev	v'	Bv'	Dv'	Std Dev
0	0.01964	1.77E-09	0.04526	26	0.01825	1.94E-09	0.06577
1	0.01959	1.75E-09	0.04155	27	0.01820	1.96E-09	0.06328
2	0.01954	1.75E-09	0.04068	28	0.01814	1.95E-09	0.06758
3	0.01949	1.79E-09	0.04788	29	0.01808	1.94E-09	0.06604
4	0.01944	1.75E-09	0.04632	30	0.01802	1.94E-09	0.06749
5	0.01939	1.77E-09	0.03942	31	0.01796	1.97E-09	0.06503
6	0.01934	1.77E-09	0.04572	32	0.01791	1.98E-09	0.06664
7	0.01928	1.75E-09	0.04386	33	0.01785	1.96E-09	0.06628
8	0.01923	1.81E-09	0.04466	34	0.01779	1.98E-09	0.06679
9	0.01918	1.80E-09	0.04398	35	0.01773	2.01E-09	0.06340
10	0.01913	1.79E-09	0.04631	36	0.01767	1.99E-09	0.06702
11	0.01907	1.80E-09	0.06298	37	0.01761	2.01E-09	0.06586
12	0.01902	1.81E-09	0.05967	38	0.01755	2.02E-09	0.06539
13	0.01897	1.83E-09	0.06678	39	0.01749	2.04E-09	0.06785
14	0.01891	1.83E-09	0.06355	40	0.01743	2.01E-09	0.06582
15	0.01886	1.85E-09	0.06396	41	0.01737	2.04E-09	0.06741
16	0.01881	1.88E-09	0.06698	42	0.01731	2.03E-09	0.06630
17	0.01875	1.87E-09	0.06822	43	0.01724	2.02E-09	0.06538
18	0.01870	1.88E-09	0.06595	44	0.01718	2.04E-09	0.06739
19	0.01864	1.87E-09	0.06709	45	0.01712	2.06E-09	0.06370
20	0.01859	1.89E-09	0.06591	46	0.01706	2.07E-09	0.06461
21	0.01853	1.91E-09	0.06606	47	0.01700	2.09E-09	0.06556
22	0.01848	1.88E-09	0.06657	48	0.01693	2.08E-09	0.06397
24	0.01836	1.91E-09	0.06335	49	0.01687	2.08E-09	0.06552
25	0.01831	1.90E-09	0.06423	50	0.01681	2.13E-09	0.06200

v'	Bv'	Dv'	Std Dev	v'	Bv'	Dv'	Std Dev
51	0.01675	2.10E-09	0.06522	70	0.01549	2.26E-09	0.06174
52	0.01668	2.12E-09	0.06560	71	0.01542	2.25E-09	0.06635
53	0.01662	2.14E-09	0.06028	72	0.01535	2.26E-09	0.06282
54	0.01655	2.13E-09	0.06330	73	0.01528	2.28E-09	0.06151
55	0.01649	2.14E-09	0.06465	74	0.01522	2.31E-09	0.06548
56	0.01643	2.18E-09	0.06431	75	0.01515	2.32E-09	0.06188
57	0.01636	2.16E-09	0.06279	76	0.01507	2.27E-09	0.06769
58	0.01629	2.16E-09	0.06324	77	0.01500	2.31E-09	0.06609
59	0.01623	2.16E-09	0.06233	78	0.01493	2.31E-09	0.06286
60	0.01616	2.18E-09	0.06418	79	0.01486	2.34E-09	0.06395
61	0.01610	2.19E-09	0.06541	80	0.01479	2.34E-09	0.06403
62	0.01603	2.20E-09	0.06663	81	0.01472	2.34E-09	0.06112
63	0.01596	2.21E-09	0.06600	82	0.01465	2.36E-09	0.06176
64	0.01590	2.21E-09	0.06461	83	0.01458	2.37E-09	0.06210
65	0.01583	2.22E-09	0.06529	85	0.01443	2.38E-09	0.04292
66	0.01576	2.28E-09	0.06980	86	0.01436	2.39E-09	0.04426
67	0.01569	2.20E-09	0.06247	87	0.01429	2.41E-09	0.04446
68	0.01563	2.26E-09	0.06472	88	0.01422	2.46E-09	0.06244
69	0.01556	2.24E-09	0.06455	91	0.01399	2.40E-09	0.06684

Appendix D

Positional information on the vibrational band system for the $Bi_2(A{\to}X)$ laser excitation spectrum, Tables D-1 and D-2, and the resulting rotational assignments from bands $(v',v'') = (21,0)$ and $(22,0)$, Table D-3, are presented in this appendix. All band head and line positions are in units of cm^{-1}.

Table D-1. Vibrational band head locations for the $Bi_2\ A0_u^+ \to X^1\Sigma_g^+$ band system

v' \ v"	0	1	2	3	4	5	6	7
8	18756.86							
9	18884.90							
10	19011.17	18839.04						
11	19136.12		18792.25					
12	19261.12		18917.71					
13	19384.52	19212.68	19041.40					
14	19507.14	19335.63	19164.38		18823.12			
15	19629.68	19458.70	19286.78			18776.85		
16	19751.70	19579.90		19239.20				
17	19873.14	19701.55		19360.11				
18	19993.73	19822.41			19311.72			
19	20114.16	19942.12	19770.60	19600.38	19431.37			
20	20233.39	20061.56	19890.53		19550.01			
21	20352.05	20179.67	20008.87		19667.81			
22	20469.68	20298.51	20127.32	19956.75				
23	20587.01	20415.03	20244.43	20074.58		19734.80		
24	20703.46	20531.81	20360.52	20191.04				
25	20818.68	20647.95	20476.83	20307.21				
26	20934.60	20763.50	20592.15	20421.68				
27	21049.54	20877.36	20706.57	20536.57	20366.53			
28	21164.22	20991.18	20820.24	20650.29	20480.95			
29	21278.92	21104.75	20933.67	20763.50	20594.25			
30	21390.34	21219.78	21046.54	20875.88	20706.57	20538.20		
31	21502.46	21331.04	21159.01	20987.54	20818.68	20650.29		
32	21613.26	21442.25	21271.70	21099.07	20929.53		20594.25	
33	21724.06	21551.69	21382.03	21211.73	21040.41		20703.46	20538.20
34	21835.13	21661.25	21491.58	21321.64	21150.47	20981.08	20813.32	
35	21944.38	21770.27	21599.63	21430.70	21261.34	21090.46	20922.35	
36			21707.98	21540.20	21369.45	21199.68	21031.15	
37				21645.95	21477.42	21308.38	21138.91	20971.53
38		21939.39				21415.39	21248.07	21078.60
39			21873.38			21521.77	21354.05	21186.51
40					21808.51		21458.88	21292.48
41					21909.36	21743.28		21397.34
42						21843.57		

Table D-2. Deslandres table (second differences, ΔG, in v') for Bi_2 $A0_u^+ \to X^1\Sigma_g^+$

v'+1 \ v"	0	1	2	3	4	5	6	7
9	128.04							
10	126.27							
11	124.95							
12	125.00		125.46					
13	123.40		123.69					
14	122.62	122.95	122.98					
15	122.54	123.07	122.40					
16	122.02	121.20						
17	121.44	121.65		120.91				
18	120.59	120.86						
19	120.43	119.71			119.65			
20	119.23	119.44	119.93		118.64			
21	118.66	118.11	118.34		117.80			
22	117.63	118.84	118.45					
23	117.33	116.52	117.11	117.83				
24	116.45	116.78	116.09	116.46				
25	115.22	116.14	116.31	116.17				
26	115.92	115.55	115.32	114.47				
27	114.94	113.86	114.42	114.89				
28	114.68	113.82	113.67	113.72	114.42			
29	114.70	113.57	113.43	113.21	113.30			
30	111.42	115.03	112.87	112.38	112.32			
31	112.12	111.26	112.47	111.66	112.11	112.09		
32	110.80	111.21	112.69	111.53	110.85			
33	110.80	109.44	110.33	112.66	110.88		109.21	
34	111.07	109.56	109.55	109.91	110.06		109.86	
35	109.25	109.02	108.05	109.06	110.87	109.38	109.03	
36			108.35	109.50	108.11	109.22	108.80	
37				105.75	107.97	108.70	107.76	
38						107.01	109.16	107.07
39						106.38	105.98	107.91
40							104.83	105.97
41				100.85				104.86
42					100.29			

Table D-3. Rotational assignments and second differences, $\Delta \equiv R(J)-P(J)$, for vibrational manifolds $(v',v'') = (21,0)$ and $(22,0)$

| J | (21,0) | | | (22,0) | | |
	R(J) (cm^{-1})	P(J) (cm^{-1})	Δ (cm^{-1})	R(J) (cm^{-1})	P(J) (cm^{-1})	Δ (cm^{-1})
16		20348.393				
17		20348.182				
18		20347.921				
19		20347.660				
20		20347.391				
21		20347.118				
22		20346.840				
23		20346.576				
24		20346.278				
25		20345.942				
26		20345.594				
27		20345.284				
28		20344.927				
29		20344.629				
30		20344.229				
31		20343.851				
32		20343.455				
33		20343.124				
34		20342.689				
35		20342.300				
36		20341.890				
37		20341.493				
38		20341.047				
39		20340.620				
40		20340.157				
41		20339.744				
42		20339.259				
43		20338.821				
44		20338.324				
45		20337.885				
46		20337.389				
47		20336.872				
48		20336.376				
49		20335.905				
50		20335.362				
51		20334.883				
52		20334.354				
53		20333.849				
54		20333.287				
55		20332.774				
56		20332.134			-	
57		20331.650			20452.334	
58		20331.058			20451.834	
59		20330.514			20451.265	
60		20329.877			20450.749	
61		20329.303			20450.208	
62		20328.686			20449.590	
63		20328.125			20449.055	
64		20327.484		-	20448.454	-

J	(21,0)			(22,0)		
	R(J) (cm⁻¹)	P(J) (cm⁻¹)	Δ (cm⁻¹)	R(J) (cm⁻¹)	P(J) (cm⁻¹)	Δ (cm⁻¹)
65		20326.897		20452.640	20447.827	4.813
66		20326.216		20452.206	20447.251	4.955
67		20325.608		20451.625	20446.615	5.010
68		20324.926		20451.088	20445.979	5.109
69		20324.287		20450.529	20445.358	5.170
70		20323.625		20449.971	20444.727	5.244
71		20322.956		20449.403	20444.112	5.291
72		20322.254		20448.880	20443.427	5.453
73		20321.573		20448.189	20442.794	5.395
74		20320.855		20447.625	20442.088	5.537
75		20320.177		20447.013	20441.428	5.585
76		20319.462		20446.444	20440.743	5.701
77		20318.731		20445.787	20440.065	5.722
78	-	20318.001	-	20445.150	20439.328	5.822
79	20323.084	20317.266	5.818	20444.467	20438.602	5.865
80	20322.395	20316.490	5.905	20443.880	20437.873	6.006
81	20321.688	20315.714	5.974	20443.169	20437.131	6.037
82	-	20314.955	-	20442.528	20436.407	6.121
83	20320.318	20314.154	6.164	20441.839	20435.645	6.194
84	-	20313.349	-	20441.136	20434.926	6.211
85	20318.893	20312.570	6.323	20440.461	20434.133	6.328
86	20318.182	20311.749	6.434	20439.776	20433.367	6.408
87	20317.440	20310.932	6.508	20439.081	20432.553	6.528
88	20316.664	20310.099	6.565	20438.329	20431.766	6.564
89	20315.879	20309.274	6.605	20437.551	20430.963	6.589
90	20315.140	20308.395	6.745	20436.908	20430.139	6.770
91	20314.344	20307.591	6.753	20436.061	20429.331	6.730
92	20313.581	20306.667	6.914	20435.420	20428.489	6.931
93	20312.747	20305.847	6.900	20434.572	20427.666	6.906
94	20311.963	20304.947	7.015	20433.847	20426.818	7.029
95	20311.118	20304.058	7.060	20433.014	20426.000	7.015
96	20310.347	20303.158	7.188	20432.263	20425.161	7.102
97	20309.475	20302.244	7.232	20431.383	20424.297	7.086
98	20308.651	20301.324	7.326	20430.672	20423.405	7.268
99	20307.793	20300.455	7.337	20429.806	20422.526	7.280
100	20306.923	20299.500	7.423	-	20421.678	-
101	20306.048	20298.564	7.484	20428.180	20420.743	7.438
102	20305.182	20297.579	7.603	20427.349	20419.875	7.474
103	20304.309	20296.639	7.670	20426.488	20418.950	7.538
104	20303.394	20295.638	7.755	-	20418.018	-
105	20302.495	20294.692	7.803	20424.782	20417.146	7.636
106	20301.596	20293.695	7.901	-	20416.181	-
107	20300.661	-	-	20423.055	20415.245	7.811
108	20299.779			-	-	-
109	20298.819					
110	20297.806					
111	20296.936					
112	20295.944					
113	20294.930					
114	20293.958					
115	-					
116	20291.899					
117	20290.903					

Appendix E

Results of lifetime analyses detailed in Chapter 4 are presented in Tables E-1 and E-2 below. These tables contain inverse lifetimes, $1/\tau$, inverse collision-free lifetimes, $1/\tau_o$, quenching rates, k_q, and the associated error in each quantity for each J-level investigated. The pressure, P, is the product of several non-specific outgas products, see Section 4.2.

Table E-1. Lifetime analysis results for $(v',v'') = (22,0)$

J	J(J+1)	$1/\tau_0$ (10^6 sec^{-1})	$\sigma 1/\tau_0$ (10^3 sec^{-1})	P (mtorr)	$1/\tau$ (10^6 sec^{-1})	$\sigma 1/\tau$ (10^4 sec^{-1})	k_q $(10^3 \text{ mtorr}^{-1} \text{ sec}^{-1})$	σk_q $(10^2 \text{ mtorr}^{-1} \text{ sec}^{-1})$
58	3422	3.684	29.909	10	3.781	1.135	3.487	3.76
				18	3.747	.9086		
				30	3.755	.7716		
				50	3.787	.9058		
				75	3.930	1.000		
				100	4.045	1.060		
				140	4.190	1.275		
63	4032	4.427	18.853	22	4.456	2.317	1.306	1.66
				50	4.467	1.974		
				75	4.547	2.499		
				100	4.569	2.839		
				127	4.591	22.80		
68	4692	4.988	73.402	27	5.039	4.376	2.237	7.22
				50	5.202	3.050		
				75	5.117	4.268		
				100	5.162	8.880		
				125	5.288	16.92		
88	7832	6.567	8.215	18	6.572	4.942	2.732	8.34
				50	6.618	4.823		
				75	6.646	4.277		
				100	6.664	5.449		
				125	6.881	8.292		
93	8742	8.152	64.048	18	8.220	14.07	2.015	9.69
				50	8.165	7.629		
				75	8.295	9.529		
				100	8.384	10.52		

Table E-2. Lifetime analysis for $(v',v'') = (21,0)$

J	J(J+1)	$1/\tau_0$ (10^6 sec^{-1})	$\sigma 1/\tau_0$ (10^3 sec^{-1})	P (mtorr)	$1/\tau$ (10^6 sec^{-1})	$\sigma 1/\tau$ (10^3 sec^{-1})	k_q $(10^3 \text{ mtorr}^{-1} \text{ sec}^{-1})$	σk_q $(10^2 \text{ mtorr}^{-1} \text{ sec}^{-1})$
18	342	2.117	6.060	13	2.161	1.383	3.189	1.15
				18	2.166	1.328		
				25	2.207	1.223		
				50	2.268	1.286		
				75	2.359	1.269		
				86	2.392	1.390		
28	812	2.251	17.570	20	2.286	1.327	2.848	1.90
				50	2.407	1.407		
				75	2.475	3.064		
				100	2.538	2.854		
				125	2.599	3.391		
38	1482	2.323	12.562	20	2.376	1.937	2.303	1.62
				50	2.439	1.731		
				75	2.475	1.366		
				100	2.554	1.219		
				125	2.622	1.320		
48	2352	2.471	10.559	25	2.561	2.046	3.040	1.13
				50	2.615	3.564		
				75	2.702	4.141		
				100	2.771	6.350		
				125	2.856	6.306		
58	3422	2.501	24.327	50	2.707	3.825	4.178	2.59
				100	2.933	2.426		
				125	3.016	3.111		
68	4692	2.669	7.802	50	2.865	14.034	3.935	0.86
				75	2.970	9.882		
				100	3.059	13.290		
				125	3.163	11.104		
78	6162	3.162	28.979	25	3.230	14.400	3.519	3.33
				50	3.356	18.922		
				75	3.413	14.789		
				100	3.543	18.958		
				125	3.584	21.968		
88	7832	3.185	17.081	25	3.281	14.105	3.843	2.62
				50	3.366	5.042		
				75	3.499	5.350		
				100	3.562	9.060		

Appendix F

This appendix contains the MCAD™ workbook used to calculate the synthetic

spectra as described in Chapter 4. All parameters, other than $k_{pd,v'}$, are have been

determined experimentally. Therefore, $k_{pd,v'}$ can be uniquely determined via this method.

Synthetic Spectrum Tool:

This workbook will produce a predicted laser excitation spectrum for a user defined (v',v")
transition. Furthermore, the effects of predissociation can also bee seen if the predissociation
rate, kpd, and the radiative decay rate, Γo, are defined. The necessary user input data is
contained in Sections 1 and 2.

(1) Define spectral constants:

$B" := .02262 \cdot cm^{-1}$ $\qquad\qquad\qquad B' := .01767 cm^{-}$

(2) Input Section:

Input v':	$v' := 3$	**J min (-):**	$J_{min} = -9$
Input v":	$v" =$	**J max (+):**	$J_{max} := 10$
Input v_0:	$v_0 := 21544.1 cm^{-}$	**Kpd:**	$K_{pd} := 140000 sec^{-}$
Input Laser Doppler Width:	$\Delta v_D := .3 \cdot cm^{-}$	**Γo:**	$\Gamma_0 := 1.76 \cdot 10^6 \cdot sec^{-}$
Input ASE Doppler Width:	$\Delta v_{ase} := 1.55 \cdot cm^{-}$	**kT (cm^{-1}):**	$kT := 208 \cdot cm^{-}$
Input max steps along v axis:	IncMax $:= 50$	**% ASE:**	$ase := 0.2$
Input vmin:			
Input step size:	$v_{step} := 0.02 \cdot cm^{-}$		$v_{min} := 21535 cm^{-}$

[# data points < 64K]

$v_{max} := v_{min} + IncMax \cdot v_{step}$

data $_{JP'} := \left(|J_{min}| + 1 \right) \cdot (IncMax + 1)$

data $_{JR'} := J_{max} (IncMax + 1)$

Input suggest a range from :

$v_{min} = 21535 \cdot$ to $v_{max} = 21545 \cdot$

With IncMax $= 50$ data points in v, and data $_{JP'} = 48$ data $_{JR'} = 52$ in JP' and JR' respectively.

----

(3) Data Analysis:

Define the range variables used in computations:

$i := 0 .. \text{IncMa}$ $\qquad$ $j := 0 .. \left| J_{min} \right|$ $\qquad$ $jj := 0 .. \left(J_{max} - 1 \right)$ $\qquad$ $k := 0 .. \left(\text{IncMax} + 1 \right) \cdot \left(\left| J_{min} \right| + 1 \right) -$

$v_i := v_{min} + v_{step} \cdot$ $\qquad$ $JP'_j := j - \left| J_{min} \right|$ $\qquad$ $JR'_{jj} := 1 + j$ $\qquad$ $kk = 0 .. \left(\text{IncMax} + 1 \right) \cdot J_{max} -$

Define the P and R branch peak energies:

$$EP_j := v_0 + \left[(B' + B'') \cdot \left(JP'_j + 1 \right) + (B' - B'') \cdot \left(JP'_j + 1 \right)^2 \right]$$

$$ER_{jj} := v_0 + \left[(B' + B'') \cdot \left(JR'_{jj} - 1 \right) + (B' - B'') \cdot \left(JR'_{jj} - 1 \right)^2 \right]$$

Define the ratio of signal area under the gate to the total signal (i.e. Ratio = AreaSignalGate/AreaSignal total) of the fluorescence decay curve:

$$RatioP_j := \exp\left[\left(-9.2 \cdot 10^9 \cdot \sec \right) \cdot \left[\Gamma_0 + K_{pd} \cdot \left| JP'_j \right| \cdot \left(\left| JP'_j \right| + 1 \right) \right] \right] - \exp\left[- \left(77.8 \cdot 10^9 \cdot \sec \right) \cdot \left[\Gamma_0 + K_{pd} \cdot \left| JP'_j \right| \cdot \left(\left| JP'_j \right| + 1 \right) \right] \right]$$

$$RatioR_{jj} := \exp\left[\left(-9.2 \cdot 10^9 \cdot \sec \right) \cdot \left[\Gamma_0 + K_{pd} \cdot \left| JR'_{jj} \right| \cdot \left(\left| JR'_{jj} \right| + 1 \right) \right] \right] - \exp\left[- \left(77.8 \cdot 10^9 \cdot \sec \right) \cdot \left[\Gamma_0 + K_{pd} \cdot \left| JR'_{jj} \right| \cdot \left(\left| JR'_{jj} \right| + 1 \right) \right] \right]$$
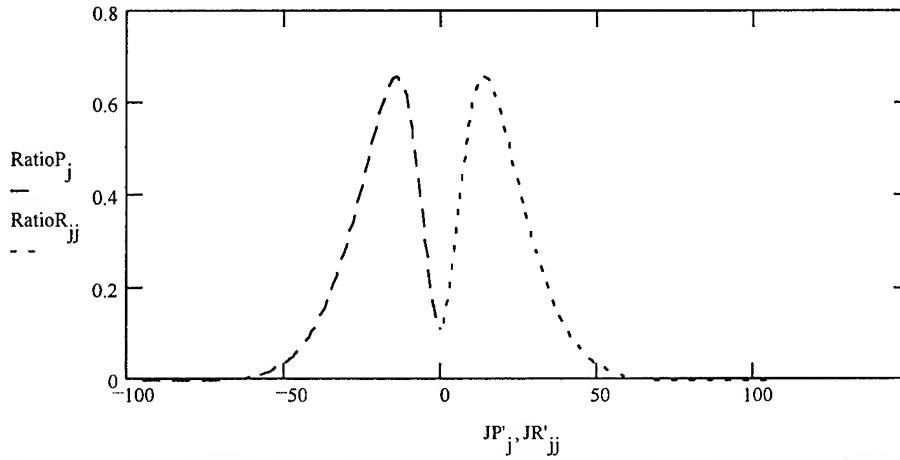
Define the P and R rotational number distributions. These terms include factors for degeneracy, M-B statistics, predissociation, nuclear spin, and variable gate ratios.

$$NrotP_j := \frac{B'' \cdot \left(\left| JP'_j + 1 \right| + \left| JP'_j \right| + 1 \right) \cdot \exp\left[\dfrac{- B'' \cdot \left| JP'_j + 1 \right| \cdot \left(\left| JP'_j + 1 \right| + 1 \right)}{kT} \right]}{kT} \cdot \frac{\Gamma_0 \cdot \left[1.22 - 0.22 \bmod\left(\left(JP'_j + 1 \right), 2 \right) \right]}{\Gamma_0 + K_{pd} \cdot \left| JP'_j \right| \cdot \left(\left| JP'_j \right| + 1 \right)} \cdot RatioP_j$$

$$NrotR_{jj} := \frac{B'' \cdot \left(2 \cdot JR'_{jj} \right) \cdot \exp\left[\dfrac{- B'' \cdot \left| JR'_{jj} - 1 \right| \cdot \left(\left| JR'_{jj} - 1 \right| + 1 \right)}{kT} \right]}{kT} \cdot \frac{\Gamma_0 \cdot \left[1.22 - 0.22 \bmod\left(\left(JR'_{jj} - 1 \right), 2 \right) \right]}{\Gamma_0 + K_{pd} \cdot JR'_{jj} \cdot \left(JR'_{jj} + 1 \right)} \cdot RatioR_{jj}$$

F-2

NrotP$_j$
◇◇◇

NrotR$_{jj}$
·o o o

$\dfrac{NrotR_{jj}}{RatioR_{jj}}$
✕✕✕

5•10^{-4}

4•10^{-4}

3•10^{-4}

2•10^{-4}

1•10^{-4}

0

$-100 \quad -80 \quad -60 \quad -40 \quad -20 \quad 0 \quad 20 \quad 40 \quad 60 \quad 80 \quad 100 \quad 12$

$JP'_j, JR'_{jj}, JR'_{jj}$
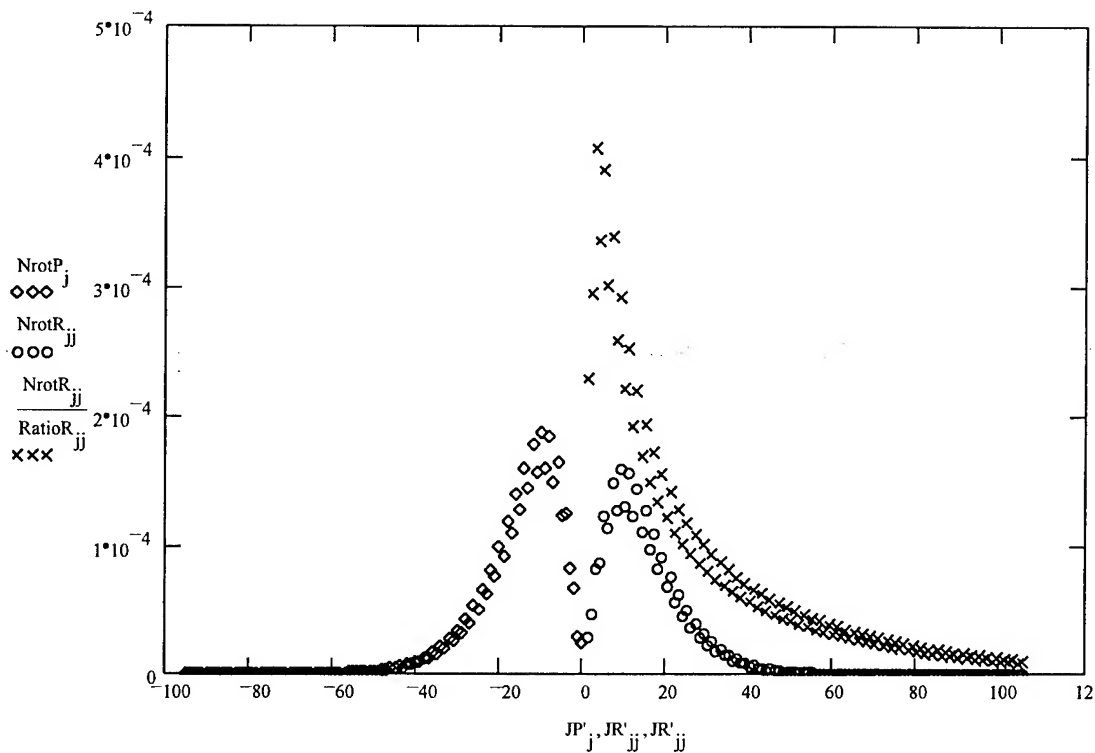
Define the energy differences [ν-E(J)], as a matrix of values, for use in the exponential terms in the lineshape functions:

$$ENGPT_{j,i} := \frac{\nu_i - EP_j}{cm^{-1}} \qquad\qquad ENGRT_{jj,i} := \frac{\nu_i - ER_{jj}}{cm^{-1}}$$

Manipulate the above matricies into a single column matrix:

$ENGP :=$
$\quad B \leftarrow ENGPT^{<0>}$
$\quad x \leftarrow 1$
$\quad while \ x \leq (IncMax - 1)$
$\qquad B \leftarrow stack\left(B, ENGPT^{<x>}\right)$
$\qquad x \leftarrow x + 1$
$\quad stack\left(B, ENGPT^{<x>}\right) \cdot cm^{-1}$

$NROTP :=$
$\quad i \leftarrow 0$
$\quad A \leftarrow NrotP$
$\quad while \ i \leq (IncMax - 1)$
$\qquad A \leftarrow stack(A, NrotP)$
$\qquad i \leftarrow i + 1$
$\quad A$

$ENGR :=$
$\quad B \leftarrow ENGRT^{<0>}$
$\quad x \leftarrow 1$
$\quad while \ x \leq (IncMax - 1)$
$\qquad B \leftarrow stack\left(B, ENGRT^{<x>}\right)$
$\qquad x \leftarrow x + 1$
$\quad stack\left(B, ENGRT^{<x>}\right) \cdot cm^{-1}$

$NROTR :=$
$\quad i \leftarrow 0$
$\quad A \leftarrow NrotR$
$\quad while \ i \leq (IncMax - 1)$
$\qquad A \leftarrow stack(A, NrotR)$
$\qquad i \leftarrow i + 1$
$\quad A$

Define the lineshapes of individual spectral features assuming Gaussian Lineshapes and an ASE component which also has a Gaussian Line Shape. (Note: These functions are area normalized)

$$\text{LineShapeP}_k = \text{NROTP}_k \left[\sqrt{\frac{4\ln(2)}{\pi}} \cdot \left(\frac{1}{\Delta v_D + \Delta v_{ase}} \right) \right] \cdot \left[(1 - ase) \cdot \exp\left[\frac{-\left[4\ln(2) \cdot \left(\text{ENGP}_{kj} \right)^2 \right]}{\Delta v_D{}^2} \right] + ase \cdot \exp\left[\frac{-\left[4\ln(2) \cdot \left(\text{ENGP}_{kj} \right)^2 \right]}{\Delta v_{ase}{}^2} \right] \right]$$

$$\text{LineShapeR}_{kk} = \text{NROTR}_{kk} \cdot \left[\sqrt{\frac{4\ln(2)}{\pi}} \cdot \left(\frac{1}{\Delta v_D + \Delta v_{ase}} \right) \right] \cdot \left[(1 - ase) \cdot \exp\left[\frac{-\left[4\ln(2) \cdot \left(\text{ENGR}_{kk} \right)^2 \right]}{\Delta v_D{}^2} \right] + ase \cdot \exp\left[\frac{-\left[4\ln(2) \cdot \left(\text{ENGR}_{kk} \right)^2 \right]}{\Delta v_{ase}{}^2} \right] \right]$$

Define the total intensity function for the desired spectrum. The lineshapes of individual spectral features are summed at each step along the wavenumber axis producing the final spectrum.

$$\text{Intensity2} := \begin{vmatrix} i \leftarrow 0 \\ k \leftarrow 0 \\ \text{while } i \leq \text{IncMax} \\ \quad \begin{vmatrix} D_i \leftarrow \sum_{k = i \cdot \left(|J_{min}| + 1 \right)}^{(i+1) \cdot \left(|J_{min}| + 1 \right) - 1} \text{LineShapeP}_k + \sum_{kk = i \cdot J_{max}}^{(i+1) \cdot J_{max} - 1} \text{LineShapeR}_{kk} \\ i \leftarrow i + 1 \end{vmatrix} \\ D \cdot cm^{-2} \end{vmatrix}$$

Export routine sends results to a user-defined Excel file (Note evaluation set to disable - reset when spectrum meets desired standards):

$$\text{EXPORT} := \text{augment}(v, \text{Intensity2})$$

Appendix G

This appendix contains output from the University of Tennessee Space Institute's

RKR program [35]. Pages G-1 through G-4 present data for $Bi_2(X)$ using constants from

Barrow et al [1] and pages G-4 through G-6 contain data for $Bi_2(A)$ using constants from

the current analysis, Table 3-2.

$Bi_2(X)$

Planck's constant = 6.626176E-27
Speed of light = 2.99792458E+10
Avogadro's number = 6.022045E+23
Reduced mass = 104.4902000
Constant = .4016617572

Gauss-Mehler points and weights

n	x(n)	w(n)
1	.99533273887160	.27305660498044
2	.95825570463284	.27050715004823
3	.88548311653283	.26543204386565
4	.77972646163861	.25787867157142
5	.64492620420617	.24791755739443
6	.48610496464900	.23564170629830
7	.30918037738183	.22116573583373
8	.12074460018195	.20462480641877
9	-7.21813100060393E-02	.18617336031175
10	-.26240900411126	.16598368178583
11	-.44285068651552	.14424429412712
12	-.60678322854758	.12115821587893
13	-.74809874165061	9.69411235330222E-02
14	-.86153241961259	7.18196062740425E-02
15	-.94286010338110	4.60309394957198E-02
16	-.98907042030188	1.98516269287997E-02

vibrational constants	rotational constants
Yoo = .0000000000	2.2807660000E-02
173.0090000	-5.3315800000E-05
-.3689000000	
-1.1564000000E-03	
2.4400000000E-05	
-6.1430000000E-07	
6.1123000000E-09	
-2.0057000000E-11	

Table G-1. Tabulated output from the RKR program for the $Bi_2(X)$ – state

v	Bv (cm^{-1})	Gv (cm^{-1})	r-min (Å)	r-max (Å)
0	2.28E-02	86.41213	2.61778688	2.70423552
1	2.27E-02	258.6797	2.58879263	2.73879547
2	2.27E-02	430.1997	2.56958365	2.76358884
3	2.26E-02	600.9662	2.55440184	2.78437401
4	2.26E-02	770.9738	2.54157501	2.8028234
5	2.25E-02	940.2173	2.5303388	2.81970166
6	2.25E-02	1108.692	2.52026787	2.83543436
7	2.24E-02	1276.393	2.51109679	2.8502872
8	2.24E-02	1443.316	2.50264673	2.86443925
9	2.23E-02	1609.456	2.49479049	2.87801798
10	2.22E-02	1774.811	2.48743375	2.89111796
11	2.22E-02	1939.375	2.48050431	2.90381167
12	2.21E-02	2103.144	2.47394541	2.91615613
13	2.21E-02	2266.115	2.46771149	2.92819719
14	2.20E-02	2428.283	2.46176529	2.93997238
15	2.20E-02	2589.644	2.45607591	2.95151292
16	2.19E-02	2750.195	2.45061733	2.96284513
17	2.19E-02	2909.93	2.44536741	2.97399145
18	2.18E-02	3068.846	2.44030713	2.98497127
19	2.18E-02	3226.937	2.43541995	2.99580142
20	2.17E-02	3384.2	2.43069144	3.00649672
21	2.17E-02	3540.629	2.42610885	3.01707028
22	2.16E-02	3696.22	2.42166088	3.02753378
23	2.16E-02	3850.968	2.41733744	3.03789771
24	2.15E-02	4004.866	2.41312947	3.04817154
25	2.14E-02	4157.911	2.40902878	3.05836387
26	2.14E-02	4310.096	2.40502795	3.06848258
27	2.13E-02	4461.416	2.40112023	3.07853487
28	2.13E-02	4611.864	2.39729943	3.0885274
29	2.12E-02	4761.436	2.39355986	3.09846634
30	2.12E-02	4910.124	2.3898963	3.10835741
31	2.11E-02	5057.924	2.38630389	3.11820598
32	2.11E-02	5204.828	2.38277816	3.12801706
33	2.10E-02	5350.83	2.37931493	3.13779537
34	2.10E-02	5495.924	2.37591029	3.14754536
35	2.09E-02	5640.104	2.37256062	3.15727125
36	2.09E-02	5783.362	2.36926249	3.16697703
37	2.08E-02	5925.693	2.36601272	3.17666648
38	2.08E-02	6067.09	2.36280828	3.18634324
39	2.07E-02	6207.546	2.35964634	3.19601075
40	2.06E-02	6347.056	2.35652423	3.20567232
41	2.06E-02	6485.613	2.35343942	3.21533111
42	2.05E-02	6623.21	2.35038952	3.22499016
43	2.05E-02	6759.841	2.34737227	3.23465237
44	2.04E-02	6895.502	2.34438554	3.24432055
45	2.04E-02	7030.185	2.3414273	3.2539974

v	Bv (cm^{-1})	Gv (cm^{-1})	r-min (Å)	r-max (Å)
46	2.03E-02	7163.884	2.33849563	3.26368551
47	2.03E-02	7296.596	2.3355887	3.27338736
48	2.02E-02	7428.314	2.3327048	3.28310538
49	2.02E-02	7559.033	2.32984228	3.29284186
50	2.01E-02	7688.749	2.32699961	3.30259905
51	2.01E-02	7817.457	2.32417531	3.31237908
52	2.00E-02	7945.153	2.32136801	3.32218401
53	2.00E-02	8071.833	2.31857639	3.33201583
54	1.99E-02	8197.494	2.31579922	3.34187644
55	1.98E-02	8322.132	2.31303535	3.35176766
56	1.98E-02	8445.746	2.31028367	3.36169123
57	1.97E-02	8568.332	2.30754318	3.37164884
58	1.97E-02	8689.889	2.3048129	3.38164205
59	1.96E-02	8810.415	2.30209195	3.3916724
60	1.96E-02	8929.909	2.29937951	3.40174132
61	1.95E-02	9048.37	2.29667479	3.41185016
62	1.95E-02	9165.798	2.2939771	3.42200023
63	1.94E-02	9282.194	2.29128579	3.43219271
64	1.94E-02	9397.558	2.28860026	3.44242876
65	1.93E-02	9511.892	2.28591998	3.45270944
66	1.93E-02	9625.196	2.28324446	3.46303572
67	1.92E-02	9737.474	2.28057327	3.47340852
68	1.92E-02	9848.727	2.27790604	3.48382869
69	1.91E-02	9958.959	2.27524242	3.494297
70	1.90E-02	10068.17	2.27258213	3.50481416
71	1.90E-02	10176.37	2.26992493	3.51538082
72	1.89E-02	10283.56	2.2672706	3.52599756
73	1.89E-02	10389.75	2.26461898	3.5366649
74	1.88E-02	10494.93	2.26196994	3.54738333
75	1.88E-02	10599.13	2.25932337	3.55815328
76	1.87E-02	10702.33	2.25667918	3.56897515
77	1.87E-02	10804.55	2.25403733	3.5798493
78	1.86E-02	10905.79	2.25139777	3.59077608
79	1.86E-02	11006.07	2.24876046	3.60175582
80	1.85E-02	11105.38	2.24612538	3.61278886
81	1.85E-02	11203.74	2.2434925	3.62387554
82	1.84E-02	11301.15	2.24086177	3.63501626
83	1.84E-02	11397.62	2.23823314	3.64621143
84	1.83E-02	11493.15	2.23560653	3.65746155
85	1.82E-02	11587.76	2.2329818	3.66876718
86	1.82E-02	11681.45	2.23035881	3.68012901
87	1.81E-02	11774.22	2.22773732	3.69154785
88	1.81E-02	11866.09	2.22511705	3.70302466
89	1.80E-02	11957.07	2.22249763	3.71456061
90	1.80E-02	12047.14	2.21987859	3.72615707

v	Bv (cm^{-1})	Gv (cm^{-1})	r-min (Å)	r-max (Å)
91	1.79E-02	12136.33	2.21725935	3.73781568
92	1.79E-02	12224.64	2.21463923	3.74953836
93	1.78E-02	12312.07	2.21201738	3.76132738
94	1.78E-02	12398.62	2.2093928	3.7731854
95	1.77E-02	12484.3	2.20676431	3.7851155
96	1.77E-02	12569.11	2.20413054	3.79712124
97	1.76E-02	12653.06	2.20148989	3.80920677
98	1.76E-02	12736.13	2.19884051	3.82137682
99	1.75E-02	12818.33	2.19618028	3.83363681

$Bi_2(A)$

Planck's constant = 6.626176E-27
Speed of light = 2.99792458E+10
Avogadro's number = 6.022045E+23
Reduced mass = 104.4902000
Constant = .4016617572

Gauss-Mehler points and weights

n	x(n)	w(n)
1	.99533273887160	.27305660498044
2	.95825570463284	.27050715004823
3	.88548311653283	.26543204386565
4	.77972646163861	.25787867157142
5	.64492620420617	.24791755739443
6	.48610496464900	.23564170629830
7	.30918037738183	.22116573583373
8	.12074460018195	.20462480641877
9	-7.21813100060393E-02	.18617336031175
10	-.26240900411126	.16598368178583
11	-.44285068651552	.14424429412712
12	-.60678322854758	.12115821587893
13	-.74809874165061	9.69411235330222E-02
14	-.86153241961259	7.18196062740425E-02
15	-.94286010338110	4.60309394957198E-02
16	-.98907042030188	1.98516269287997E-02

vibrational constants
Yoo = .0000000000
132.3835000
-.3109310000
-2.7494000000E-04

rotational constants
1.9641200000E-02
-5.0080000000E-05
-1.3170000000E-07

Table G-2. Tabulated output from the RKR program for the $Bi_2(A)$ - state

v	Bv (cm^{-1})	Gv (cm^{-1})	r-min (Å)	r-max (Å)
0	1.96E-02	66.11398	2.81822993	2.91706572
1	1.96E-02	197.8747	2.78519332	2.9567195
2	1.95E-02	329.0111	2.76334807	2.98522689
3	1.95E-02	459.5216	2.74611374	3.00916875
4	1.94E-02	589.4043	2.73157988	3.03045597
5	1.94E-02	718.6578	2.71887337	3.04996206
6	1.93E-02	847.2804	2.70750853	3.06817317
7	1.93E-02	975.2704	2.69718231	3.08539278
8	1.92E-02	1102.626	2.68769064	3.10182542
9	1.92E-02	1229.346	2.67888838	3.11761668
10	1.91E-02	1355.428	2.67066798	3.13287457
11	1.90E-02	1480.871	2.66294714	3.14768187
12	1.90E-02	1605.674	2.65566122	3.16210371
13	1.89E-02	1729.834	2.64875838	3.17619241
14	1.89E-02	1853.349	2.64219627	3.18999081
15	1.88E-02	1976.219	2.63593981	3.20353453
16	1.88E-02	2098.442	2.6299595	3.21685355
17	1.87E-02	2220.015	2.6242303	3.22997346
18	1.87E-02	2340.938	2.61873073	3.24291626
19	1.86E-02	2461.208	2.61344219	3.2557011
20	1.86E-02	2580.824	2.60834846	3.26834475
21	1.85E-02	2699.785	2.60343529	3.28086204
22	1.84E-02	2818.088	2.59869008	3.29326613
23	1.84E-02	2935.732	2.59410162	3.30556881
24	1.83E-02	3052.716	2.5896599	3.31778071
25	1.83E-02	3169.037	2.58535591	3.32991142
26	1.82E-02	3284.695	2.58118154	3.34196969
27	1.82E-02	3399.687	2.57712942	3.35396349
28	1.81E-02	3514.011	2.57319287	3.36590017
29	1.80E-02	3627.667	2.56936578	3.37778649
30	1.80E-02	3740.652	2.56564256	3.3896287
31	1.79E-02	3852.965	2.56201807	3.40143263
32	1.79E-02	3964.605	2.55848757	3.41320369
33	1.78E-02	4075.568	2.5550467	3.42494698
34	1.78E-02	4185.855	2.55169139	3.43666726
35	1.77E-02	4295.463	2.5484179	3.44836903
36	1.76E-02	4404.39	2.54522271	3.46005653
37	1.76E-02	4512.636	2.54210257	3.47173381
38	1.75E-02	4620.197	2.53905442	3.4834047
39	1.75E-02	4727.074	2.5360754	3.49507284
40	1.74E-02	4833.263	2.53316283	3.50674174
41	1.73E-02	4938.763	2.53031419	3.51841475
42	1.73E-02	5043.574	2.5275271	3.5300951
43	1.72E-02	5147.692	2.52479931	3.54178589
44	1.72E-02	5251.117	2.52212871	3.55349013
45	1.71E-02	5353.846	2.51951329	3.56521073

v	Bv (cm^{-1})	Gv (cm^{-1})	r-min (Å)	r-max (Å)
46	1.70E-02	5455.878	2.51695115	3.57695052
47	1.70E-02	5557.212	2.51444048	3.58871225
48	1.69E-02	5657.846	2.51197956	3.6004986
49	1.68E-02	5757.778	2.50956675	3.6123122
50	1.68E-02	5857.006	2.50720049	3.62415563
51	1.67E-02	5955.529	2.50487928	3.6360314
52	1.66E-02	6053.346	2.50260171	3.647942
53	1.66E-02	6150.453	2.50036639	3.65988988
54	1.65E-02	6246.851	2.49817202	3.67187746
55	1.65E-02	6342.537	2.49601732	3.68390714
56	1.64E-02	6437.51	2.4939011	3.69598128
57	1.63E-02	6531.767	2.49182217	3.70810225
58	1.63E-02	6625.308	2.48977941	3.72027239
59	1.62E-02	6718.13	2.48777173	3.73249404
60	1.61E-02	6810.232	2.48579807	3.74476952
61	1.61E-02	6901.613	2.4838574	3.75710117
62	1.60E-02	6992.271	2.48194875	3.76949132
63	1.59E-02	7082.203	2.48007113	3.78194232
64	1.59E-02	7171.409	2.47822361	3.79445651
65	1.58E-02	7259.886	2.47640528	3.80703624
66	1.57E-02	7347.634	2.47461525	3.81968391
67	1.57E-02	7434.65	2.47285264	3.8324019
68	1.56E-02	7520.933	2.4711166	3.84519264
69	1.55E-02	7606.481	2.46940629	3.85805856
70	1.55E-02	7691.292	2.4677209	3.87100215
71	1.54E-02	7775.366	2.46605961	3.8840259
72	1.53E-02	7858.699	2.46442164	3.89713235
73	1.52E-02	7941.291	2.46280619	3.91032408
74	1.52E-02	8023.14	2.4612125	3.92360371
75	1.51E-02	8104.244	2.45963979	3.93697391
76	1.50E-02	8184.602	2.45808732	3.95043737
77	1.50E-02	8264.212	2.45655433	3.96399687
78	1.49E-02	8343.072	2.45504007	3.97765523
79	1.48E-02	8421.18	2.45354381	3.99141531
80	1.48E-02	8498.536	2.45206479	4.00528007
81	1.47E-02	8575.137	2.45060228	4.0192525
82	1.46E-02	8650.982	2.44915554	4.03333568
83	1.45E-02	8726.068	2.44772383	4.04753277
84	1.45E-02	8800.395	2.4463064	4.061847
85	1.44E-02	8873.961	2.44490252	4.07628168
86	1.43E-02	8946.764	2.44351142	4.09084022
87	1.43E-02	9018.802	2.44213236	4.10552611
88	1.42E-02	9090.075	2.44076456	4.12034296
89	1.41E-02	9160.579	2.43940726	4.13529447
90	1.40E-02	9230.314	2.43805967	4.15038445
91	1.40E-02	9299.277	2.436721	4.16561683

The following data is the input file, prein.dat, for use with the FCF program

provided by Michael Heaven [27].

PREDISSOCIATION OF Bi2(A) Data 01/15/2001
208.9804,208.9804
3 3
132.3836 -0.31093 -0.000275
0.0196412 -0.00005008 -0.000000132
17740.693
 6 0 0
 127
27039.970,2.437,26541.088,2.446,26083.765,2.455,25516.059,2.466,
25000.579,2.476,24550.925,2.486,24083.230,2.496,23597.699,2.507,
23196.517,2.517,22784.267,2.528,22467.767,2.536,22145.083,2.545,
21816.261,2.555,21481.345,2.566,21140.380,2.577,20909.730,2.585,
20558.781,2.599,20321.517,2.608,20081.631,2.619,19839.135,2.630,
19716.912,2.636,19470.527,2.649,19346.367,2.656,19096.121,2.671,
18970.039,2.679,18843.319,2.688,18715.963,2.697,18587.973,2.708,
18459.351,2.719,18330.097,2.732,18200.214,2.746,18069.704,2.763,
17938.567,2.785,17806.807,2.818,17740.693,2.868,17806.807,2.917,
17938.567,2.957,18069.704,2.985,18200.214,3.009,18330.097,3.030,
18459.351,3.050,18587.973,3.068,18715.963,3.085,18843.319,3.102,
18970.039,3.118,19096.121,3.133,19221.564,3.148,19346.367,3.162,
19470.527,3.176,19594.042,3.190,19716.912,3.204,19839.135,3.217,
19960.708,3.230,20081.631,3.243,20201.901,3.256,20321.517,3.268,
20440.478,3.281,20558.781,3.293,20676.425,3.306,20793.409,3.318,
20909.730,3.330,21025.388,3.342,21140.380,3.354,21254.704,3.366,
21368.360,3.378,21481.345,3.390,21593.658,3.401,21705.298,3.413,
21816.261,3.425,21926.548,3.437,22036.156,3.448,22145.083,3.460,
22253.329,3.472,22360.890,3.483,22467.767,3.495,22573.956,3.507,
22679.456,3.518,22784.267,3.530,22888.385,3.542,22991.810,3.553,
23094.539,3.565,23196.571,3.577,23297.905,3.589,23398.539,3.600,
23498.471,3.612,23597.699,3.624,23696.222,3.636,23794.039,3.648,
23981.146,3.660,23987.544,3.672,24083.230,3.684,24178.203,3.696,
24272.460,3.708,24366.001,3.720,24458.823,3.732,24550.925,3.745,

24642.306,3.757,24732.964,3.769,24822.896,3.782,24912.102,3.794,
25000.579,3.807,25088.327,3.820,25175.343,3.832,25261.626,3.845,
25347.174,3.858,25431.985,3.871,25516.059,3.884,25599.392,3.897,
25681.984,3.910,25763.833,3.924,25844.937,3.937,25925.295,3.950,
26004.905,3.964,26083.765,3.978,26161.873,3.991,26239.229,4.005,
26315.830,4.019,26391.675,4.033,26466.761,4.048,26541.088,4.062,
26614.654,4.076,26687.457,4.091,26759.495,4.106,26830.768,4.120,
26901.272,4.135,26971.007,4.150,27039.970,4.166
29913.22
  17
2.0 4.1 0.010 0.05
  20
  2 0
5.00E05,8.991,0.0,0.92
A /(R-D)**B
2.5 5.0
14877.68
  34,35,36,37,38,39
  0
  0 0 0
  1
  70
  0 0 0
  0
  0
  0
  0

A sample output data file, preout.dat, from the FCF program provided by Michael

Heaven [27]. The six rows at the end of the file provide predissociation probabilities,

right-most number, as a function of vibrational level reported on the left.

FRANK-CONDON DENSITIES AND R-CENTROIDS FOR RADIATIONLESS
TRANSITIONS

MASSES OF NUCLEI (BASED ON C12=12) ARE   208.98040   208.98040
FUNDAMENTAL CONSTANT=   .6198245E+01

  3 VIBRATIONAL PARAMETERS FOR BOUND STATE

132.383600000000000 -3.109300000000000E-001 -2.750000000000000E-004

  3 ROTATIONAL PARAMETERS FOR BOUND STATE

1.964120000000000E-002 -5.008000000000000E-005 -1.320000000000000E-007

Y00(/CM)= 17740.693

INPUT POTENTIAL CURVE FOR BOUND STATE (UNITS A AND /CM)
HAVING DISS. E=   29913.22

2.43700 27039.970   2.44600 26541.088   2.45500 26083.765
2.46600 25516.059   2.47600 25000.579   2.48600 24550.925
2.49600 24083.230   2.50700 23597.699   2.51700 23196.517
2.52800 22784.267   2.53600 22467.767   2.54500 22145.083
2.55500 21816.261   2.56600 21481.345   2.57700 21140.380
2.58500 20909.730   2.59900 20558.781   2.60800 20321.517
2.61900 20081.631   2.63000 19839.135   2.63600 19716.912

2.64900	19470.527	2.65600	19346.367	2.67100	19096.121
2.67900	18970.039	2.68800	18843.319	2.69700	18715.963
2.70800	18587.973	2.71900	18459.351	2.73200	18330.097
2.74600	18200.214	2.76300	18069.704	2.78500	17938.567
2.81800	17806.807	2.86800	17740.693	2.91700	17806.807
2.95700	17938.567	2.98500	18069.704	3.00900	18200.214
3.03000	18330.097	3.05000	18459.351	3.06800	18587.973
3.08500	18715.963	3.10200	18843.319	3.11800	18970.039
3.13300	19096.121	3.14800	19221.564	3.16200	19346.367
3.17600	19470.527	3.19000	19594.042	3.20400	19716.912
3.21700	19839.135	3.23000	19960.708	3.24300	20081.631
3.25600	20201.901	3.26800	20321.517	3.28100	20440.478
3.29300	20558.781	3.30600	20676.425	3.31800	20793.409
3.33000	20909.730	3.34200	21025.388	3.35400	21140.380
3.36600	21254.704	3.37800	21368.360	3.39000	21481.345
3.40100	21593.658	3.41300	21705.298	3.42500	21816.261
3.43700	21926.548	3.44800	22036.156	3.46000	22145.083
3.47200	22253.329	3.48300	22360.890	3.49500	22467.767
3.50700	22573.956	3.51800	22679.456	3.53000	22784.267
3.54200	22888.385	3.55300	22991.810	3.56500	23094.539
3.57700	23196.571	3.58900	23297.905	3.60000	23398.539
3.61200	23498.471	3.62400	23597.699	3.63600	23696.222
3.64800	23794.039	3.66000	23981.146	3.67200	23987.544
3.68400	24083.230	3.69600	24178.203	3.70800	24272.460
3.72000	24366.001	3.73200	24458.823	3.74500	24550.925
3.75700	24642.306	3.76900	24732.964	3.78200	24822.896
3.79400	24912.102	3.80700	25000.579	3.82000	25088.327
3.83200	25175.343	3.84500	25261.626	3.85800	25347.174
3.87100	25431.985	3.88400	25516.059	3.89700	25599.392
3.91000	25681.984	3.92400	25763.833	3.93700	25844.937
3.95000	25925.295	3.96400	26004.905	3.97800	26083.765
3.99100	26161.873	4.00500	26239.229	4.01900	26315.830
4.03300	26391.675	4.04800	26466.761	4.06200	26541.088
4.07600	26614.654	4.09100	26687.457	4.10600	26759.495
4.12000	26830.768	4.13500	26901.272	4.15000	26971.007
4.16600	27039.970				

ROUTINE POTH PRODUCES WORKING POTENTIAL CURVE AT 211 POINTS, WITH
    RMIN(ANGSTROMS) = 2.000   RMAX= 4.100   DR= .01000

    8 POINTS USED IN DIVIDED DIFFERENCES INTERPOLATION

POTENTIAL OF FORM A+C(1/R)** 17 IS ATTACHED TO L BRANCH,
WITH A= -1.1086205E+04 AND C= 3.0977290E+10

POTENTIAL OF FORM C(1/R)**P IS ATTACTED TO RIGHT BRANCH,
WITH P= 6.16377 AND C= -1.89748E+07

POTENTIAL FOR CONTINUUM STATE IS GENERATED FROM FUN OF FORM
A /(R-D)**B
PARAMETERS A,B,C,D ARE .5000E+06 .8991E+01 .0000E+00 .9200E+00

ROUTINE POTH PRODUCES WORKING POTENTIAL CURVE AT 361 POINTS
WITH
RMIN(ANGSTROMS)= 2.500 RMAX= 6.100 DR= .01000

ENERGY DIFFERENCE (/CM) AT DISSOCIATION LIMITS OF CUR= 14877.68

SOLUTIONS TO RADIAL EQUATIONS FOR BOUND STATE
CONVERGENCE CRITERION (/CM)= .050

ROTATIONAL NUMBER J= 1

V E(TRIAL) E(FOUND) E(CONTINUUM) F-C DENSITY R-CENTROID PRED. PROB.

V	E(TRIAL)	E(FOUND)	E(CONTINUUM)	F-C DENSITY	R-CENTROID	PRED. PROB.
34	21926.59	21891.36	6855.82	.2583E-05	.2559E+01	.6589E+05
35	22036.19	21998.11	6962.57	.2006E-04	.3026E+01	.2967E+06
36	22145.12	22104.06	7068.52	.1609E-04	.3232E+01	.1796E+06
37	22253.37	22209.09	7173.55	.7635E-07	.7510E+01	.4756E+04
38	22360.93	22313.80	7278.26	.1024E-08	.1762E+02	.1329E+04
39	22467.80	22417.47	7381.93	.3485E-05	.3835E+01	.1206E+05

1

1. Barrow, R. F., F. Taher, J. d'Incan, C. Effantin, A. J. Ross, and J. Vergès. "Electronic States of Bi_2," Molec. Phys., 87(4)725-733, 1996.

2. Gerber, G., K. Sakurai, and H. P. Broida. "Laser Photoluminescence of Bi_2^*," J. Chem. Phys., 66(8)3410-3422, 1976.

3. Ehret, G. and G. Gerber. "Polarization Labeling Spectroscopy of the $A(0_u^+)$ state of Bi_2 with Narrowband Pulsed Dye-Lasers," Optics Communications, 51(3)145-150, 1984.

4. Gerber, G., H. Honninger, and J. Janes. "Rotational Analysis of the A-X Band System of Bi_2," Chem. Phys. Lett., 85(4):415-417, 1981.

5. Effatin, C., A. Topouzkhanian, J. Figuet, J. d'Incan, R.F. Barrow, and J. Vergès. "Electronic States of Bi_2 Studied by Laser-Excited Fluorescence," J. Phys. B.: Atomic and Molecular Physics, 15:3829-3840, 1982.

6. Franklin, Robert E. and Glen P. Perram. "Laser Excitation Spectra and Frank-Condon Factors for Bi_2 $X^1\Sigma_g^+ \rightarrow A(0_u^+)$," J. of Molec. Spec., 194:1-7, 1999.

7. Balasubramanian, K. and Dai-Wei Liao. "Spectroscopic Constants and Potential Energy Curves of Bi_2 and Bi_2^-," J. Chem Phys., 95(5):3064-3073, 1991.

8. Blondeau, J.M., G. Gandara, P. Carette, and J. Messelyn. "Lifetimes of the $A(O_u^-)$ State and Quenching Cross Sections of Bi_2," Chem. Phys. Lett., 71(2):246-252, 1980.

9. Ehret, G. and G. Gerber. "Lifetimes and Transition Moment of the A-X Band System of Bi_2," Chem. Phys., 66:27-38, 1982.

10. Das, Kalyan K., Heinz-Peter Liebermann, and Robert J. Buenker. "Relativistic Configuration Interaction Study of the Low-Lying Electronic States of Bi_2," J. Chem. Phys., 102(11):4518-4530, 1995.

11 . Bloembergen, N. and C. K. N., Co-chairs. "APS Study Group Patel," Rev. Mod. Phys., 59(3):S33-S47, 1987.

12. Perram, Glen P. "Tutorial on Chemical Lasers," Air Force Institute of Technology, Department of Engineering Physics (AU), Wright-Patterson AFB OH, No date.

13. Perram, G. P. "Visible Chemical Lasers," Proceedings of the International Conference on Lasers '89, 1989.

14. Capelle, Gene A., David G. Sutton, and Jeffery I. Steinfeld. "Near-resonant Electronic Energy Transfer from $NF(a^1\Delta)$ to Bi," J. Chem. Phys., 69(11): 5140-5146, 1978.

15. Herbelin, J. M., R. R. Giedt, and H. A. Bixler. "Production of Electronically Excited Bismuth in a Supersonic Flow," J. Appl. Phys., 54(1): 28-32, 1983.

16. Benard, D. J. "Threshold Oscillation of an $NF(a^1\Delta)$/BiF Visible Wavelength Chemical Laser," J. Appl. Phys., 74(4):2900-2907, 1993.

17. Clyne, Michael A., Michael C. Heaven, and Joel Tellinghuisen. "Theoretical Treatment of the Spontaneous Predissociation of Br_2, $B^3\Pi(0_u^+)$," J. Chem. Phys., 76(11):5341-5349, June 1982.

18. Steinfeld, Jeffery I. Molecules and Radiation. An Introduction to Modern Molecular Spectroscopy (Second edition). Cambridge MA: The MIT Press, 1985.

19. Arfken, George. Mathematical Methods for Physicist (Third edition). San Diego CA: Academic Press, 1985.

20. Herzberg, Gerhard. Molecular Spectra and Molecular Structure I.. Spectra of Diatomic Molecules. Malabar FL: Krieger Publishing Company, 1989.

21. Shankar, Ramamurti. Principles of Quantum Mechanics. New York NY: Plenum Press, 1980.

22. Bernath, Peter F. Spectra of Atoms and Molecules. New York NY: Oxford University Press, Inc., 1995.

23. Moore, Charolotte E. Atomic Energy Levels As Derived From the Analysis of Atomic Spectra Vol III. Circular of the National Bureau of Standards 467: 220, Washington DC, US Government Printing Office, 1958.

24. Candler, Albert C. Atomic Spectra and the Vector Model (Second edition). Princeton NJ: D. Van Nostrand Company, Inc., 1964.

25. Demtröder, Wolfgang. <u>Laser Spectroscopy, Basic Concepts and Instrumentation</u> (Second edition). Berlin, Germany: Springer-Verlag, 1996.

26. Verdeyen, Joseph, T. <u>Laser Electronics</u> (Third edition). Englewood Cliffs NJ: Prentice Hall, 1995.

27. Heaven, Michael, C. <u>PC-Based Program for the Determination of $V_{rep}(R)$ for Cases of Heterogeneous Predissociation</u>. Personal Contact, April 1999.

28. <u>Table Curve™ 2D Version 4.0 for Windows®</u> (User's Manual). Chicago, IL: SPSS Inc., 1997

29. Dolezal, Michael W. and Sammuel D. Herbert. <u>DataFit</u>. Computer software. Air Force Technical Applications Center, Patrick AFB, FL, 2000.

30 . Franklin, Robert E. Computer software. 3.5 inch diskette. Personal conversation, June, 1999.

31. Dolezal, Michael W. and Sammuel D. Herbert. <u>GlobalFit</u>. Computer software. Air Force Technical Applications Center, Patrick AFB, FL, 2000.

32. Tellinghuisen, Joel. "Photodissociation and Photoionization, The Frank-Condon Principle in Bound-Free Transitions," <u>Advances in Chemical Physics-Volume LX</u>. Chichester: Wiley and Sons Ltd., 1985.

33. Bomem, Hartmann, and Braun. <u>PCDA Software User's Guide</u> (Revision 1.1). Quebec Canada: Bomem, Inc., 1993.

34. Bevington, Philip R. <u>Data Reduction and Analysis for the Physical Sciences</u>. New York New York: McGraw-Hill, Inc., 1969.

35. Hornkohl, James O. <u>RKR Program</u>. Computer software. The University of Tennessee Space Institute, Tullahoma TN, 1996.

36. Hume, Mark D. <u>DataPlot</u>, Computer software. Marcat Technologies, Dayton OH, Oct 2000.

Vita

Captain Michael Wayne Dolezal was born on October 30, 1967 in Des Moines, Iowa. After graduating from Thomas Jefferson High School in Bloomington, Minnesota in 1986 he enrolled at the University of Minnesota Institute of Technology and in the Air Force Reserved Officers Training Corps, Detachment 415. After studying physics at both the University of Minnesota and the University of North Dakota, he graduated with a Bachelor of Physics from the University of Minnesota in the summer of 1991. After accepting his commission as a second lieutenant, Captain Dolezal was assigned to undergraduate pilot training (UPT), Reese Air Force Base, Texas in May of 1992. A routine medical evaluation led to his disqualification from the program. After UPT he was assigned to the United States Strategic Command (USSTRATCOM) Omaha, Nebraska as a Warhead Lethality and Infrared Systems Physicist. While in Omaha he earned a Masters Degree in Physics from Creighton University. After his tour of duty at STRATCOM he was accepted into the Ph.D. program at the Air Force Institute of Technology (AFIT) Wright-Patterson Air Force Base, Ohio in the summer of 1996. Michael married Jennifer Wren, of Roseville, Minnesota, in May of 1992. They have one daughter, Maria Nichole, born in November of 1993 and one son, Jonathan Michael, born in February of 1996. Captain Dolezal's follow-on assignment is to the Air Force Technical Applications Center (AFTAC) Patrick Air Force Base, Florida.

Permanent Address: 8224 Stevens Avenue South
                     Bloomington, MN 55434

REPORT DOCUMENTATION PAGE

1. REPORT DATE *(DD-MM-YYYY)*	2. REPORT TYPE	3. DATES COVERED *(From - To)*
20-03-2001	Doctoral Dissertation	Jun 1996-Mar 2001

4. TITLE AND SUBTITLE	5a. CONTRACT NUMBER
SPECTROSCOPIC CONSTANTS, LIFETIMES AND PREDISSOCIATION RATES FOR BI2 A(0U+)	
	5b. GRANT NUMBER
	5c. PROGRAM ELEMENT NUMBER

6. AUTHOR(S)	5d. PROJECT NUMBER
Dolezal, Michael W., Captain, USAF	
	5e. TASK NUMBER
	5f. WORK UNIT NUMBER

7. PERFORMING ORGANIZATION NAME(S) AND ADDRESS(ES)	8. PERFORMING ORGANIZATION REPORT NUMBER
Air Force Institute of Technology Graduate School of Engineering and Management (AFIT/EN) 2950 P Street, Building 640 WPAFB OH 45433-7765	AFIT/DS/ENP/01-01

9. SPONSORING/MONITORING AGENCY NAME(S) AND ADDRESS(ES)	10. SPONSOR/MONITOR'S ACRONYM(S)
AFOSR/NL Attn: Michael R. Berman 801 N. Randolf St., Rm 732 Arlington, VA 22203-1977 Phone: (703) 696-7781	
	11. SPONSOR/MONITOR'S REPORT NUMBER(S)

12. DISTRIBUTION/AVAILABILITY STATEMENT

APPROVED FOR PUBLIC RELEASE; DISTRIBUTION UNLIMITED

13. SUPPLEMENTARY NOTES

14. ABSTRACT

This research determined spectroscopic constants, lifetimes and predissociation rates for the A-state of Bi2. More than 100,000 spectral features from a Bi2 X to A absorption spectrum, encompassing $0 < v' < 92$, $0 < v'' < 7$, and $J < 204$, have been assigned. Vibrational and rotational spectroscopic constants for Bi2(A) were improved. These constants redefine the A-state potential using RKR methods and set the A-state dissociation energy at 29913 1/cm correlating A-state dissociation products to quartet S + doublet D atoms. A pulsed dye laser apparatus was used to obtain lifetime data for Bi2 A to X transitions. The collision-free lifetimes for $v' = 20$ to $v' = 39$, and $J < 105$, were investigated for effects of heterogeneous predissociation. observed predissociation rates, $k_{pd} J(J+1)$, establish the range $k_{pd} = 153$ to 1.5 E+05 1/sec for $v' = 21$ to $v' = 39$. Rapid predissociation and the dense Bi2 (A-X) spectrum required both traditional lifetime measurements and synthetic spectrum fits to determine the full range of observed rates. Numerical analysis fails to produce a repulsive potential responsible for predissociation implying that current theoretical knowledge of predissociation is inadequate to describe the results of this study.

15. SUBJECT TERMS

Bismuth, Molecular Spectroscopy, Laser Induced Fluorescence, Molecular States, Predissociation

16. SECURITY CLASSIFICATION OF:			17. LIMITATION OF ABSTRACT	18. NUMBER OF PAGES	19a. NAME OF RESPONSIBLE PERSON
a. REPORT	b. ABSTRACT	c. THIS PAGE	U	146	LtCol Glen P. Perram, ENP
U	U	U			19b. TELEPHONE NUMBER *(Include area code)* (937)255-3636 x4504